CLUES ON THE ORIGIN AND DIFFERENTIATION OF PRIMITIVE ARC MAGMAS: THE COARSE GRAINED, HIGH-MG BASALTIC ENCLAVES OF CAPO MARARGIU (SARDINIA, ITALY)

SAPIENZA
UNIVERSITÀ DI ROMA

a thesis submitted to attain the degree of
Doctor of Philosophy

by

VANNI TECCHIATO
Dipartimento di Scienze della Terra
Sapienza – Università di Roma

Supervisor
Prof. Mario Gaeta

Co-Supervisor
Prof. Silvio Mollo

2017

Alle mie radici:

la mia famiglia
vicina e lontana

la mia nonna
una maestosa fortezza

il nonno Toni
e i nonni Bruno e Dina
eroi

con infinita gratitudine

Table of contents

Summary

Recent models depict thermally mature magmatic systems as transcrustal crystal mushes where, from the base to the roof, primary magmas evolve towards silicic end-members through crystal fractionation. In these cumulitic piles, igneous distillation is variably overprinted by open system dynamics, with the result that plutonic and volcanic rocks show puzzling textures and hybrid bulk compositions.

The first evolutionary stage of primary arc magmas occurs at the mantle-crust transition, where high pressure conditions may prevent water loss, thus promoting the fractionation of pyroxenitic to hornblenditic cumulates. Intriguingly, the average composition of continental crust is too felsic to be in equilibrium with the mantle, implying that (i) preserved mafic cumulates are too scarce than predicted according to mass balance principles, and (ii) high pressure cumulitic rocks and inclusions eventually exposed at Earth surface provide precious insights on the lower crustal evolution of arc basalts and picrites.

The goal of this PhD project is to give a contribution to the scientific debate about arc magma evolution by investigating the basaltic to andesitic rocks from Capo Marargiu Volcanic District (i.e., CMVD). This is an Oligo-Miocene calc-alkaline complex located in north-western Sardinia (Italy) and characterised by the widespread occurrence of basaltic andesitic domes and dikes. One of these domes hosts abundant crystal-rich enclaves containing ~50% of millimetre- to centimetre-sized clinopyroxene and amphibole crystals with intriguing textures.

Based on textural, geochemical, and experimental data, it is demonstrated that the CMVD plumbing system is a complex polybaric structure developed from the base of Sardinian crust to hypabyssal depths, where hydrous high-Mg basalts produce basaltic andesitic magmas by fractional crystallisation of high-pressure assemblages and assimilation of the Hercynian basement. Buoyant basaltic andesites undergo a second stage of differentiation in the shallow crust, leading the more evolved andesitic melts intruded as dikes.

Enclave mineral texture and chemistry constrain the hybrid nature of these rocks due to entrainment of lower crustal clinopyroxene + amphibole cumulates in a basaltic andesitic magma ascending towards shallow depths.

Introduction

Volcanic eruptions are among the most impressive natural phenomena on Earth. They can be extremely hazardous for humans, even “catastrophic” when erupted materials destroy entire cities and civilisations. To cite a few examples, the Minoan eruption of Santorini caused the decline of the Minoan civilisation, the well-known eruption of Mount Vesuvius in 79 AD buried the cities of Pompeii and Herculaneum, and the 1883 eruption of Krakatoa killed about forty thousand people and altered the global climate for about five years.

Volcanic eruptions represent the spectacular result of deep igneous processes triggered by the physico-chemical gradients characteristic of our dynamic planet. These processes include partial melting of mantle and crustal rocks, and magmatic differentiation within reservoirs located at different levels in the crust. Both partial melting and magmatic differentiation can generate compositionally heterogeneous magmas: in the former case, depending on the characteristics of the source and on the degree of partial melting (i.e., primary variability); in the latter case, according to the evolution of an initial, single, parental magma towards a variety of different products (i.e., secondary variability). Despite both mechanisms are of fundamental importance in igneous petrology, magmatic differentiation is widely considered as the main responsible for the most evolved, viscous and potentially explosive magmas produced by Earth. Understanding the modalities, loci, and timing of magmatic differentiation processes is a crucial task towards a more precise evaluation of volcanic hazard and, thus, for the mitigation of volcanic risk.

Mechanisms of magmatic differentiation

The fact that igneous rocks are extremely variable both in mineralogy and chemical composition leads petrologists to think automatically in evolutionary terms. Magmatic differentiation is therefore defined as “the formation of a variety of substances from an initial, single, parental material” (Cox et al., 1979). Magmatic differentiation is thought to operate either in the liquid state (liquid

immiscibility and thermogravitational diffusion) or by the physical separation of crystals from liquid (cf. Wilson, 1995). Although liquid state differentiation (especially liquid immiscibility) may be important for the segregation of carbonatitic melts from alkaline magmas (e.g., Freestone and Hamilton, 1980; Pinkerton et al., 1995) or of sulphide liquids from basalts (e.g., Pedersen, 1979; Keays, 1995), crystal-liquid fractionation is considered as the main drive for magmatic differentiation (at least since Harker, 1894). This latter can be theoretically achieved by:

1. gravitational or Stokes settling (Daly, 1933), at crystallinity lower than ~40 vol.% and depending on melt density, viscosity, and on the presence of convective movements (convective fractionation; Rice, 1981; Sparks et al., 1984; Langmuir, 1989). At such conditions, crystal agglomeration may promote particle sedimentation (e.g., Masotta et al., 2012);
2. micro-settling (Miller et al., 1988) in magmas of intermediate crystallinity (between ~40-60 vol.%), when the establishment of a self-supporting skeleton of crystals causes micro-rearrangements of the crystalline framework and the expulsion of some interstitial melt;
3. compaction (McKenzie, 1985; Bachmann and Bergantz, 2004; Hildreth, 2004) and/or filter-pressing (including mush fracturing, Bachmann and Bergantz, 2006; Parmigiani et al., 2017) at crystallinity higher than ~60 vol%.

Besides these closed system differentiation mechanisms, open-system processes such as magma mixing, and wall-rock assimilation also contribute to petrological diversity. The blending of two melt-dominated magmas has been long recognised as an important magmatic process (at least since Bunsen, 1851) and the assimilation of crustal melts by hot, mantle-derived magmas (often accompanied by crystallisation) is commonly invoked to explain the variations in magmatic series (e.g., DePaolo, 1981).

From the mush model to transcrustal magma reservoirs

In the last decade, the classical model of magmatic systems as massive vats of near-liquidus material (e.g., Marsh, 1989) has been revised in favour of the concept that magmas are prominently stored in the crust as high-crystallinity bodies (Hildreth, 1981; Lipman, 1984; Bachmann and Bergantz, 2004; Hildreth,

2004; Huber et al. 2009). Indeed, intruding magmas are typically much hotter than surrounding crustal rocks and undergo rapid cooling due to high thermal gradients. At magma-country rock interface, important heat loss leads to extensive crystallisation with the formation of solidification fronts (Marsh, 1989, 2002; Masotta et al., 2012; Gutierrez et al., 2013) acting as thermal buffers between the hot, inner region of intrusions and the cold crust. As the temperature contrast and the cooling rate decrease, magmas encounter favourable conditions to spend most of their life (~10^5-10^6 years; Schmitt, 2011; Cooper, 2015) in a near-solidus state (Koyaguchi and Kaneko, 1999; Huber et al., 2009) as crystal mushes (i.e., "mixture of crystals and silicate liquid whose mobility, and hence eruptibility, is inhibited by a high fraction of solid particles"; Miller and Wark, 2008). Such high-crystallinity magmas (~50 vol.%) are ideal systems for melt segregation, since the presence of an interconnected crystal framework prevents the interference between settling and convection, and porosity conditions still allow for efficient liquid extraction (Dufek and Bachmann, 2010).

On this basis and with the support of field observations (e.g., Miller and Miller, 2002; Quick et al., 2009; Jagoutz and Schmidt, 2012), petrological data (e.g., Hildreth, 2004; Putirka et al., 2014; Lipman and Bachmann, 2015), geophysical surveys (e.g., Ward et al., 2014; Huang et al., 2015; Kiser et al., 2016) and thermal models (e.g., Annen et al., 2006; Karakas et al., 2017), petrologists recently converged in the unified view of thermally mature magmatic systems as complex "transcrustal" (Cashman et al., 2017) structures, that develop vertically from nearby the Moho to subvolcanic depths (e.g., Hildreth and Moorbath, 1988; Bachmann and Huber, 2016). These crustal-scale mushy reservoirs act as distillation columns where, from the base to the roof, mantle-derived basalts differentiate towards silicic end members by crystal fractionation (e.g., Dufek and Bachmann, 2010). Rationally, buoyant residual melts can ascend through the layered continental crust until density traps cause them to pond, accumulate, fractionate, and ascend again (Dufek and Bachmann, 2010). The final result is a vertical compositional gradient from lower crustal mafic cumulates to upper crustal felsic plutons, as recorded in crustal sections exposed worldwide (e.g., Miller and Miller, 2002; Quick et al., 2009; Jagoutz and Schmidt, 2012). Moreover, petrological evidence and numerical modelling results also demonstrate that open system processes, such as magma recharge (Bergantz et al., 2015; Forni

et al., 2015) and gas sparging (Bachmann and Bergantz, 2003), may advect enough heat to efficiently remobilise locked mushes (Huber et al., 2011; Parmigiani et al., 2014) and favour magma mixing and homogenisation (e.g., Bachmann et al, 2002; Burgisser and Bergantz, 2011). In this framework, the effect of igneous distillation is potentially mixed or overprinted by that of open system dynamics, leading to the extreme variability typical of arc magmas (cf. Eichelberger et al., 2006).

Primitive arc magmas

Magmas produced in arc settings represent the primary ingredient for the growth of continental crust. While early models of arc petrogenesis recognised andesites as primary magmas derived by melting of subducting oceanic slab (e.g., Green and Ringwood, 1968), current models emphasise the basaltic nature of arcs resulting from partial melting of the hydrated mantle wedge (e.g., Gust and Perfit, 1987; Eggins, 1993; Pichavant and Macdonald, 2007; Melekhova et al., 2015). In this view, primary magmas are MgO-rich basalts (or picrites) with ~4 wt.% dissolved H_2O (Plank et al., 2013), being rarely erupted at the surface. As supported by field (e.g., Best, 1975; Blundy and Sparks, 1992; DeBari and Coleman, 1989; Ducea and Saleeby, 1996; Lewis, 1973; Smith, 2014; Stamper et al., 2014) and experimental (Alonso-Perez et al., 2009; Foden and Green, 1992; Gust and Perfit, 1987; Holloway and Burnham, 1972; Melekhova et al., 2015; Pichavant and Macdonald, 2007) data, the first evolutionary stage of primary magmas occurs at the mantle-crust transition, where high pressure conditions may prevent water loss, thus promoting the fractionation of pyroxenitic to hornblenditic cumulates.

Intriguingly, the average composition of continental crust is too felsic to be in equilibrium with the mantle, implying that preserved mafic cumulates are too scarce than predicted according to mass balance principles. This necessarily suggests that part of these materials was recycled into the mantle (e.g., Arndt and Goldstein, 1989; Kay and Mahlburg Kay, 1993; Rudnick, 1995), being sometimes partially assimilated into ascending basaltic melts (Dungan and Davidson, 2004; Streck et al., 2007). Hence, high pressure cumulitic rocks and inclusions eventually exposed at Earth surface provide precious insights on the lower crustal evolution of arc basalts and picrites.

Aim of the PhD project

The goal of this PhD project is to give a contribution to the scientific debate about arc magma evolution by investigating the origin of mafic, crystal-rich enclaves entrapped in a basaltic andesitic dome from the Capo Marargiu Volcanic District (CMVD; Sardinia, Italy). This is a calc-alkaline complex where near-primary high-Mg basalts to more evolved andesites were erupted during Oligo-Miocene. Enclaves contain a high crystal fraction (>50% crystals) of primitive olivine, clinopyroxene, and amphibole fractionated under lower crustal conditions. For this reason, they represent a potential source of information on the early differentiation of arc basalts.

Structure of the PhD thesis

This PhD thesis is divided in 4 chapters:

- **Chapter 1** is a paper published in Journal of Volcanology and Geothermal Resource about the origin of CMVD basaltic to andesitic products. This work is based on mineral textural and compositional characteristics to (i) infer the differentiation processes, (ii) model major and trace element bulk-rock data, and (iii) estimate magma crystallisation conditions by comparing thermometric, barometric, hygrometric, and oxygen barometric results with phase relation diagrams.

  The candidate is the first author and the main responsible for fieldwork, analytical work, data analysis and interpretation, picture production, and for the writing of the manuscript draft.
- **Chapter 2** is a manuscript about the intriguing zoning patterns of clinopyroxenes from crystal-rich enclaves. Clinopyroxene major, trace element and isotopic data are interpreted on the basis of theoretical model to infer detailed information on magma evolution, reinforcing some aspect of the overall scenario provided in the first chapter.

  The candidate is the first author and the main responsible for sample preparation, analytical work, data analysis and interpretation, picture production, and for the writing of the manuscript draft.

- **Chapter 3** is a paper published in Periodico di Mineralogia about the stability of amphibole in primitive alkaline and calc-alkaline magmas. The paper discusses experimental results obtained from two basaltic starting materials with different alkali compositions (Na_2O+K_2O = 4.40 wt.% and 2.59 wt.%, respectively) at pressure of 800 MPa, in the temperature range of 975-1225 °C, and with variable contents of initial H_2O (from 0 to 5 wt.%). A comparative study with experimental data from literature and results obtained through thermodynamic simulations allows to constrain the stability field of amphibole in such primitive magmas.

  The candidate is the fourth author and contributed with the sampling and preliminary preparation of the calc-alkaline starting material, with the production of panels b and c of Figure 1, and with the revision and correction of the manuscript draft.
- **Chapter 4** contains the final discussion and conclusions.

Electronic appendixes A-C include the supplementary material of Chapters 1-3.

References

Alonso-Perez, R., Müntener, O., Ulmer, P., 2009. Igneous garnet and amphibole fractionation in the roots of island arcs: experimental constraints on andesitic liquids. Contributions to Mineralogy and Petrology 157, 541–558. doi:10.1007/s00410-008-0351-8

Annen, C., Blundy, JD., Sparks, RSJ., 2006. The genesis of intermediate and silicic magmas in deep crustal hot zones. J Petrol 47(3):505-539

Arndt, N.T., Goldstein, S.L., 1989. An open boundary between lower continental crust and mantle: its role in crust formation and crustal recycling. Tectonophysics 161, 201–212.

Bachmann, O., Bergantz, G.W., 2003. Rejuvenation of the Fish Canyon magma body: a window into the evolution of large volume silicic magma systems. Geology 31 (9), 789–792.

Bachmann, O., Bergantz, G.W., 2004. On the origin of crystal-poor rhyolites: extracted from batholithic crystal mushes. Journal of Petrology 45, 1565–1582.

Bachmann, O., Bergantz, G.W., 2006. Gas percolation in upper-crustal silicic crystal mushes as a mechanism for upward heat advection and rejuvenation of near-solidus magma bodies. Journal of Volcanology and Geothermal Research 149 (1–2), 85–102.

Bachmann, O., Huber, C., 2016. Silicic magma reservoirs in the Earth's crust. Am Mineral 101(11):2377-2404

Bachmann, O., Dungan, M. A., 2002. Temperature-induced Al-zoning in hornblendes of the Fish Canyon magma, Colorado. American Mineralogist, 87(8-9), 1062-1076.

Bergantz, G.W., Schleicher, J.M., and Burgisser, A., 2015. Open-system dynamics and mixing in magma mushes. Nature Geoscience, 8, 793–796

Best, M.G., 1975. Amphibole bearing cumulate inclusions, Grand Canyon, Arizona, and their bearing on silica undersaturated hydrous magma in the upper mantle. Journal of Petrology 16, 212–236.

Blundy, J. D., Sparks, R. S. J., 1992. Petrogenesis of mafic inclusions in granitoids of the Adamello Massif, Italy. Journal of Petrology, 33(5), 1039-1104.

Bunsen, R., 1851. Ueber die prozesse der vulkanishen Gesteinsbildungen Islands. Annalen der Physik (Leipzig) 83, 197–272.

Burgisser, A., and Bergantz, G.W. (2011) A rapid mechanism to remobilize and homogenize highly crystalline magma bodies. Nature, 471, 212–215.

Cashman, K.V., Sparks, R.S.J., Blundy, J.D., 2017. Vertically extensive and unstable magmatic systems: a unified view of igneous processes. Science 355, eaag3055.

Cooper, KM., 2015. Timescales of crustal magma reservoir processes: insights from U-series crystal ages. Geol Soc Spec Publ 422:141-174

Cox, K.G., Bell, J.D., Pankhurst, RJ., 1979. The interpretation of igneous rocks.

Daly, R. A., 1933. Igneous Rocks and the Depths of the Earth.

DeBari, S.M., Coleman, R.G., 1989. Examination of the deep levels of an island arc: evidence from the Tonsina ultramafic-mafic assemblage, Tonsina, Alaska. Journal of Geophysical Research 94, 4373–4391.

DePaolo, D.J., 1981. Trace element and isotopic effects of combined wallrock assimilation and fractional crystallization. Earth and Planetary Science Letters 53, 189–202. doi:10.1016/0012-821X(81)90153-9

Ducea, M.N., Saleeby, J.B., 1996. Buoyancy sources for a large, unrooted mountain range, the Sierra Nevada, California: evidence from xenolith thermobarometry. Journal of Geophysical Research: Solid Earth 101.B4, 8229-8244.

Dufek, J., Bachmann, O., 2010. Quantum magmatism: Magmatic compositional gaps generated by melt-crystal dynamics. Geology 38, 687–690.

Dungan, M. A., Davidson, J., 2004. Partial assimilative recycling of the mafic plutonic roots of arc volcanoes: an example from the Chilean Andes. Geology 32, 773–776.

Eggins, S.M., 1993. Origin and differentiation of picritic arc magmas, Ambae (Aoba), Vanuatu. Contributions to Mineralogy and Petrology, 114(1), 79-100.

Eichelberger, J.C., Izbekov, P.E., Browne, B.L., 2006. Bulk chemical trends at arc volcanoes are not liquid lines of descent. Lithos, 87(1), 135-154.

Foden, J.D., Green, D.H., 1992. Possible role of amphibole in the origin of andesite: some experimental and natural evidence. Contrib. to Mineral. Petrol. 109, 479–493. doi:10.1007/BF00306551

Forni, F., Ellis, B. S., Bachmann, O., Lucchi, F., Tranne, C. A., Agostini, S., & Dallai, L. (2015). Erupted cumulate fragments in rhyolites from Lipari (Aeolian Islands). Contributions to Mineralogy and Petrology, 170(5-6), 49.

Freestone, I.C., Hamilton, D.L., 1980. The role of liquid immiscibility in the genesis of carbonatite. Contributions to Mineralogy and Petrology 73, 105–117.

Green, T.H., Ringwood, A.E., 1968. Genesis of the calc-alkaline igneous rock suite. Contributions to Mineralogy and Petrology 18, 105–162.

Gust, D.A., Perfit, M.R., 1987. Phase relations of a high-Mg basalt from the Aleutian Island Arc: implications for primary island arc basalts and high-Al

basalts. Contributions to Mineralogy and Petrology 97, 7–18. doi:10.1007/BF00375210

Gutierrez, F., Payacan, I., Gelman, S.E., Bachmann, O., Parada, M.A., 2013. Late stage magma flow in a shallow felsic reservoir: Merging the anisotropy of magnetic susceptibility record with numerical simulations in La Gloria Pluton, central Chile. Journal of Geophysical Research-Solid Earth, 118, 1984–1998.

Harker, A., 1894. Carrock Fell: A study of the variation of igneous rock masses. Part I. The gabbros. Quaterly Journal of the Geological Society of London 50, 311–337.

Hildreth, W., Moorbath, S., 1988. Crustal contributions to arc magmatism in the Andes of central Chile. Contributions to mineralogy and petrology, 98(4), 455-489.

Hildreth, W., 1981. Gradients in silicic magma chambers: implications for lithospheric magmatism. Journal of Geophysical Research 86 (B11), 10153–10192.

Hildreth, W., 2004. Volcanological perspectives on Long Valley, Mammoth Mountain, and Mono Craters: several contiguous but discrete systems. Journal of Volcanology and Geothermal Research 136 (3–4), 169–198.

Holloway, J.R., Burnham, C.W., 1972. Melting relations of basalt with equilibrium water pressure less than total pressure. Journal of Petrology 13, 1–29. doi:10.1093/petrology/13.1.1

Huang, H.H., Lin, F.C., Schmandt, B., Farrell, J., Smith, R.B., Tsai, V.C., 2015. The Yellowstone magmatic system from the mantle plume to the upper crust. Science 348(6236):773-776

Huber, C., Bachmann, O., Manga, M., 2009. Homogenization processes in silicic magma chambers by stirring and mushification (latent heat buffering). Earth and Planetary Science Letters, 283, 38–47.

Huber, C., Bachmann, O., Dufek, J., 2011. Thermo-mechanical reactivation of locked crystal mushes: Melting-induced internal fracturing and assimilation processes in magmas. Earth and Planetary Science Letters, 304, 443–454

Jagoutz, O., Schmidt, M.W., 2012. The formation and bulk composition of modern juvenile continental crust: The Kohistan arc. Chem Geol 298:79-96

Karakas, O., Degruyter, W., Bachmann, O., Dufek, J., 2017. Lifetime and size of shallow magma bodies controlled by crustal-scale magmatism. Nature Geosci 10(6):446-450

Kay, R.W., Mahlburg Kay, S., 1993. Delamination and delamination magmatism. Tectonophysics 219, 177–189.

Keays, R.R., 1995. The role of komatiitic and picritic magmatism and S-saturation in the formation of ore deposits. Lithos, 34(1-3), 1-18.

Kiser, E., Palomeras, I., Levander, A., Zelt, C., Harder, S., Schmandt, B., Hansen, S., Creager, K., Ulberg, C., 2016. Magma reservoirs from the upper crust to the Moho inferred from high-resolution Vp and Vs models beneath Mount St. Helens, Washington State, USA. Geology 44(6):411-414

Koyaguchi, T., Kaneko, K., 1999. A two-stage thermal evolution model of magmas in continental crust. Journal of Petrology 40 (2), 241–254.

Langmuir, C.H., 1989. Geochemical consequences of in situ crystallization. Nature, 340(6230), 199-205.

Lewis, J.F., 1973. Petrology of ejected plutonic blocks of Soufriere volcano, St. Vincent, West Indies. Journal of Petrology 14, 81–112.

Lipman, P.W., Bachmann, O., 2015. Ignimbrites to batholiths: Integrating perspectives from geological, geophysical, and geochronological data. Geosphere, 11.

Lipman, P.W., 1984. The roots of ash-flow calderas in western North America: windows into the tops of granitic batholiths. Journal of Geophysical Research 89 (B10), 8801–8841.

Marsh, B.D., 1989. Magma chambers. Annual Review of Earth and Planetary Sciences, 17, 439–474.

Marsh, B.D., 2002. On bimodal differentiation by solidification front instability in basaltic magmas, part 1: basic mechanics. Geochimica et Cosmochimica Acta, 66, 2211–2229.

Masotta, M., Freda, C., Gaeta, M., 2012. Origin of crystal-poor, differentiated magmas: insights from thermal gradient experiments. Contributions to Mineralogy and Petrology, 163(1), 49-65.

McKenzie, D., 1985. The extraction of magma from the crust and mantle. Earth and Planetary Science Letters, 74(1), 81-91.

Melekhova, E., Blundy, J., Robertson, R., Humphreys, M.C.S., 2015. Experimental evidence for polybaric differentiation of primitive arc basalt beneath St. Vincent, Lesser Antilles. Journal of Petrology 56, 161–192. doi:10.1093/petrology/egu074Miller and Miller, 2002;

Miller, C.F., Miller, J.S., 2002. Contrasting stratified plutons exposed in tilt blocks, Eldorado Mountains, Colorado River Rift, NV, USA. Lithos 61, 209–224.

Miller, C.F., Wark, D.A., 2008. Supervolcanoes and their explosive supereruptions. Elements, 4, 11–16.

Miller, C.F., Watson, E.B., Harrison, T.M., 1988. Perspectives on the source, segregation and transport of granitoid magmas. Transactions of the Royal Society of Edinburgh. Earth Sciences 79, 135–156.

Parmigiani, A., Huber, C., Bachmann, O., 2014. Mush microphysics and the reactivation of crystal-rich magma reservoirs. Journal of Geophysical Research: Solid Earth, 119, 6308–6322.

Parmigiani, A., Degruyter, W., Leclaire, S., Huber, C., Bachmann, O., 2017. The mechanics of shallow magma reservoir outgassing. Geochemistry, Geophysics, Geosystems.

Pedersen, A.K., 1979. Basaltic glass with high-temperature equilibrated immiscible sulphide bodies with native iron from Disko, central West Greenland. Contributions to Mineralogy and Petrology, 69(4), 397-407.

Pichavant, M., Macdonald, R., 2007. Crystallization of primitive basaltic magmas at crustal pressures and genesis of the calc-alkaline igneous suite: experimental evidence from St Vincent, Lesser Antilles arc. Contributions to Mineralogy and Petrology 154, 535–558. doi:10.1007/s00410-007-0208-6

Pinkerton, H., Norton, G.E., Dawson, J.B., Pyle, D.M., 1995. Carbonatite volcanism: Oldoinyo Lengai and the petrogenesis of natrocarbonatites. Springer-Verlag, Berlin.

Plank, T., Kelley, K.A., Zimmer, M.M., Hauri, E.H., Wallace, P.J., 2013. Why do mafic arc magmas contain ~ 4wt% water on average?. Earth and Planetary Science Letters, 364, 168-179.

Putirka, K.D., Canchola, J., Rash, J., Smith, O., Torrez, G., Paterson, S.R., Ducea, M.N., 2014. Pluton assembly and the genesis of granitic magmas: Insights from the GIC pluton in cross section, Sierra Nevada Batholith, California. Am Mineral 99(7):1284-1303

Quick, J.E., Sinigoi, S., Peressini, G., Demarchi, G., Wooden, J.L., Sbisa, A., 2009. Magmatic plumbing of a large Permian caldera exposed to a depth of 25 km. Geology 37(7):603-606

Rice, A. 1981. Convective fractionation: A mechanism to provide cryptic zoning (macrosegregation), layering, crescumulates, banded tufts and explosive volcanism in igneous processes. Journal of Geophysical Research, 86, 405-417.

Rudnick, R.L., 1995. Making continental crust. Nature 378, 571–578.

Schmitt, A.K., 2011. Uranium series accessory crystal dating of magmatic processes. Annu Rev Earth Pl Sc 39:321-349

Smith, D.J., 2014. Clinopyroxene precursors to amphibole sponge in arc crust. Nature Communications 5, 4329. doi:10.1038/ncomms5329

Sparks, R.S.J., Huppert, H.E., Turner, J.S., Sakuyama, M., O'Hara, M.J., 1984. The fluid dynamics of evolving magma chambers. Philosophical Transactions of the Royal Society of London A: Mathematical, Physical and Engineering Sciences, 310(1514), 511-534.

Stamper, C.C., Blundy, J.D., Arculus, R.J., Melekhova, E., 2014. Petrology of plutonic xenoliths and volcanic rocks from Grenada, Lesser Antilles. Journal of Petrology 55, 1353–1387. doi:10.1093/petrology/egu027

Streck, M. J., Leeman, W. P., Chesley, J., 2007. High-magnesian andesite from Mount Shasta: a product of magma mixing and contamination, not a primitive mantle melt. Geology 35, 351–354.

Ward, K.M., Zandt, G., Beck, S.L., Christensen, D.H., McFarlin, H., 2014. Seismic imaging of the magmatic underpinnings beneath the Altiplano-Puna volcanic complex from the joint inversion of surface wave dispersion and receiver functions. Earth and Planetary Science Letters, 404, 43–53.

Wilson, M., 1995. Magmatic differentiation. In: Le Bas, M.J. (Ed.), Milestones in Geology. Geological Society Memoirs, London.

Chapter 1

Petrological constraints on the high-Mg basalts from Capo Marargiu (Sardinia, Italy): evidences of cryptic amphibole fractionation in polybaric environments

Vanni Tecchiato[a], Mario Gaeta[a], Silvio Mollo[a], Piergiorgio Scarlato[b], Olivier Bachmann[c], Cristina Perinelli[a]

[a] Dipartimento di Scienze della Terra, Sapienza-Università di Roma, Piazzale Aldo Moro 5, 00185 Roma, Italy

[b] Istituto Nazionale di Geofisica e Vulcanologia, Via di Vigna Murata 605, 00143 Roma, Italy

[c] Institute of Geochemistry and Petrology, ETH Zürich, Clausiusstrasse 25, 8092 Zurich, Switzerland

Published in Journal of Volcanology and Geothermal Resource 349, 31-46.

Abstract

This study deals with the textural and compositional characteristics of the calc-alkaline stratigraphic sequence from Capo Marargiu Volcanic District (CMVD; Sardinia island, Italy). The area is dominated by basaltic to intermediate hypabyssal (dikes and sills) and volcanic rocks (lava flows and pyroclastic deposits) emplaced during the Oligo-Miocene orogenic magmatism of Sardinia. Interestingly, a basaltic andesitic dome hosts dark-grey, crystal-rich enclaves containing up ~50% of millimetre- to centimetre-sized clinopyroxene and amphibole crystals. This mineral assemblage is in equilibrium with a high-Mg basalt recognised as the parental magma of the entire stratigraphic succession at CMVD. Analogously, centimetre-sized clots of medium- and coarse-grained amphibole + plagioclase crystals are entrapped in andesitic dikes that ultimately intrude the stratigraphic sequence. Amphibole-plagioclase cosaturation occurs at equilibrium with a differentiated basaltic andesite. Major and trace element modelling indicates that the evolutionary path of magma is controlled by a two-step process driven by early olivine + clinopyroxene and late amphibole + plagioclase fractionation. In this context, enclaves represent parts of a cumulate horizon segregated at the early stage of differentiation of the precursory high-Mg basalt. This is denoted by i) resorption effects and sharp transitions between Mg-rich and Mg-poor clinopyroxenes, indicative of pervasive dissolution phenomena followed by crystal re-equilibration and overgrowth, and ii) reaction minerals found in amphibole coronas formed at the interface with more differentiated melts infiltrating within the cumulate horizon, and carrying the crystal-rich material with them upon eruption. Coherently, the mineral chemistry and phase relations of enclaves indicate crystallisation in a high-temperature, high-pressure environment under water-rich conditions. On the other hand, the upward migration and subsequent fractionation of the residual basaltic andesite in a shallower, colder, and hydrous region of the CMVD plumbing system lead to the formation of the amphibole-plagioclase crystal clots finally entrained by the andesitic dikes. Indeed, phenocrysts from these more evolved products record the final crystallisation path of magma during ascent towards the surface. Magma decompression and volatile loss cause the formation of amphibole reaction coronas and the crystallisation of a more sodic plagioclase in equilibrium with basaltic andesitic to andesitic melts. The bulk-rock geochemical signature of

these products testifies to open-system, polybaric magma dynamics, accounting for variable degrees of crustal assimilation of the Hercynian basement of Sardinia.

Keywords: Crystal-rich enclaves; High-Mg basalts; Cryptic amphibole fractionation; Crystal entrainment; Polybaric crystallisation; Sardinia magmatism.

1.1. Introduction

Differentiation of hydrous, mantle-derived basalts is a fundamental process to generate intermediate to SiO_2-rich products commonly erupted in continental and island arc settings. The stratigraphic architecture of the crust encountered by primary magma *en route* to surface dictates how and where differentiation acts. The most important density trap that primarily constrains cooling and crystallisation of primitive magmas is likely located at the mantle-crust transition (i.e., Mohorovičić discontinuity), where high pressure conditions may prevent water loss, thus promoting amphibole formation. Calc-alkaline melts extracted from such deep-seated crystal mushes typically inherit the geochemical signature of amphibole fractionation (i.e., trends of decreasing Dy/Yb and increasing La/Yb with SiO_2), reflecting leverage of this mineral on the behaviour of both trace (Rare Earth Elements) and major (SiO_2) elements during earlier stages of magmatic evolution (Davidson et al., 2007). Despite the intriguing paucity of this mineral as a major constituent in arc lavas (e.g., Tilley, 1950), a number of experimental works (Alonso-Perez et al., 2009; Cawthorn and O'Hara, 1976; Foden and Green, 1992; Green and Ringwood, 1968; Grove et al., 2003; Gust and Perfit, 1987; Holloway and Burnham, 1972; Melekhova et al., 2015; Pichavant and Macdonald, 2007) provide significant evidence that such a process "cryptically" occurs at the roots of volcanic arcs. Accordingly, large volumes of unerupted amphibole gabbros, diorites, tonalites, and amphibolites outcrop in exhumed deep crustal suites derived from subduction environments (Abd El-Rahman et al., 2012; Larocque and Canil, 2010; Best, 1975; Davidson et al., 2007; DeBari and Coleman, 1989; Dessimoz et al., 2012; Ducea and Saleeby, 1996; Lewis, 1973; Smith, 2014; Stamper et al., 2014; Yamamoto, 1984). Alternatively, portions of these plutonic rocks or individual amphibole megacrysts entrapped within erupted products provide textural and compositional information to qualitatively and quantitatively infer magmatic processes and intensive parameters of crystallisation at depth (Bachmann and Dungan, 2002; Chadwick et al., 2013; De Angelis et al., 2013; Shane and Smith, 2013; Turner et al., 2013).

Prior to eruption, buoyant high Al-basaltic, basaltic andesitic and andesitic melts (Melekhova et al., 2015; Pichavant and Macdonald, 2007) extracted from lower crustal mushes and ascending through the crust have more than one opportunity to be further stopped at variable depths, depending on how their

physical properties differ from those of country rocks (Gudmundsson, 2011). This can lead to complexly structured plumbing systems built by multiple magma chambers and reservoirs more or less interconnected to each other (e.g., Elsworth et al., 2008). In the shallower portions of these systems, the intermediate melts are subjected to additional steps of differentiation towards more evolved compositions (Lipman et al., 1978; Foden and Green, 1992; Dufek and Bachmann, 2010; Bachmann and Huber, 2016; Cashman et al., 2017). Residual cumulates fractionated at shallow levels are typically more siliceous than those segregated at higher depths, providing modal and chemical heterogeneities throughout the entire crustal cumulate pile (Dufek and Bachmann, 2010). Identifying the discrete mineral assemblages determining the multistage physicochemical evolution of arc series is fundamental for a correct interpretation of magmatic processes.

The Capo Marargiu Volcanic District (i.e., CMVD; Sardinia island, Italy) represents an interesting case of amphibole-driven polybaric differentiation from near-primary high-Mg basaltic to andesitic products. In this contribution, mineral textures and compositions of crystal-rich enclaves (up ~50% of millimetre- to centimetre-sized clinopyroxene and amphibole crystals) and amphibole-plagioclase crystal clots hosted in intermediate domes and dikes are used to (1) model major and trace element bulk-rock data, (2) estimate magma crystallisation conditions by comparing thermometric, barometric, hygrometric, and oxygen barometric data with phase relation diagrams.

1.2. Geological setting

Sardinia is one of the largest islands in the central-western Mediterranean region, at the subduction-collisional boundary between the European and the westward-subducted Ionian and Adria plates. In this geodynamic context, the Apennine-Maghrebide fold-and-thrust belt migrated from eastward to southward from the late Cretaceous (~80 Ma) and during the Cenozoic (Carminati et al., 2012; Lustrino et al., 2004, 2009). Afterwards, this migration was followed by back-arc stretching and boudinage of the European upper plate, driving the formation of a series of V-shaped basins and to the isolation of lithospheric ribbons in the middle of Central-Western Mediterranean area (Carminati et al., 2012, and references therein). Sardinia represents one of these lithospheric

ribbons rotated ~55-60° counter-clockwise away from the European paleo-margin during the Late Oligocene-Early Miocene (Cherchi et al., 2008; Dieni et al., 2008, and references therein). The rotation was the result of an initial stage of rifting and subsequent drifting, also accompanied by the widespread production of magmas with subduction fingerprint (Lustrino et al., 2013).

The orogenic magmatism ranged from ~38 to ~13 Ma (Late Eocene-Middle Miocene) with a productivity peak at ~22-18 Ma (Lustrino et al., 2009). Igneous rocks were almost exclusively erupted in a graben structure crossing the island from north to south, called the Fossa Sarda (Sardinian Trough). In particular, intense volcanism interested the Logudoro-Bosano domain (north-western Sardinia), where four eruptive sequences were identified: basal (or lower) andesitic series, lower ignimbritic series, upper andesitic series, and upper ignimbritic series (Coulon and Baque, 1973; Coulon et al., 1978; Deriu, 1964). The overall compositions of rocks in the Logudoro-Bosano domain span from basalt to rhyolite. The most primitive terms are high-Mg basalts from the Montresta locality, ~10 km northeast of Capo Marargiu area (Morra et al., 1997). From a geochemical point of view, the Montresta rocks evolve towards calc-alkaline basalts and high-K calc-alkaline basaltic andesites. The incompatible trace element variation denotes the typical subduction-related geochemical characteristics of arc magmas (e.g., Avanzinelli et al., 2009; Duggen et al., 2005; Lustrino et al., 2011). The faintly LREE-enriched and HREE-flattened chondrite-normalised patterns point to a spinel-bearing mantle source (Brotzu et al., 1997b; Franciosi et al., 2003; Lustrino et al., 2009; Morra et al., 1997). An important feature of the Logudoro–Bosano rocks is also represented by the variation of Nd-Sr isotopes relative to SiO_2, interpreted as either the effect of magma-crust interaction processes at shallow-levels (Morra et al., 1997; Franciosi et al., 2003; Lustrino et al., 2013), or the involvement of terrigenous subducted sediments/fluids in the mantle source (Franciosi et al., 2003; Lustrino et al., 2013). The CMVD is located at ~10 km south-westward of Montresta (Fig. 1a). Lecca et al. (1997) categorised the stratigraphic succession in andesitic domes, andesitic autoclastic and blocky lava flows (i.e., lower andesitic series), dikes, and welded ignimbrites. Geochronological studies conducted with the K-Ar method provided ages between 24 ± 1.2 Ma (Montigny et al., 1981) and 17.3-17.7 ± 0.4 Ma (Coulon et al., 1974) from the bottom (andesitic domes) to the top

(welded ignimbrites) of the Oligo-Miocene stratigraphic succession. The high-Mg basalts at Montresta have K–Ar ages of 18.5 ± 1.2 Ma (Montigny et al., 1981) comparable to those of products at the CMVD (Coulon et al., 1974; Montigny et al., 1981). At the end of magmatism, the volcanic edifice was eroded exposing hypabyssal and volcanic rocks from the shallowest part of the plumbing system.

1.3. Field characters and rock sampling

The fieldwork targeted the geological formations of the Capo Marargiu area previously described by other authors (cf. Deriu, 1964; Lecca et al., 1997). Lava domes are the main products, being usually in lateral contact with volcanic breccias. Locally, lava flows or stratified pyroclastic deposits are found. Dikes and sills are abundant and intrude both the domes and the volcanic breccias. All these rocks belong to the first (i.e., lower andesitic series) eruptive sequence described by Coulon et al. (1978). The shift from older volcanic to younger hypabyssal products testifies to the accretion of the volcanic edifice as a result of multiple eruptive episodes. The sampling focused on the coast of Cala Bernardu (Fig. 1b), where a cliff exposed the inner part of an andesitic dome hosting abundant crystal-rich enclaves (Fig. 1c). The dome appears as a yellowish, porphyritic rock with ~15% of phenocrysts. In contrast, the dark-grey enclaves are centimetre-to-metre-sized rounded blocks with ~50% of coarse-grained crystals (Fig. 1c). Some portions of the dome are also slightly darker and richer in crystals due to enclave disaggregation in the surrounding magma. Dikes intruding the andesitic dome are characterised by radial orientation variable thickness (0.3-2 m), and the occurrence of centimetre-sized clots of medium- and coarse-grained amphibole + plagioclase crystals.

For the purpose of this study, a total amount of twenty-eight rocks were collected and investigated for mineral and bulk-rock major elements. These rocks comprise seven samples for the enclaves, ten samples for the host dome, six samples for dikes, and five samples for the crystal clots (Tab. A1).

1.4. Analytical methods

Major element analyses of minerals (Tabs. A2-A6) were carried out with a Jeol-JXA8200 microprobe installed at the HPHT Laboratory of Experimental Volcanology and Geophysics of the Istituto Nazionale di Geofisica e Vulcanologia

(INGV) in Rome, Italy. The accelerating voltage and beam current were 15 kV and 10 nA, respectively. The beam size was 5 μm with a counting time of 20 and 10 s on peaks and background, respectively. The following standards have been adopted for the various chemical elements: jadeite (Si and Na), corundum (Al), forsterite (Mg), andradite (Fe), rutile (Ti), orthoclase (K), barite (Ba), apatite (P), spessartine (Mn) and chromite (Cr). Sodium and potassium were analysed first to prevent alkali migration effects. The precision of the microprobe was measured through the analysis of well-characterised synthetic oxides and minerals. Data quality was ensured by analysing these test materials as unknowns according to Iezzi et al. (2014).

Images were collected at the INGV using the backscattered electron (BSE) mode of a field emission gun-scanning electron microscopy (FE-SEM) Jeol 6500F equipped with an energy-dispersive spectrometer (EDS) detector.

Bulk-rock major element analyses (Tab. A7) were performed at Department of Earth Sciences, Sapienza University of Rome (Italy) by X-ray fluorescence (Philips PW1480/10). The organic material was removed by sample washing, i.e., soaking in a hot mixture of HCl and H_2O_2 and cleaning in acetone using ultrasound. Loss-on-ignition (LOI) was calculated by measuring the weight loss from 2 g of powdered sample after heating to 1050 °C for 2 h. Then, 1 g of the devolatilised sample powder was mixed with di-lithium tetraborate, melted in Pt crucibles at 1300 °C, and poured to form homogenous glassy beads. Matrix effects for major elements were corrected according to Franzini et al. (1972).

Bulk-rock trace element analyses (Tab. A7) were measured at Actlabs (Activation Laboratories Ltd.) by lithium metaborate/tetraborate fusion – ICP-MS (inductively coupled plasma mass spectrometry). The fused samples were diluted and analysed by a Perkin Elmer Sciex ELAN 9000 ICP/MS. Three blanks and five controls (three before sample group and two after) were analysed per group of samples.

1.5. Petrography and mineral chemistry

In this section, each rock type (i.e., enclaves, host dome, dikes, crystal clots) is described combining textural observations and mineral chemistry data (Figs. 1-4). Comparisons are also provided to point out the compositional difference of

the most abundant minerals (i.e., amphibole, plagioclase, and clinopyroxene) among the studied products (Figs. 3-4).

1.5.1. Enclaves

Enclaves are crystal-rich, porphyritic rocks (Fig. 1d) containing ~40-50% of coarse-grained (not univocally phenocrysts) clinopyroxene + amphibole + plagioclase + olivine + titanomagnetite/ilmenite ± Cr-spinel (in order of abundance). The millimetre-to-centimetre-sized minerals are dispersed in a microcrystalline groundmass of plagioclase + clinopyroxene + titanomagnetite ± low-Ca pyroxene. The most striking textural and compositional characteristics consist of the occurrence of two types of clinopyroxenes (Fig. 2):

- Type 1 clinopyroxenes appear as large crystal cores (> 1 mm) showing intense fracturing and disequilibrium dissolution features (Fig. 2a and 2b), i.e., sub-rounded edges, spongy cellular textures, and patchy zoning. The crystal composition is diopsidic (Wo_{41-48}-En_{40-50}-Fs_{5-14}; Morimoto, 1988) with Mg-number [$Mg\# = 100 \cdot Mg/(Mg + Fe_{tot})$] ranging from 75 to 91 (Tab. A2). Al_{tot} is negatively correlated with Mg# (Fig. 2d). Patchy zoning along cracks (Fig. 2a) and around the voids of spongy crystals (Fig. 2b) results when Type 1 clinopyroxenes are in the process of reaction with the surrounding melt feeding the growth of Type 2 clinopyroxenes;

- Type 2 clinopyroxenes occur either as thick (0.1 - 0.5 mm) crystal rims around Type 1 cores entrapping Usp_{20-40} titanomagnetite + An_{88-93} plagioclase ± altered olivine (Fig. 2a), or as millimetre-sized glomerocrysts together with the same plagioclases and titanomagnetites (Fig. 2c). The clinopyroxene composition is augitic (Wo_{41-45}-En_{42-45}-Fs_{12-16}; Tab. A2) with $Mg\#_{72-79}$ lower than that measured for Type 1. The concentration of Al_{tot} is generally low (0.211 - 0.230 apfu) and decoupled with respect to Mg# (Fig. 2d). Clinopyroxene microlites (≤30 µm) show the most evolved compositions, i.e., $Mg\#_{70-76}$ and Al_{tot} contents in the range of 0.057-0.208 apfu (Fig. 2d).

Amphibole consists of large crystals (from 1 to 20 mm in size; Fig. 3a) with dark, fine-grained (<5 µm) reaction rims including groundmass minerals of clinopyroxene + plagioclase + titanomagnetite/ ilmenite ± low-Ca pyroxene (Fig. 3b and 3c). These crystal rims may also develop on amphibole cores with spongy cellular textures (Fig. 3a) and the thickness of the reaction boundary is highly variable from 0.02 to 0.5 mm. According to the classification scheme of Leake et

al. (1997), the composition of amphibole is magnesiohastingsite (Tab. A3). The $Mg\#_{68-76}$ is also positively correlated with Al_{tot} (Fig. 3d), but most of the analytical dataset is restricted to a nearly constant value of Al_{tot} between 2.6 and 2.8 apfu. Generally, amphibole crystals including An_{72-93} plagioclase show the lowest values of Mg# (between 68 and 71) and Al_{tot} (between 2.2 and 2.6 apfu).

Plagioclase is found as either large, isolated crystals of a few millimetres in size, or small crystals entrapped in Type 2 clinopyroxenes (Fig. 2c) and, less frequently, in $Mg\#_{68-71}$ amphiboles. Plagioclase is characterised by continuous normal zoning with anorthite (An_{78-94}) content variable from core-to-rim (Fig. 4a; Tab. A4). Microlites are generally less calcic showing An_{72-88} compositions.

Olivine occurs as millimetre-sized crystals typically altered to secondary iddingsite and, for this reason, it is rarely analysable for mineral texture and composition. Normally zoned crystals show primitive cores characterised by forsterite (Fo) contents from 84 to 87, whereas the rims are more evolved with Fo_{75-79} (Tab. A5). The concentration of CaO (≤0.22 wt.%) is also inversely proportional to the forsterite component.

Titanomagnetite grains have maximum size of 0.5 mm and are frequently associated with Type 2 clinopyroxenes. The ulvöspinel (Usp) content ranges between 3 and 42 (Tab. A6).

Low-Ca pyroxene microlites are rare, showing Wo_{2-7}-En_{65-74}-Fs_{24-35} compositions and $Mg\#_{67-76}$ (Tab. A2).

Cr-spinel has been found only in one sample (i.e., CM42) and in association with the most primitive olivine (Fo_{87}). The chemical composition is Usp_{38} with Cr-number [Cr# = Cr/ (Cr + Al)] of 0.58.

1.5.2. Host dome

The host dome is porphyritic with plagioclase and clinopyroxene phenocrysts (≤15%) clashing abruptly with the plagioclase + clinopyroxene + low-Ca pyroxene + titanomagnetite groundmass.

Millimetre-sized (≤3 mm) plagioclase phenocrysts occur either as single, isolated crystals or as monomineralic glomerocrysts. Phenocrysts are characterised by normal zoning with An_{75-95} cores that are sharply overgrown by thin (20-30 µm) An_{45-71} rims (Fig. 4a; Tab. A4). Plagioclase microlites (≤0.05 mm) are euhedral and unzoned, showing An_{49-72} compositions comparable to those of

plagioclase rims. In spite of the extreme phenocryst-to-microlite variability of anorthite content (i.e., difference of ~45 mol.% of An), the FeO concentration of plagioclase stays almost constant around an average of ~0.6 wt.%.

Clinopyroxene phenocrysts are rare and frequently associated with titanomagnetite. The crystal size (≤1 mm) is usually smaller than that of plagioclase. Both clinopyroxene phenocrysts (Wo_{23-44}-En_{41-51}-Fs_{13-26}) and microlites (Wo_{36-42}-En_{38-44}-Fs_{15-20}) are augites showing almost homogeneous compositions with $Mg\#_{64-77}$ and Al_{tot} contents from 0.037 to 0.218 apfu (Fig. 4b). Low-Ca pyroxene is more abundant with respect to enclaves and its chemistry is Wo_{1-14}-En_{54-68}-Fs_{30-39} and $Mg\#_{60-69}$ (Tab. A2).

Titanomagnetite occurs as small, Usp_{10-50} crystals (Tab. A6).

Two samples (i.e., TG21C and B6) show an apparent high crystallinity (≤35%) caused by the mechanical disaggregation of the enclaves into the host dome. Clinopyroxene and amphibole xenocrysts are the most abundant minerals with textural evidences of disequilibrium with the host magma, and compositions identical to those documented for the enclaves. Clinopyroxene xenocrysts exhibit corroded Wo_{44-48}-En_{40-51}-Fs_{4-15} cores with $Mg\#_{71-93}$ and low Al_{tot} contents ranging from 0.062 to 0.383 apfu (Fig. 4b). These diopsidic cores are marked by the overgrowth of idiomorphic augitic rims with compositions (Wo_{39-47}-En_{39-46}-Fs_{10-20}, $Mg\#_{68-77}$, and Al_{tot} from 0.056 to 0.251 apfu) comparable to those of microlites in the groundmass (Fig. 4b). Amphiboles show thick (≤0.5 mm) reaction rims due to the occurrence of coarse-grained (0.05–0.1 mm) mineral associations of clinopyroxene + plagioclase + ilmenite. The composition of amphibole is prevalently magnesiohastingsite with $Mg\#_{69-74}$ and Al_{tot} contents ranging from 2.490 to 2.726 apfu (Tab. A3).

1.5.3. Dikes

Dike samples are fine-grained (≤0.5 mm), weakly porphyritic (<10% phenocrysts), and glomeroporphyritic rocks. The paragenesis consists of plagioclase + clinopyroxene + titanomagnetite, either as single phenocrysts or polymineralic glomerocrysts. The same mineral assemblage is found in the groundmass.

Plagioclase composition is relatively sodic, being An_{50-71} (Fig. 4a). Interestingly, its composition overlaps with that measured for both phenocryst

rims and microlites from host dome. Clinopyroxene is augite (Wo_{40-44}-En_{39-43}-Fs_{14-20}) with $Mg\#_{67-76}$ and low Al_{tot} concentrations (0.064 – 0.163 apfu), as observed for the most evolved microlites from enclaves and phenocrysts from host dome (Fig. 4b).

Titanomagnetite is Usp_{31-50} (Tab. A6).

The occurrence of secondary minerals testifies to post-magmatic hydrothermal alteration. Tiny crystals of calcite, chlorite, and quartz, are found to replace the small igneous crystals (likely pyroxenes) or filling voids and fractures.

1.5.4. Crystal clots

Medium-grained (millimetre-sized) to coarse-grained (centimetre-sized) gabbroic crystal clots of amphibole + plagioclase + titanomagnetite are hosted in dike rocks (Fig. 3).

Amphibole in the coarse-grained clots is subhedral to euhedral with size up 3 cm (Fig. 3e). Centimetre-sized amphiboles occur either as texturally homogeneous crystals (Fig. 3e), or as oikocrysts including An_{77-92} plagioclase + Usp_{15-58} titanomagnetite. Dark, thin (≤0.1 mm) reaction rims of micron-sized clinopyroxene + plagioclase + ilmenite + low-Ca pyroxene develop at the edges of amphibole crystals and in direct contact with the groundmass.

The composition of amphibole is magnesiohastingsite, but some crystals are also tschermakitic pargasite (Tab. A3). The $Mg\#_{60-73}$ is positively correlated with Al_{tot}, although the majority of data are restricted to Al_{tot} between 2.2 and 2.4 apfu (Fig. 3d). Notably, the centimetre-sized amphiboles show the most primitive compositions ($Mg\#_{70-73}$) and contain scarce mineral inclusions (Fig. 3e).

Plagioclase is subhedral with maximum size in the order of a few millimetres. The overall compositional variation is An_{77-92}. (Fig. 4a). Plagioclase abundance is exiguous in the coarse-grained clots (Fig. 3e), whereas it increases in the medium-grained samples up to levels comparable to the amphibole contents (Fig. 3f).

Small titanomagnetite crystals are Usp_{15-58} and their compositions resemble those from the host dome (Tab. A6).

1.6. Bulk-rock geochemistry

Bulk-rock data from this study are reported in Table A7, also in comparison with the calc-alkaline basalts and high-K calc-alkaline basaltic andesites from Montresta (cf. Morra et al., 1997). According to the TAS (total alkali vs. silica) classification scheme of Le Bas et al. (1986), rock samples are basalts, basaltic andesites, and andesites (Fig. 5) whose geochemical affinity shifts from calc-alkaline to high-K calc-alkaline (cf. Peccerillo and Taylor, 1976). Enclaves are high-Mg basalts (9.3–10.7 wt.% MgO and 46.0–48.6 wt.% SiO_2), whereas the host dome samples are basalts and basaltic andesites (3.8–6.5 wt.% MgO and 49.8–54.2 wt.% SiO_2). The most primitive host dome compositions (6.4–6.5 wt.% MgO and 49.8–52.4 wt.% SiO_2) are found for the high crystallinity samples (i.e., TG21C and B6) due to the mechanical disaggregation of enclaves into the basaltic andesitic host magma. Rationally, these compositions are outliers to the typical host dome chemistry, and their use is not contemplated for the following calculations (see below). Dikes are basaltic andesites to andesites (2.5–5.1 wt.% MgO and 52.9–60.9 wt.% SiO_2), except for the basaltic sample CM27 (4.9 wt.% MgO and 50.5 wt.% SiO_2) whose composition is affected by entrainment of abundant crystal clots.

From enclaves to host dome to dikes, SiO_2 (Fig. 6a) and Al_2O_3 (Fig. 6b) are negatively correlated with MgO. Conversely, Fe_2O_3 (Fig. 6c) and CaO (Fig. 6d) monotonically decrease with decreasing MgO, showing kinks at ~4-5 wt.% MgO. Notably, the concentration of Al_2O_3 slightly decreases in the more evolved andesites (≤4 wt.% MgO) due to the crystallisation of plagioclase (Fig. 6b).
Chondrite-normalised patterns (Fig. 7a) of Rare Earth Elements (REE) show enrichments in Light Rare Earth Elements (LREE) relative to Heavy Rare Earth Elements (HREE). From enclaves to host dome to dikes, the La_N/Lu_N ratio increases from 3.1 to 6.5 (Tab. A7). A more pronounced negative Eu anomaly is observed from primitive to more evolved rock types (Fig. 7a), whereas the Eu/Eu* ratio (i.e., $Eu_N/ [\sqrt{(Sm_N)} \times \sqrt{(Gd_N)}]$) decreases from 1.06 to 0.78.

Primitive mantle-normalised trace element patterns (Fig. 7b) show the typical geochemical characteristic of subduction-related rocks, consisting of variable enrichments in Large Ion Lithophile Elements (LILE; i.e., K, Rb, Sr, Ba, U, Th, and Pb) coupled with remarkable negative anomalies for some High Field Strength Elements (HFSE; i.e., Nb and Ta). Substantial enrichments of

incompatible trace elements are also observed from enclaves to dikes, except for Cs and Ti in dike rocks (Fig. 7b).

1.7. Discussion

1.7.1. Constraining the parental magma composition

By comparing the compositions of Mg-rich enclaves and the most primitive basalts from Sardinia, it is possible to identify the parental magma feeding the volcanic activity at CMVD. High-Mg basaltic rocks (MgO > 7 wt.%) are quite rare in the Sardinian orogenic area, exposed only in a few localities: i) Montresta and Capo Marargiu (i.e., CMVD) from the northern part of the island, and ii) Capo Frasca and Marmilla (cf. Lustrino et al., 2013), Arcuentu (cf. Brotzu et al., 1997b), and Villanovaforru (cf. Mattioli et al., 2000), from the southern part. Concerning the Montresta stratigraphic succession, Morra et al. (1997) categorised two types of basaltic products on the basis of their major element analyses (Fig. 5): 1) near-primary, mantle-derived high-Mg basalts (HMB), and 2) more differentiated high-Al basalts (HAB). In this context, enclaves, host dome, and dikes from this study are compositionally very similar to HMB, HAB, and basaltic andesites (BA) from Montresta (Figs. 5 and 6). However, Cr (186-338 ppm) and Ni (26-133 ppm) concentrations of enclaves are significantly lower than those (Cr = 186-739 ppm and Ni = 47-226 ppm) measured for HMB products. In turn, Sc (74-81 ppm) and V (457-470 ppm) contents of the former are 1.5–2 times higher than those (Sc = 42-51 ppm and V = 261-318 ppm) found in the latter. Chondrite-normalised REE and primordial mantle-normalised trace element patterns also denote compositional discrepancies between HMB products from Montresta and enclaves (Fig. 7). HMB products are clearly the most primitive rocks of the entire stratigraphic succession at CMVD (cf. Morra et al., 1997), especially for their extremely low concentrations of LREE (Fig. 7a) and incompatible trace element (mostly HFSE; Fig. 7b). In contrast, enclaves are plainly more similar to the more evolved HAB and BA products.

In this view, crystal-rich enclaves do not indeed represent the parental magma composition but rather a derivative melt from a primitive precursory crystallising primitive olivines (Fo_{84-87}), Type 1 clinopyroxenes ($Mg\#_{83-91}$), and Cr-spinel. Through the Fe-Mg exchange between olivine/clinopyroxene and melt, the composition of such primitive progenitor has been recalculated assuming

equilibrium exchange partition coefficients of $^{ol\text{-}melt}Kd_{Fe-Mg} = 0.30 \pm 0.03$ (Roeder and Emslie, 1970) and $^{cpx\text{-}melt}Kd_{Fe-Mg} = 0.27 \pm 0.03$ (Putirka et al., 2003). It is found that $Fo_{84\text{-}87}$ olivines and $Mg\#_{83\text{-}91}$ Type 1 clinopyroxenes from enclaves are, on average, in equilibrium with magmas ($Mg\#_{64\text{-}65}$) resembling the compositions ($Mg\#_{58\text{-}68}$) of HMB products erupted at Montresta. Therefore, the most primitive HMB rock is recognised as the parental magma at CMVD.

To confirm this hypothesis, mass balance calculations have been performed to quantify the degree of crystallisation driving the HMB magma towards BA and andesitic compositions. A two-step calculation approach has been adopted by subtracting 1) the enclave coarse-grained paragenesis (i.e., Fo_{86} olivine + $Mg\#_{87}$ Type 1 clinopyroxene + $Mg\#_{73}$ amphibole + An_{91} plagioclase + Usp_5 titanomagnetite) to the composition of HMB, and 2) the crystal clot paragenesis (i.e., $Mg\#_{67}$ amphibole + An_{90} plagioclase + Usp_{30} titanomagnetite) to the residual melt derived by step 1 (see details in Table A8). The MgO vs. TiO_2 diagram (Fig. 8) shows that enclave compositions cannot be reproduced by simple subtraction of minerals to the parental HMB magma, i.e., the sum of squared residuals (SSR) is higher than 1, denoting weak statistics for step 1. In contrast, the host dome composition is fairly reproduced (SSR = 0.44) by the crystallisation of olivine (~11%) + Type 1 clinopyroxene (~16%) + amphibole (~12%) + plagioclase (~11%) + titanomagnetite (~3%). In step 2 (Fig. 8), the dike composition is also adequately reconstructed (SSR = 0.13) by subtraction of amphibole (~23%) + plagioclase (~16%) + titanomagnetite (~3%). Results from mass balance calculations indicate that the segregation of primitive Type 1 clinopyroxene plays a major role at the early stage of HMB differentiation to form BA. On the contrary, the late crystallisation of $Mg\#_{67}$ amphibole + An_{90} plagioclase (i.e., the crystal clot paragenesis) drives the magmatic evolution from BA to andesites, accounting for the prevalent segregation of amphibole over plagioclase.

The negative correlation between Al_{tot} and Mg# observed for Type 1 clinopyroxene (Fig. 2d) is consistent with a progressive Al_2O_3 enrichment in the primitive magma crystallising clinopyroxene. Accordingly, this tendency is reflected by the increase of Al_2O_3 with decreasing MgO from HMB to BA (Fig. 6b), pointing to the early crystallisation of mafic minerals (i.e., clinopyroxene and olivine) with typically low Al_2O_3 concentrations rather than feldspar. The crystallisation of olivine also influences the early differentiation of HMB, in

agreement with the almost constant CaO content of magma when MgO varies between 7 and 12 wt.% (Fig. 6d). Moreover, the textural association of Fo-rich olivine + Cr-spinel suggests that this latter mineral cosaturated the melt at the onset of olivine crystallisation, before the formation of Type 1 clinopyroxene (cf. Morra et al., 1997).

Textural evidences point out that the crystallisation of primitive (~$Mg\#_{75}$) amphibole occurs at higher temperature than plagioclase. On one hand, centimetre-sized, $Mg\#_{68\text{-}71}$ amphiboles from enclaves, showing the lowest Al_{tot} concentrations (2.2-2.6 apfu; Fig. 3d), are observed to frequently entrap small $An_{72\text{-}93}$ plagioclase crystals. On the second hand, the more primitive ($Mg\#_{71\text{-}76}$) and Al-rich (Al_{tot} = 2.6-2.8 apfu) amphiboles do not exhibit mineral inclusions. Analogously, plagioclase inclusions are almost lacking in the more primitive ($Mg\#_{70\text{-}73}$) and Al-rich (Al_{tot} = 2.5-2.6 apfu) amphibole from the coarse-grained crystal clots (Fig. 3d, 3e), whereas feldspar abundance increases significantly in the medium-grained samples where more evolved amphiboles ($Mg\#_{60\text{-}69}$ and Al_{tot} = 2.2-2.5 apfu) crystallise (Fig. 3f). This leads to the conclusion that the crystallisation sequence of HMB products is Fo-rich olivine (± Cr-spinel) + primitive Type 1 clinopyroxene + high-Mg# amphibole + An-rich plagioclase. Olivine and Type 1 clinopyroxene control the early differentiation of magma, despite being not the only mineral phases to be crystallised during the HMB to BA evolution (step 1). Conversely, amphibole and plagioclase progressively dominate the latest stage of magma differentiation towards andesitic compositions (step 2). Assuming equilibrium crystallisation when $^{amp\text{-}melt}Kd_{Fe\text{–}Mg}$ = 0.34 ± 0.06 (cf. Li et al., 2017), the most primitive $Mg\#_{76}$ amphiboles from enclaves are effectively in equilibrium with the HAB magma (i.e., sample CM43 with $Mg\#_{52}$). On the contrary, the late formation of An-rich plagioclase is attested by the negative trajectory in the Al_2O_3 vs. MgO diagram (Fig. 6b); this is dictated by abundant feldspar fractionation in correspondence of the more differentiated (<$Mg\#_{50}$) BA and andesitic terms.

1.7.2. Trace element modelling

Due to the scarce sensitivity of major elements to open-system contamination phenomena, bulk-rock trace element modelling can more adequately clarify the geochemical evolution of CMVD products during interaction between magma and

crustal materials. Indeed, geochemical data for Montresta products indicate that crustal contamination plays a focal role in the evolution of magma (Franciosi et al., 2003; Morra et al., 1997). Coherently, Sr isotope ratios have been commonly observed to increase from basalts to andesites (Brotzu et al., 1997a; Dupuy et al., 1974; Lonis et al., 1997; Lustrino et al., 2013; Morra et al., 1997), suggesting that contamination phenomena take place within the middle-lower crust, at depths of 20-30 km (i.e., 500-700 MPa; Coulon et al., 1978 and Morra et al., 1994). Sr isotope ratios reported by Morra et al. (1997) increase from ~0.704 to ~0.706, along with variations in SiO_2 and incompatible trace elements from HMB to andesitic rocks. FC (fractional crystallisation) and AFC (assimilation and fractional crystallisation) modelling conducted by these authors denote that HMB magmas assimilated up to 13% of granitoid materials from the sialic lower crust ($^{87}Sr/^{86}Sr$ = ~0.715).

In this view, we have modelled the geochemical behaviour of transition elements (i.e., Cr and Ti), HFSE (i.e., Zr), and REE (i.e., La, Ce, Nd, Sm, Eu, Gd, Dy, Er, Yb and Lu) during FC and AFC processes at CMVD. According to the Rayleigh fractionation law, FC is expressed as:

$$C_l = C_0 \cdot F^{D-1}$$

where C_0 and C_l are, respectively, the concentrations of the trace element in parental liquid and melt remaining during fractional crystallisation. F is the melt fraction and D is the bulk partition coefficient of the element for the n-fractionating mineral phases, calculated as:

$$D = \sum_i^n x_i \cdot K_{D_i}$$

with x_i as the weight fraction of mineral phase *i* and K_{Di} as the partition coefficient of the element in mineral phase *i*. In turn, AFC is formulated after DePaolo (1981):

$$C_l = C_0 \cdot \left[F^{-z} + \left(\frac{r}{r-1}\right) \cdot \frac{C_a}{z \cdot C_0} \cdot (1 - F^{-z})\right]$$

with C_0, C_l, D, and F as above. C_a is the concentration of the element of interest in the contaminant (wall rock), whereas r is the mass ratio of assimilated to crystallised material. The value of *z* can be derived as:

$$z = \frac{r + D - 1}{r - 1}$$

Following the strategy designed for mass balance calculations, a two-step modelling approach is adopted. The most primitive basalt from HMB and the less differentiated basaltic andesite at CMVD are used as starting compositions. Two distinct vectors are calculated for step 1 and step 2, accounting for either prevalent fractionation of Fo-rich olivine + primitive Type 1 clinopyroxene (i.e., FC1 and AFC1), or $Mg\#_{67}$ amphibole + An_{90} plagioclase (i.e., FC2 and AFC2). The assimilant composition comes from Tommasini et al. (1995) and corresponds to the Hercynian granite from Sardinian-Corsan Batholith, as inferred by Brotzu et al. (1997a) and Conte (1997). Values for F and x_i are those recovered by mass balance calculations (Tab. A8). Input and output data concerning FC and AFC modelling are listed in Table A9, together with the values of partition coefficients specifically derived for calc-alkaline magmas (i.e., Bacon and Druitt, 1988; Dostal et al., 1983; Duke, 1976; Dunn and Sen, 1994; Forsythe et al., 1994; Frey, 1969; Fujimaki et al., 1984; Green et al., 1993; Irving and Frey, 1984; Jones and Drake, 1986; Klöck and Palme, 1988; Luhr and Carmichael, 1980; McKay and Weill, 1976; McKay et al., 1994; Oberti et al., 2000; Okamoto, 1979; Reid, 1983; Skulski et al., 1994; Villemant et al., 1981).

The Y vs. Cr diagram (Fig. 9) shows that, after ~53% of mineral segregation, FC and AFC vectors from step 1 and step 2 virtually overlap. The residual melt composition changes slightly under the effect of fractional crystallisation (Y ≈ 32 ppm and Cr ≈ 0.4 ppm) and country rock assimilation (Y ≈ 33 ppm and Cr ≈ 0.2 ppm). The evolutionary trajectories evidence as HMB products are mostly dominated by fractionation of mafic minerals (i.e., FC1 and AFC1), whereas the differentiation of basaltic andesites to andesites proceeds by $Mg\#_{67}$ amphibole and An_{90} plagioclase saturation (i.e., FC2 and AFC2; Fig. 9). In terms of LREE vs. HFSE ratios (Fig. 10a), the FC1 vector cannot reproduce in full the transition from HMB magmas to basaltic andesites. This geochemical evolution is captured only by the AFC1 vector when the ratio of the assimilation rate to the crystallisation rate (i.e., r = 0.16) is close to the degree of assimilation derived by Morra et al. (1997). On the other hand, both FC2 and AFC2 trajectories describe plausible differentiation paths for the basaltic andesitic magmas (Fig. 10a). The AFC2 vector denotes lower degrees of contamination (i.e., r = 0.1) for the more differentiated melts, perhaps responding to the colder thermal regime of the system (cf. Bohrson and Spera, 2001). The same conclusion applies to the

behaviour of REE (Fig. 10b). The crustal contribution is more effective during step 1, producing remarkable LREE enrichments in the basaltic andesitic melt.

The role played by crustal assimilation during the geochemical evolution of magma is also documented by Sr isotope data for Montresta products (Fig. 11a). Modelling results (Tab. A10) based on the formalism of DePaolo (1981) indicate that the parental HMB magma ($^{87}Sr/^{86}Sr$ = 0.7039) differentiated towards the andesitic rocks ($^{87}Sr/^{86}Sr$ = 0.7062-0.7068) by assimilation of the Hercynian crust ($^{87}Sr/^{86}Sr$ = 0.732). To estimate the maximum degree of assimilation, the energy-constrained assimilation–fractional crystallisation (EC-AFC) formulation of Spera and Bohrson (2001) has been used (Fig. 11b). This model builds on previous treatments of open-system processes (e.g., DePaolo, 1981) but it also considers the mass, chemical, and thermal properties of a magma body, as well as the energy conservation and country rock partial melting. According to Bohrson and Spera (2001), the input parameters for the granitic country rock are solidus (675 °C) and liquidus (950 °C) of the assimilant with isobaric specific heat capacity of 1388 J kg^{-1} K^{-1}, whereas those of magma are the liquidus temperature (1250 °C) and isobaric specific heat capacity of 1555 J kg^{-1} K^{-1}. The mass of fractionated material is much higher than that of crustal rock assimilated, causing that the highest $^{87}Sr/^{86}Sr$ ratio measured for HMB products is related to a maximum crustal assimilation of 10% and fractional crystallisation of 55% (Fig. 11b). Both these derived values conform to (i) the high radiogenic nature of the Hercynian basement of Sardinia island (Di Vincenzo et al., 1996), (ii) the trace element patterns of CMVD rocks (Fig. 10), and (iii) the review study of Lustrino et al. (2013) denoting as the degree of assimilation cannot exceeds the value of ~20% during interaction between primitive Sardinian basalts and Hercynian basement.

1.7.3. Origin of enclaves

Textural (Figs. 2 and 3), mineralogical (Fig. 4), and geochemical (Figs. 7 and 8) data point out that the formation of enclaves is controlled by evolutionary mechanisms rather different from those driving the petrogenesis of basaltic andesitic and andesitic rocks. Importantly, the overgrowth of Type 2 clinopyroxene rims on early-formed Type 1 cores (Fig. 2a) evidences open-system magma dynamics ascribable to entrainment of early-formed crystals in a compositionally distinct melt (Dungan and Davidson, 2004; Streck, 2008; Streck

et al., 2007). Sharp transitions from Mg-rich (Type 1) to Mg-poor (Type 2) mineral portions (Figs. 2a) and resorption textures forming patchy zoning (Fig. 2b) are both the effect of pervasive dissolution phenomena followed by crystal re-equilibration (Streck, 2008). Reaction minerals in amphibole coronas (i.e., clinopyroxene + plagioclase + titanomagnetite/ilmenite ± low-Ca pyroxene; Fig. 3c) developed at the interface with a more differentiated magma that, in turn, underwent abundant groundmass crystallisation at the time of eruption. Additionally, HAB products and enclaves share a common trace element signature (Fig. 7) indicative of cogenetic origin. In this framework, it is argued that enclaves represent the crystal-rich portion of a volatile-rich, basaltic magma stored at depth and in equilibrium with Type 1 clinopyroxene and $Mg\#_{73\text{-}75}$ amphibole (cf. Stamper et al., 2014). Conversely, the sharp textural discontinuity between Type 1 and Type 2 clinopyroxenes denotes the injection of a compositionally distinct magma (Fig. 2a). Field and petrographic characters of the host dome evidence that the basaltic andesitic melt infiltrated, disaggregated and reacted within the cumulate horizon, feeding the overgrowth of Type 2 clinopyroxene rims onto Type 1 cores (Fig. 1c). The dome formation is indeed petrogenetically related to the emplacement of a more differentiated melt carrying crystal-rich enclaves. During magma ascent, rapid decompression and volatile loss may have caused the progress of amphibole reaction coronas (e.g., De Angelis et al., 2015) and the crystallisation of a more sodic plagioclase in equilibrium with basaltic andesitic to andesitic melts (e.g. Frey and Lange, 2011). According to Ruprecht and Worner (2007), the abrupt shifts in the anorthite component associated to almost constant iron concentrations are consistent with crystallisation under variable temperature and/or partial pressure of H_2O upon magma ascent in the volcanic conduit. In this context, the compositional trend observed for plagioclase from host dome (from An_{90} phenocryst cores to An_{45} microlites with ~0.6 wt.% FeO) may effectively result from a higher efficacy of decompression-induced degassing (e.g., Blundy and Cashman, 2001) rather than heating during ascent-driven crystallisation and latent heat release (Blundy et al, 2006).

On this basis, the least square method has been used to model the composition of the enclaves by entrainment of Fo_{86} olivine + $Mg\#_{87}$ Type 1 clinopyroxene + $Mg\#_{73}$ amphibole + An_{91} plagioclase + Usp_5 titanomagnetite in

the basaltic andesitic host dome. The mineral compositions adopted for the calculation correspond to those previously used to model magma fractional crystallisation (step 1; Tab. A8). Modelling data confirm that the enclave compositions are well reproduced (SSR = 0.02-0.04) by addition of olivine (3-4%), Type 1 clinopyroxene (20-21%), amphibole (20-21%), plagioclase (5-6%) and titanomagnetite (2-3%) to the basaltic andesitic magma (Fig. 8). In terms of trace element contents, Sc (74-81 ppm) and V (457-474 ppm) measured for the enclaves are intriguingly higher than transition elements typically measured for Island Arc Basalts (i.e., IAB with Sc ≤ 55 ppm and V ≤ 450 ppm; cf. Doe, 1997). The high compatibility of scandium in clinopyroxene and amphibole is controlled by its ionic radius (74.5 pm in six-fold coordination) and electronegativity (1.36 from the Pauling's scale) that are both very similar to those (72 pm and 1.31, respectively) of magnesium (Iain and Chassé, 2016). The geochemical behaviour of vanadium resembles that of scandium, despite the fact that vanadium can be more favourably incorporated in Mg-rich amphiboles due to the crystal-chemical control effect on trace element partitioning (Meurer and Claeson, 2002). Consequently, partition coefficients of Sc and V for clinopyroxene (K_{Sc} = 2.5 and K_V = 2.3; Dale and Henderson, 1972 and Duke, 1976), amphibole (K_{Sc} = 4 and K_V = 1.49; Sisson, 1994), and titanomagnetite (K_{Sc} = 3,3 and K_V = 6.8; Luhr and Carmichael, 1980 and Nielsen, 1992) are much higher than those measured for olivine (K_{Sc} = 0.3 and K_V = 0.08; Luhr and Carmichael, 1980 and Duke, 1976) and plagioclase (K_{Sc} = 0.02 and K_V = 0.02; Luhr and Carmichael, 1980 and Dunn and Sen, 1994). Eluding the low solid fraction of titanomagnetite, the entrainment of Type 1 clinopyroxene and amphibole within the basaltic andesitic melt can be described by the following mixing expression:

$$C_m = X \cdot (C_s - C_{BA}) + C_{BA}$$

where C_s, C_{BA}, and C_m are the concentrations of the cumulate horizon, the basaltic andesite, and the final hybrid rock, whereas X is the degree of mixing. The concentrations of V and Sc in Type 1 clinopyroxene and amphibole crystals come from equilibrium partitioning calculations performed on HMB (sample KB24) and HAB (sample CM43) compositions (further details are given in Table A11). The V vs. Sc diagram (Fig. 12) shows that enclaves lie on a mixing trajectory resulting from entrainment of Type 1 clinopyroxene (51%) and amphibole (49%) in the basaltic andesitic magma (note that the mineral content

come from mass balance data normalised to 100). Through the same approach, modelling calculations for REE attest that enclave compositions result from hybridisation phenomena due to the entrainment of a pre-existing crystal cargo (50-60%) of Type 1 clinopyroxene + $Mg\#_{71-76}$ amphibole into the original basaltic andesitic magma (Fig. 13).

1.7.4. Magma crystallisation conditions

To retrieve the intensive variable of the magmatic system during evolution of HMB towards more differentiated basaltic andesites and andesites, phase equilibrium experiments of Grove et al., (2003), Pichavant and Macdonald (2007), and Melekhova et al. (2015) have been compared with the mineral assemblage of natural products from the CMVD. The compositions investigated by these authors consists of high-Mg basalts to andesites equilibrated at P = 0.1-1500 MPa, T = 940-1350 °C, H_2O = 0-8 wt.% (from anhydrous to $P_{tot} = P_{H2O}$), and fO_2 = QFM-NNO+4. Results show that, at P > 400 MPa and H_2O > 2 wt.%, the stability field of both olivine and clinopyroxene expands at the expense of plagioclase (Fig. 14). Under such circumstances, the crystallisation of 30-40% of mafic minerals (cf. Pichavant and Macdonald, 2007) drives the residual melt towards compositions comparable to those observed for HAB and basaltic andesitic products from the CMVD (Figs. 5 and 6). At 400 MPa, 1000-1025 °C, 5-6 wt.% H_2O, and NNO-0.8-NNO+2.4 buffer, Pichavant and Macdonald (2007) found that amphibole equilibrates with high-Mg basaltic melts, after segregation of olivine + Cr-spinel + clinopyroxene + plagioclase. In contrast, the same authors document that, at 1000 MPa, 1044 °C, 9.4 wt.% H_2O, and NNO+2, amphibole occurs as the liquidus phase when the crystallisation of plagioclase is suppressed. As a rule, at P >400 MPa, T > 1030 °C, H_2O > 4.5 wt.%, and fO_2 > NNO, amphibole saturates the primitive basaltic liquid after the crystallisation of olivine, Cr-spinel, and clinopyroxene (Fig. 14) but, importantly, its appearance precedes the onset of plagioclase crystallisation (Grove et al., 2003; Melekhova et al., 2015; Pichavant and Macdonald, 2007). The chemistry of experimental amphiboles ($Mg\#_{72-79}$) is also very similar to that ($Mg\#_{71-76}$) of natural minerals from enclaves, providing further constraints on the formation of amphibole at high pressures, temperatures and melt-water contents (cf. Grove et al., 2003; Melekhova et al., 2015).

In this framework, barometric, thermometric, hygrometric, and oxygen barometric equations have been used to model the *P*-*T*-H_2O-fO_2 path of the system during the differentiation of HMB magmas towards more evolved basaltic andesitic and andesitic terms. The redox state of enclaves, crystal clots, host dome, and dikes has been measured through the equations of Ariskin and Nikolaev (1996), France et al. (2010), and Ridolfi et al. (2010) based on spinel-melt (error of ±0.3 log unit), clinopyroxene-plagioclase (error of ±0.5 log unit), and amphibole-melt equilibria (error of ±0.4 log unit), respectively. The input pressures and temperatures for these models have been obtained with the independent barometric and thermometric equations described below. Results from calculations are plotted in Fig. 15a showing that, within the calibration error of each model, the oxygen fugacity of the system is constrained between NNO and NNO+2, with the majority of the estimates pointing to NNO+1. This value is consistent with previous data obtained using ilmenite-magnetite pairs from the groundmass of HMB products at Montresta (Morra et al., 1997), as well as with the more oxidised conditions commonly encountered for the subduction-related magmatism (cf. Scarlato et al., 2017).

The amount of H_2O in equilibrium with plagioclase has been determined through the Ca-Na exchange experimentally-derived by Sisson and Grove (1993) for calc-alkaline systems. Despite the anorthite content of plagioclase is positively correlated with H_2O and temperature, the value of $^{pl\text{-}melt}Kd_{Ca–Na}$ is a proxy for the amount of H_2O dissolved in the melt (i.e., P-T independent hygrometer), provided that the effects of temperature and pressure are negligible for the equilibrium Ca-Na exchange (cf. Ushioda et al., 2014). $^{pl\text{-}melt}Kd_{Ca–Na}$ values (3.4-5.5) measured in this study evidence that An-rich plagioclases from enclaves and host dome equilibrated with a basaltic andesitic melt characterised by relatively high H_2O contents ranging from 4 to 6 wt.% (Fig. 15b). This is also confirmed by the incorporation of octahedral aluminium in amphiboles from enclaves and crystal clots, translating to H_2O contents of 5.6-7.9 wt.% (error of ±0.41 wt.% H_2O), as predicted by the amphibole-based hygrometer of Ridolfi et al. (2010). In contrast, the more sodic plagioclase rims formed at the final stage of crystallisation (i.e., $^{pl\text{-}melt}Kd_{Ca–Na}$ = 1.7-3.4), recording the lower H_2O concentrations (2-4 wt.%) ultimately dissolved in host dome and dike andesitic magmas (Fig. 15b).

The crystallisation temperature of Fo_{84-87} olivines from enclaves has been estimated with the thermometer of Putirka et al. (2007) based on the partitioning of magnesium between forsterite and melt (error of ±29 °C). This model returns mineral saturation at 1176-1178 °C (Fig. 15c), in agreement with the stability field of olivine (1100-1220 °C) obtained in laboratory by Pichavant and Macdonald (2007) and Melekhova et al. (2015) at 400-700 MPa and 4.5 wt.% H_2O (Fig. 14). The crystallisation pressure of clinopyroxene has been calculated with the recent *T*-dependent barometer (error of ±140 MPa) of Neave and Putirka (2017), referring to the pressure-sensitive incorporation of jadeite. This model has been integrated with the *P*-independent thermometer (error of ±27 °C) of Putirka (1996) that, in turn, depends on the diopside-hedenbergite exchange.

The compositions of clinopyroxenes have been tested for equilibrium using the equation of Mollo et al. (2013) based on the difference (Δ) between diopside + hedenbergite (DiHd) components predicted for clinopyroxene via regression analysis of clinopyroxene-melt pairs in equilibrium conditions, and those measured in the analysed crystals. For the specific case of rocks with calc-alkaline affinity, phase equilibrium experiments indicate that near-equilibrium crystallisation conditions are achieved when the value of ΔDiHd is lower than 0.1 (Mollo et al., 2012). Type 1 clinopyroxenes ($Mg\#_{83-91}$) from enclaves yield pressures of 514-661 MPa and temperatures of 1111-1136 °C (Fig. 15c), in agreement with data from Pichavant and Macdonald (2007) and Melekhova et al. (2015) (Fig. 14). Type 2 clinopyroxenes ($Mg\#_{72-79}$) denote intermediate crystallisation conditions (i.e., 100-410 MPa and 1057-1086 °C) corresponding to the ascent of magma towards the surface. Conversely, the final closure temperature (1050-1085 °C) of the system is recorded by the more evolved clinopyroxenes ($Mg\#_{65-77}$) from host dome and dikes that, virtually, formed at the time of magma emplacement (0.1-280 MPa).

The crystallisation conditions of plagioclase have been constrained with the H_2O-dependent model of Putirka (2005) with errors of ±240 MPa and ±26 °C for pressure and temperature, respectively. The amount of H_2O in equilibrium with plagioclase has been modulated according to values recovered by the Ca-Na exchange reaction (Fig. 15b). However, we have established that a H_2O change of ±2 wt.% produces temperature and pressures variations of only ±12 °C and ±15MPa, which are well below the errors of estimates of the model.

The empirical formulations of Ridolfi et al. (2010) and Ridolfi and Renzulli (2012) have been adopted to retrieve, respectively, the saturation temperature (error of ±22 °C) and pressure (error of ±37 MPa) of amphibole. For the specific case of crystal clots, consistently with the petrography of these rocks, the barometer (error of ±150 MPa) of Molina et al. (2015) based on Al-Si partitioning between amphibole and plagioclase has been employed. Coherently with the textural characteristics of enclaves (Figs. 1d, 3a and 3b), these calculations suggest the early crystallisation of $Mg\#_{71\text{-}76}$ amphibole (978-1088 °C) respect to An-rich plagioclase (1031-1048 °C), at pressures of 355-713 MPa (Fig. 15c). On the other hand, the more evolved amphibole ($Mg\#_{60\text{-}69}$) from crystal clots (Figs. 3e and 3f) is in cosaturation with An_{90} plagioclase at lower temperatures and pressures (i.e., 962-1060 °C and 145-427 MPa; Fig. 15c). Nonetheless, the more sodic plagioclase crystals from host dome and dikes equilibrated at the last stage of eruption (Fig. 15c) in a more degassed magma ascending along the uppermost part of the volcanic conduit (i.e., 0.1-16 MPa and 1017-1027 °C). Similarly, the two-pyroxene model of Putirka (2008) suggests near-equilibrium crystallisation (i.e., $^{cpx\text{-}opx}Kd_{Fe\text{–}Mg}$ = 1.09±0.14) for low-Ca pyroxenes and augites in the host dome groundmass, providing information on the final quenching temperature during lava flowage onto the surface (i.e., 961-970 °C with error of ±38 °C).

Enclaves are interpreted as the cumulate assemblage of a high-temperature, water-rich magma stored at depth with composition close to that of HMB products (Fig. 15c). The segregation of mafic crystals at relatively high crustal pressures has been documented for basaltic rocks from Montresta (>500 MPa; Morra et al., 1997), as well as for the more differentiated products outcropping at both the northern and southern parts of Sardinia (500-700 MPa; Coulon et al., 1978 and Morra et al., 1994). In this scenario, the enclaves formed prevalently by Fo-rich olivine + primitive Type 1 clinopyroxene + high-Mg# amphibole accumulation and, minor An-rich plagioclase + titanomagnetite fractionation. Similarly, crystal clots represent the solid fractionated by a colder, hydrous basaltic andesite in a shallower region of the CMVD plumbing system, where the simultaneous precipitation of more evolved amphibole and An-rich plagioclase was favoured. These two gabbroid assemblages may therefore be ascribed to different portions of the polybaric crystal mush formed during the multi-stage HMB to basaltic andesitic to andesitic differentiation (e.g. Cashman et al., 2017; Chadwick et al.,

2013; Deering et al., 2011; Dufek and Bachmann, 2010). The stable paragenesis of infiltrating basaltic andesite consists of Type 2 clinopyroxene + An_{88-93} plagioclase + titanomagnetite, followed by late groundmass crystallisation at the time of eruption. Type 2 clinopyroxenes are euhedral and compositionally homogeneous (Fig. 2c), in sharp contrast with the pervasive dissolution phenomena forming the spongy cellular texture of Type 1 crystals (Fig. 2b). Moreover, augitic Type 2 clinopyroxenes ($Mg\#_{72-79}$ and Al_{tot} = 0.211-0.230 apfu) are comparatively more evolved than diopsidic Type 1 clinopyroxenes (Fig. 2d), accounting for magma dynamics controlled by progressive melt evolution and crystal entrainment. Therefore, enclaves and crystal clots were entrapped by cogenetic magmas formed from the same HMB progenitor, as attested by modelling data (Figs. 8, 9, and 10) and the strong correlation coefficients (R^2 = 0.86-0.96) measured for the incompatible trace element ratios (e.g., La/Ce = 0.41-0.53 and Zr/Hf = 30-46).

1.8. Conclusions

This study focused on better understanding the textural and compositional characteristics of crystal-rich enclaves sampled from an andesitic dome outcropping at the Capo Marargiu Volcanic District (Sardinia island, Italy). Based on petrological and geochemical evidence, the following conclusions can be drawn:

1) enclaves formed during crystallisation of high-Mg basalts with trace element patterns resembling those of more differentiated basaltic andesitic to andesitic products found in the same stratigraphic succession;
2) diopsidic clinopyroxene and high-Mg# amphibole from enclaves show strong disequilibrium textures caused by entrainment in magmas that, subsequently, underwent decompression and volatile loss;
3) the mineral chemistry of enclaves reflects crystallisation in a high-temperature, high-pressure environment under water-rich conditions. In contrast, low-Mg# amphibole and An-rich plagioclase cosaturation recorded by crystal clots in andesites indicate crystallisation under hydrous conditions in a colder and shallower region of the plumbing system. In the end, phenocryst compositions from the more differentiated products constrain the final *P*-*T*-H_2O path of magma during ascent towards the surface.

4) enclaves and crystal clots represent different portions of a polybaric mush column formed during the two-step HMB to basaltic andesitic to andesitic differentiation. In particular, enclaves are the “cryptic” solid fraction of a cumulate horizon segregated from the deep-seated crystallisation of parental magma driven by Fo_{87} olivine + $Mg\#_{90}$ clinopyroxene, whereas crystal clots belong to the cumulate removed during the shallow fractionation of $Mg\#_{65}$ amphibole + An_{90} plagioclase from the basaltic andesite extracted at depth;
5) the geochemical signature of basalts, basaltic andesites, and andesites at Capo Marargiu Volcanic District has been also influenced by variable degrees of crustal assimilation involving the Hercynian granitic basement, with the highest contamination during the early evolutionary stage of parental magma in proximity of the Moho.

Acknowledgements

We gratefully acknowledge Joan Andújar and an anonymous reviewer for their useful and constructive criticisms. The authors thank also J. Marti for his valuable editorial guidance. V.T. is grateful to F. Forni, A. Parmigiani (tetris), and J. Leuthold for their suggestions during the preparation of the manuscript. M. Nazzari is acknowledged for assistance during electron microprobe analysis. The authors are grateful to V. Piras for the logistic support on the field. This work was supported by the Sapienza - Università di Roma doctoral scholarship.

References

Abd El-Rahman, Y., Helmy, H.M., Shibata, T., Yoshikawa, M., Arai, S., Tamura, A., 2012. Mineral chemistry of the Neoproterozoic Alaskan-type Akarem Intrusion with special emphasis on amphibole: implications for the pluton origin and evolution of subduction-related magma. Lithos 155, 410–425. doi:10.1016/j.lithos.2012.09.015

Alonso-Perez, R., Müntener, O., Ulmer, P., 2009. Igneous garnet and amphibole fractionation in the roots of island arcs: experimental constraints on andesitic liquids. Contributions to Mineralogy and Petrology 157, 541–558. doi:10.1007/s00410-008-0351-8

Ariskin, A.A., Nikolaev, G.S., 1996. An empirical model for the calculation of spinel-melt equilibria in mafic igneous systems at atmospheric pressure: 1. Chromian spinels. Contributions to Mineralogy and Petrology 123, 282–292. doi:10.1007/s004100050156

Avanzinelli, R., Lustrino, M., Mattei, M., Melluso, L., Conticelli, S., 2009. Potassic and ultrapotassic magmatism in the circum-Tyrrhenian region: Significance of carbonated pelitic vs. pelitic sediment recycling at destructive plate margins. Lithos 113, 213–227. doi:10.1016/j.lithos.2009.03.029

Bachmann, O., Dungan, M. A., 2002. Temperature-induced Al-zoning in hornblendes of the Fish Canyon magma, Colorado. American Mineralogist 87, 1062–1076.

Bachmann, O., Huber, C., 2016. Silicic magma reservoirs in the Earth's crust. American Mineralogist 101, 2377–2404.

Bacon, C.R., Druitt, T.H., 1988. Compositional evolution of the zoned calcalkaline magma chamber of Mount Mazama, Crater Lake, Oregon. Contributions to Mineralogy and Petrology 98, 224–256. doi:10.1007/BF00402114

Best, M.G., 1975. Amphibole bearing cumulate inclusions, Grand Canyon, Arizona, and their bearing on silica undersaturated hydrous magma in the upper mantle. Journal of Petrology 16, 212–236.

Blundy, J., Cashman, 2001. Ascent-driven crystallization of dacite magmas at Mount St Helens, 1980-1986. Contributions to Mineralogy and Petrology 140, 631–650.

Blundy, J., Cashman, K., Humphreys, M., 2006. Magma heating by decompression-driven crystallization beneath andesite volcanoes. Nature 443, 76–80.

Bohrson, W.A., Spera, F.J., 2001. Energy-constrained open-system magmatic processes II: Application of energy-constrained assimilation-fractional crystallization (EC-AFC) model to magmatic systems. Journal of Petrology 42, 1019–1041. doi:10.1093/petrology/42.5.1019

Brotzu, P., Callegari, E., Morra, V., Ruffini, R., 1997a. The orogenic basalt-andesite suites from the Tertiary volcanic complex of Narcao, SW-Sardinia (Italy):

petrology, geochemistry and Sr-isotope characteristics. Periodico di Mineralogia 66, 101–150.

Brotzu, P., Lonis, R., Melluso, L., Morbidelli, L., Traversa, G., Franciosi, L., 1997b. Petrology and evolution of calcalkaline magmas from the Arcuentu volcanic complex (SW Sardinia, Italy). Periodico di Mineralogia 66, 151–184.

Carminati, E., Lustrino, M., Doglioni, C., 2012. Geodynamic evolution of the central and western Mediterranean: Tectonics vs. igneous petrology constraints. Tectonophysics 579, 173–192. doi:10.1016/j.tecto.2012.01.026

Cashman, K. V., Sparks, R. S. J., Blundy, J. D., 2017. Vertically extensive and unstable magmatic systems: a unified view of igneous processes. Science 355, eaag3055.

Cawthorn, R.G., O'Hara, M.J., 1976. Amphibole fractionation in calc-alkaline magma genesis. American Journal of Science 276, 309-329. doi:10.2475/ajs.276.3.309

Chadwick, J. P., Troll, V. R., Waight, T. E., Van Der Zwan, F. M., Schwarzkopf, L. M., 2013. Petrology and geochemistry of igneous inclusions in recent Merapi deposits: a window into the sub-volcanic plumbing system. Contributions to Mineralogy and Petrology 165, 259–282.

Cherchi, A., Mancin, N., Montadert, L., Murru, M., Putzu, M.T., Schiavinotto, F., Verrubbi, V., 2008. The stratigraphic response to the Oligo-Miocene extension in the western Mediterranean from observations on the Sardinia graben system (Italy). Bulletin de la Société Géologique de France 179, 267–287.

Conte, A., 1997. Petrology and geochemistry of Tertiary calcalkaline magmatic rocks from the Sarroch district (Sardinia, Italy). Periodico di Mineralogia 66, 63–100.

Coulon, C., Baque, L., 1973. Les andésites cénozoiques et les laves associées en Sardaigne Nord-Occidentale (Provinces du Logudoro et du Bosano) - Caractères minéralogiques et chimiques. Contributions to Mineralogy and Petrology 42, 125-139. doi:10.1007/BF00371502

Coulon, C., Demant, A., Bellon, H., 1974. Premieres datations par la methode K/Ar de quelques laves cenozoiques et quaternaires de Sardaigne nord-occidentale. Tectonophysics 22, 41–57. doi:10.1016/0040-1951(74)90034-1

Coulon, C., Dostal, J., Dupuy, C., 1978. Petrology and geochemistry of the ignimbrites and associated lava domes from NW Sardinia. Contribution to Mineralogy and Petrology 68, 89–98.

Dale, I.M., Henderson, P., 1972. The partition of transition elements in phenocryst-bearing basalts and the implications about melt structure, in: 24th International Geological Congress. pp. 105–111.

Davidson, J., Turner, S., Handley, H., Macpherson, C., Dosseto, A., 2007. Amphibole "sponge" in arc crust? Geology 35, 787–790. doi:10.1130/G23637A.1

De Angelis, S. H., Larsen, J., Coombs, M., 2013. Pre-eruptive magmatic conditions at Augustine Volcano, Alaska, 2006: evidence from amphibole geochemistry and textures. Journal of Petrology 54, 1939–1961.

De Angelis, S.H., Larsen, J., Coombs, M., Dunn, A., Hayden, L., 2015. Amphibole reaction rims as a record of pre-eruptive magmatic heating: an experimental approach. Earth and Planetary Science Letters 426, 235–245. doi:10.1016/j.epsl.2015.06.051

DeBari, S.M., Coleman, R.G., 1989. Examination of the deep levels of an island arc: evidence from the Tonsina ultramafic-mafic assemblage, Tonsina, Alaska. Journal of Geophysical Research 94, 4373–4391.

Deering, C. D., Bachmann, O., Dufek, J., Gravley, D. M., 2011. Rift-related transition from andesite to rhyolite volcanism in the Taupo Volcanic Zone (New Zealand) controlled by crystal-melt dynamics in mush zones with variable mineral assemblages. Journal of Petrology 52, 2243–2263.

DePaolo, D.J., 1981. Trace element and isotopic effects of combined wallrock assimilation and fractional crystallization. Earth and Planetary Science Letters 53, 189–202. doi:10.1016/0012-821X(81)90153-9

Deriu, M., 1964. Notizie sulla costituzione geologica del Bosano, della Planargia e del Montiferro settentrionale e occidentale. e. Monografia Reg. Bosano, Ass. Comm. Bosa e Cuglieri, 1-50.

Dessimoz, M., Muntener, O., Ulmer, P., 2012. A case for hornblende dominated fractionation of arc magmas: the Chelan Complex, Washington Cascades. Contributions to Mineralogy and Petrology 163, 567–589.

Dieni, I., Massari, F., Médus, J., 2008. Age, depositional environment and stratigraphic value of the Cuccuru 'e Flores Conglomerate: insight into the Palaeogene to Early Miocene geodynamic evolution of Sardinia. Bulletin de la Société Géologique de France 179, 51–72.

Doe, B.R., 1997. Geochemistry of oceanic igneous rocks-ridges, islands, and arcs-with emphasis on manganese, scandium, and vanadium. International Geology Review 39, 1053–1112. doi:10.1080/00206819709465317

Dostal, J., Dupuy, C., Carron, J.P., Le Guen de Kerneizon, M., Maury, R.C., 1983. Partition coefficients of trace elements: application to volcanic rocks of St. Vincent, West Indies. Geochimica et Cosmochimica Acta 47, 525–533. doi:10.1016/0016-7037(83)90275-2

Ducea, M.N., Saleeby, J.B., 1996. Buoyancy sources for a large, unrooted mountain range, the Sierra Nevada, California: evidence from xenolith thermobarometry. Journal of Geophysical Research: Solid Earth 101.B4, 8229-8244.

Dufek, J., Bachmann, O., 2010. Quantum magmatism: Magmatic compositional gaps generated by melt-crystal dynamics. Geology 38, 687–690.

Duggen, S., Hoernle, K., van den Bogaard, P., Garbe-Schönberg, D., 2005. Post-collisional transition from subduction-to intraplate-type magmatism in the westernmost Mediterranean: evidence for continental-edge delamination of subcontinental lithosphere. Journal of Petrology doi:10.1093/petrology/egi013

Duke, J.M., 1976. Distribution of the period four transition elements among olivine, calcic clinopyroxene and mafic silicate liquid: experimental results. Journal of Petrology 17, 499–521. doi:10.1093/petrology/17.4.499

Dungan, M. A., Davidson, J., 2004. Partial assimilative recycling of the mafic plutonic roots of arc volcanoes: an example from the Chilean Andes. Geology 32, 773–776.

Dunn, T., Sen, C., 1994. Mineral/matrix partition coefficients for orthopyroxene, plagioclase, and olivine in basaltic to andesitic systems: a combined analytical and experimental study. Geochimica et Cosmochimica Acta 58, 717–733. doi:10.1016/0016-7037(94)90501-0

Dupuy, C., McNutt, R., Coulon, C., 1974. Détermination de Sr dans les andésites cénozoïques et les laves associées de Sardaigne Nord occidentale (Italie). Geochimica et Cosmochimica Acta 38, 1287–1296. doi:10.1016/0016-7037(74)90121-5

Elsworth, D., Mattioli, G., Taron, J., Voight, B., Herd, R., 2008. Implications of magma transfer between multiple reservoirs on eruption cycling. Science 322, 246–248.

Foden, J.D., Green, D.H., 1992. Possible role of amphibole in the origin of andesite: some experimental and natural evidence. Contributions to Mineralogy and Petrology 109, 479–493. doi:10.1007/BF00306551

Forsythe, L.M., Nielsen, R.L., Fisk, M.R., 1994. High-field-strength element partitioning between pyroxene and basaltic to dacitic magmas. Chemical Geology 117, 107–125. doi:10.1016/0009-2541(94)90124-4

France, L., Ildefonse, B., Koepke, J., Bech, F., 2010. A new method to estimate the oxidation state of basaltic series from microprobe analyses. Journal of Volcanology and Geothermal Research 189, 340–346. doi:10.1016/j.jvolgeores.2009.11.023

Franciosi, L., Lustrino, M., Melluso, L., Morra, V., D'Antonio, M., 2003. Geochemical characteristics and mantle sources of the Oligo-Miocene primitive basalts from Sardinia: the role of subduction components. Ofioliti 28, 105–114.

Franzini, M., Leoni, L., Saitta, M., 1972. A simple method to evaluate the matrix effects in X-Ray fluorescence analysis. X-Ray Spectrometry 1, 151–154. doi:10.1002/xrs.1300010406

Frey, H.M., Lange, R.A., 2011. Phenocryst complexity in andesites and dacites from the Tequila volcanic field, Mexico: resolving the effects of degassing vs. magma mixing. Contributions to Mineralogy and Petrology 162, 415–445. doi:10.1007/s00410-010-0604-1

Fujimaki, H., Tatsumoto, M., Aoki, K., 1984. Partition coefficients of Hf, Zr, and REE between phenocrysts and groundmasses. Journal of Geophysical Research 89, B662–B672.

Green, T., Adam, J., Site, S., 1993. Proton microprobe determined trace element partition coefficients between pargasite, augite and silicate or carbonatitic melts. American Geophysical Union Transactions 74, 340.

Green, T.H., Ringwood, A.E., 1968. Genesis of the calc-alkaline igneous rock suite. Contributions to Mineralogy and Petrology 18, 105–162.

Grove, T.L., Elkins-Tanton, L.T., Parman, S.W., Chatterjee, N., Müntener, O., Gaetani, G.A., 2003. Fractional crystallization and mantle-melting controls on calc-alkaline differentiation trends. Contributions to Mineralogy and Petrology 145, 515–533. doi:10.1007/s00410-003-0448-z

Gudmundsson, A., 2011. Deflection of dykes into sills at discontinuities and magma-chamber formation. Tectonophysics 500, 50–64.

Gust, D.A., Perfit, M.R., 1987. Phase relations of a high-Mg basalt from the Aleutian Island Arc: implications for primary island arc basalts and high-Al basalts. Contributions to Mineralogy and Petrology 97, 7–18. doi:10.1007/BF00375210

Holloway, J.R., Burnham, C.W., 1972. Melting relations of basalt with equilibrium water pressure less than total pressure. Journal of Petrology 13, 1–29. doi:10.1093/petrology/13.1.1

Iain, S., Chassé, M., 2016. Scandium. William M. White. Encyclopedia of Geochemistry, Springer International Publishing Switzerland, pp.1-4, 2016, <10.1007/978-3-319-39193-9_281-1>. <hal-01420736>

Iezzi, G., Mollo, S., Shahini, E., Cavallo, A., Scarlato, P., 2014. The cooling kinetics of plagioclase feldspar as revealed by electron-microprobe mapping. American Mineralogist 99, 898–907. doi:10.2138/am.2014.4626

Irving, A.J., Frey, F.A., 1984. Trace element abundances in megacrysts and their host basalts: constraints on partition coefficients and megacryst genesis. Geochimica et Cosmochimica Acta 48, 1201–1221. doi:10.1016/0016-7037(84)90056-5

Jones, J.H., Drake, M.J., 1986. Geochemical constraints on core formation in the Earth. Nature 322, 221–228. doi:10.1038/322221a0

Klöck, W., Plame, H., 1988. Partitioning of siderophile and chalcophile elements between sulfide, olivine, and glass in a naturally reduced basalt from Disko Island, Greenland. Lunar Planeary Science Conference Proceedings 18, 471–483.

Larocque, J., Canil, D., 2010. The role of amphibole in the evolution of arc magmas and crust: the case from the Jurassic Bonanza arc section, Vancouver Island, Canada. Contributions to Mineralogy and Petrology 159, 475–492. doi:10.1007/s00410-009-0436-z

Le Bas, M.J., Le Maitre, R.W., Streckeisen, A., Zanettin, B., 1986. A chemical classification of volcanic rocks based on the total alkali silica diagram. Journal of Petrology 27, 745–750. doi:10.1093/petrology/27.3.745

Leake, B.E., Woolley, A.R., Arps, C.E.S., Birch, W.D., Gilbert, M.C., Grice, J.D., Hawthorne, F.C., Kato, A., Kisch, H.J., Krivovichev, V.G., Linthout, K., Laird, J., Mandarino, J.A., Maresch, W. V, Nickel, E.H., Rock, N.M., Schumacher, J.C., Smith, D.C., Stephenson, N.C.N., Ungaretti, L., Whittaker, E.J.W., Youzhi, G., 1997. Nomenclature of amphiboles: report of the subcommittee on amphiboles of the International Mineralogical Association, commission on new minerals and mineral names. Canadian Mineralogist 35, 219–246.

Lecca, L., Lonis, R., Luxoro, S., Melis, E., Secchi, F., Brotzu, P., 1997. Oligo-Miocene volcanic sequences and rifting stages in Sardinia: a review. Periodico di Mineralogia 66, 7–61.

Lewis, J.F., 1973. Petrology of ejected plutonic blocks of Soufriere volcano, St. Vincent, West Indies. Journal of Petrology 14, 81–112.

Li, L., Xiong, X.L., Liu, X.C., 2017. Nb/Ta fractionation by amphibole in hydrous basaltic systems: implications for arc magma evolution and continental crust formation. Journal of Petrology 15, egw070. doi:10.1093/petrology/egw070

Lipman, P. W., Doe, B. R., Hedge, C. E., Steven, T. A., 1978. Petrologic evolution of the San Juan volcanic field, southwestern Colorado: Pb and Sr isotope evidence. Geological Society of America Bulletin 89, 59–82.

Lonis, R., Morra, V., Lustrino, M., Melluso, L., Secchi, F., 1997. Plagioclase textures, mineralogy and petrology of Tertiary orogenic volcanic rocks from Sindia (central Sardinia). Periodico di Mineralogia 66, 185–210.

Luhr, J.F., Carmichael, I.S.E., 1980. The Colima Volcanic complex, Mexico. Contributions to Mineralogy and Petrology 71, 343–372. doi:10.1007/BF00374707

Lustrino, M., Duggen, S., Rosenberg, C.L., 2011. The Central-Western Mediterranean: anomalous igneous activity in an anomalous collisional tectonic setting. Earth Science Review 104, 1-40. doi:10.1016/j.earscirev.2010.08.002

Lustrino, M., Fedele, L., Melluso, L., Morra, V., Ronga, F., Geldmacher, J., Duggen, S., Agostini, S., Cucciniello, C., Franciosi, L., Meisel, T., 2013. Origin and evolution of Cenozoic magmatism of Sardinia (Italy). A combined isotopic (Sr-Nd-Pb-O-Hf-Os) and petrological view. Lithos 180–181, 138–158. doi:10.1016/j.lithos.2013.08.022

Lustrino, M., Morra, V., Fedele, L., Franciosi, L., 2009. Beginning of the Apennine subduction system in central western Mediterranean: constraints from Cenozoic “orogenic” magmatic activity of Sardinia, Italy. Tectonics 28, 1–23. doi:10.1029/2008TC002419

Lustrino, M., Morra, V., Melluso, L., Brotzu, P., D’Amelio, F., Fedele, L., Franciosi, L., Lonis, R., Lieberckнecht, A.M.P., 2004. The Cenozoic igneous activity of Sardinia. Periodico di Mineralogia 73, 105–134.

Marsh, B.D., 1996. Solidification fronts and magmatic evolution. Mineralogical Magazine 60, 5–40. doi:10.1180/minmag.1996.060.398.03

Mattioli, M., Guerrera, F., Tramontana, M., Raffaelli, G., D’Atri, M., 2000. High-Mg Tertiary basalts in Southern Sardinia (Italy). Earth and Planetary Science Letters 179, 1–7. doi:10.1016/S0012-821X(00)00103-5

McKay, G.A., Weill, D.F., 1976. Petrogenesis of KREEP, in: Merrill, R.B., Morris, R.V., Rhodes, J.M., Usselman, T.M. (Eds.), Proceedings of the 7th Lunar Science Conference: Petrogenetic Studies of Mare and Highland Rocks. Pergamon Press, New York, pp. 427–447.

McKay, G., Le, L., Wagstaff, J., Crozaz, G., 1994. Experimental partitioning of rare earth elements and strontium: constraints on petrogenesis and redox conditions during crystallization of Antarctic angrite Lewis Cliff 86010. Geochimica et Cosmochimica Acta 58, 2911–2919. doi:10.1016/0016-7037(94)90124-4

Melekhova, E., Blundy, J., Robertson, R., Humphreys, M.C.S., 2015. Experimental evidence for polybaric differentiation of primitive arc basalt beneath St. Vincent, Lesser Antilles. Journal of Petrology 56, 161–192. doi:10.1093/petrology/egu074

Meurer, W.P., Claeson, D.T., 2002. Evolution of crystallizing interstitial liquid in an arc-related cumulate determined by LA ICP-MS mapping of a large amphibole oikocryst. Journal of Petrology 43, 607–629. doi:10.1093/petrology/43.4.607

Molina, J. F., Moreno, J. A., Castro, A., Rodriguez, C., Fershtater, G. B., 2015. Calcic amphibole thermobarometry in metamorphic and igneous rocks: New calibrations based on plagioclase/amphibole Al-Si partitioning and amphibole/liquid Mg partitioning. Lithos 232, 286–305.

Mollo, S., Misiti, V., Scarlato, P., Soligo, M., 2012. The role of cooling rate in the origin of high temperature phases at the chilled margin of magmatic intrusions. Chemical Geology 322–323, 28–46. doi:10.1016/j.chemgeo.2012.05.029

Mollo, S., Putirka, K., Misiti, V., Soligo, M., Scarlato, P., 2013. A new test for equilibrium based on clinopyroxene-melt pairs: clues on the solidification temperatures of Etnean alkaline melts at post-eruptive conditions. Chemical Geology 352, 92–100. doi:10.1016/j.chemgeo.2013.05.026

Montigny, R., Edel, J.B., Thuizat, R., 1981. Oligo-Miocene rotation of Sardinia: K-Ar ages and paleomagnetic data of Tertiary volcanics. Earth and Planetary Science Letters 54, 261–271. doi:10.1016/0012-821X(81)90009-1

Morra, V., Secchi, F.A., Assorgia, A., 1994. Petrogenetic significance of peralkaline rocks from Cenozoic calc-alkaline volcanism from SW Sardinia, Italy. Chemical Geology 118, 109–142. doi:10.1016/0009-2541(94)90172-4

Morra, V., Secchi, F. a. G., Melluso, L., Franciosi, L., 1997. High-Mg subduction-related Tertiary basalts in Sardinia, Italy. Lithos 40, 69–91. doi:10.1016/S0024-4937(96)00028-X

Neave, D.A., Putirka, K.D., 2017. A new clinopyroxene-liquid barometer, and implications for magma storage pressures under Icelandic rift zones. American Mineralogist.

Nielsen, R.L., 1992. BIGD.FOR: A FORTRAN program to calculate trace-element partition coefficients for natural mafic and intermediate composition magmas. Computers and Geosciences 18, 773–788. doi:10.1016/0098-3004(92)90024-L

Oberti, R., Vannucci, R., Zanetti, A., Tiepolo, M., Brumm, R.C., 2000. A crystal chemical re-evaluation of amphibole/melt and amphibole/clinopyroxene DTi values in petrogenetic studies. American Mineralogist 85, 407–419. doi:10.2138/am-2000-0402

Okamoto, K., 1979. Geochemical study on magmatic differentiation of Asama volcano, central Japan. Journal of Geological Society of Japan 85, 525–535. doi:10.5575/geosoc.85.525

Peccerillo, A., Taylor, S.R., 1976. Geochemistry of Eocene calc-alkaline volcanic rocks from the Katamonu area, northern Turkey. Contributions to Mineralogy and Petrology 58, 63–81.

Pichavant, M., Macdonald, R., 2007. Crystallization of primitive basaltic magmas at crustal pressures and genesis of the calc-alkaline igneous suite: experimental evidence from St Vincent, Lesser Antilles arc. Contributions to Mineralogy and Petrology 154, 535–558. doi:10.1007/s00410-007-0208-6

Putirka, K., Johnson, M., Kinzler, R., Longhi, J., Walker, D., 1996. Thermobarometry of mafic igneous rocks based on clinopyroxene-liquid equilibria, 0-30 kbar. Contributions to Mineralogy and Petrology 123, 92–108. doi:10.1007/s004100050145

Putirka, K.D., 2008. Thermometers and barometers for volcanic systems. Reviews in Mineralogy and Geochemistry 69, 61–120. doi:10.2138/rmg.2008.69.3

Putirka, K.D., 2005. Igneous thermometers and barometers based on plagioclase + liquid equilibria: tests of some existing models and new calibrations. American Mineralogist 90, 336–346. doi:10.2138/am.2005.1449

Putirka, K.D., Mikaelian, H., Ryerson, F., Shaw, H., 2003. New clinopyroxene-liquid thermobarometers for mafic, evolved, and volatile-bearing lava compositions, with applications to lavas from Tibet and the Snake River Plain, Idaho. American Mineralogist 88, 1542–1554. doi:10.2138/am.2005.431

Putirka, K.D., Perfit, M., Ryerson, F.J., Jackson, M.G., 2007. Ambient and excess mantle temperatures, olivine thermometry, and active vs. passive upwelling. Chemical Geology 241, 177–206. doi:10.1016/j.chemgeo.2007.01.014

Reid, F., 1983. Origin of the rhyolitic rocks of the Taupo volcanic zone, New Zealand. Journal of Volcanology and Geothermal Research 15, 315–338. doi:10.1016/0377-0273(83)90105-1

Ridolfi, F., Renzulli, A., 2012. Calcic amphiboles in calc-alkaline and alkaline magmas: Thermobarometric and chemometric empirical equations valid up to 1,130°C and 2.2 GPa. Contributions to Mineralogy and Petrology 163, 877–895. doi:10.1007/s00410-011-0704-6

Ridolfi, F., Renzulli, A., Puerini, M., 2010. Stability and chemical equilibrium of amphibole in calc-alkaline magmas: an overview, new thermobarometric formulations and application to subduction-related volcanoes. Contributions to Mineralogy and Petrology 160, 45–66. doi:10.1007/s00410-009-0465-7

Roeder, P.L., Emslie, R.F., 1970. Olivine-liquid equilibrium. Contributions to Mineralogy and Petrology 29, 275–289. doi:10.1007/BF00371276

Ruprecht, W., Wörner, G., 2007. Variable regimes in magma systems documented in plagioclase zoning patterns: El Misti stratovolcano and Andahua monogenetic cones. Journal of Volcanology and Geothermal Research 165, 142–162.

Rutherford, M. J., Devine, J. D., 2003. Magmatic conditions and magma ascent as indicated by hornblende phase equilibria and reactions in the 1995-2002 Soufriere Hills magma. Journal of Petrology 44, 1433–1453.

Rutherford, M. J., Hill, P. M., 1993. Magma ascent rates from amphibole breakdown: An experimental study applied to the 1980–1986 Mount St. Helens eruptions. Journal of Geophysical Research 98, 19667.

Scarlato, P., Mollo, S., Del Bello, E., von Quadt, A., Brown, R.J., Gutierrez, E., Martinez-Hackert, B., Papale, P., 2017. The 2013 eruption of Chaparrastique volcano (El Salvador): effects of magma storage, mixing, and decompression. Chemical Geology 448, 110–122. doi:10.1016/j.chemgeo.2016.11.015

Shane, P., Smith, V. C., 2013. Using amphibole crystals to reconstruct magma storage temperatures and pressures for the post-caldera collapse volcanism at Okataina volcano. Lithos 156–159, 159–170.

Sisson, T.W., 1994. Hornblende-melt trace-element partitioning measured by ion microprobe. Chemical Geology 117, 331–344. doi:10.1016/0009-2541(94)90135-X

Sisson, T.W., Grove, T.L., 1993. Experimental investigations of the role of H2O in calc-alkaline differentiation and subduction zone magmatism. Contributions to Mineralogy and Petrology 113, 143–166. doi:10.1007/BF00283225

Skulski, T., Minarik, W., Watson, E.B., 1994. High-pressure experimental trace-element partitioning between clinopyroxene and basaltic melts. Chemical Geology 117, 127–147. doi:10.1016/0009-2541(94)90125-2

Smith, D.J., 2014. Clinopyroxene precursors to amphibole sponge in arc crust. Nature Communications 5, 4329. doi:10.1038/ncomms5329

Spera, F.J., Bohrson, W.A., 2001. Energy-constrained open-system magmatic processes I: general model and Energy-Constrained Assimilation and Fractional Crystallization (EC-AFC) formulation. Journal of Petrology 42, 999–1018. doi:10.1093/petrology/42.5.999

Stamper, C.C., Blundy, J.D., Arculus, R.J., Melekhova, E., 2014. Petrology of plutonic xenoliths and volcanic rocks from Grenada, Lesser Antilles. Journal of Petrology 55, 1353–1387. doi:10.1093/petrology/egu027

Streck, M. J., 2008. Mineral textures and zoning as evidence for open system processes. Reviews in Mineralogy and Geochemistry 69, 595–622.

Streck, M. J., Leeman, W. P., Chesley, J., 2007. High-magnesian andesite from Mount Shasta: a product of magma mixing and contamination, not a primitive mantle melt. Geology 35, 351–354.

Tilley, C.E., 1950. Some aspects of magmatic evolution. Quarterly Journal of the Geological Society of London 106, 37–61.

Tommasini, S., Poli, G., Halliday, A.N., 1995. The role of sediment subduction and crustal growth in Hercynian plutonism: isotopic and trace element evidence

from the Sardinia-Corsica batholith. Journal of Petrology 36, 1305–1332. doi:10.1093/petrology/36.5.1305

Turner, S. J., Izbekov, P., Langmuir, C., 2013. The magma plumbing system of Bezymianny Volcano: insights from a 54year time series of trace element whole-rock geochemistry and amphibole compositions. Journal of Volcanology and Geothermal Research 263, 108–121.

Ushioda, M., Takahashi, E., Hamada, M., Suzuki, T., 2014. Water content in arc basaltic magma in the Northeast Japan and Izu arcs: an estimate from Ca/Na partitioning between plagioclase and melt. Earth, Planets and Space 66, 1–10. doi:10.1186/1880-5981-66-127

Villemant, B., Jaffrezic, H., Joron, J.L., Treuil, M., 1981. Distribution coefficients of major and trace-elements - fractional crystallization in the alkali basalt series of Chaine-des-Puys (Massif Central, France). Geochimica et Cosmochimica Acta 45, 1997–2016.

Yamamoto, M., 1984. Origine of calc-alkaline andesite from Oshima-Oshima volcano, north Japan. Journal of the Faculty of Science, Hokkaido University. Series 4, Geology and mineralogy 21, 77–131.

Chapter 1: Figures

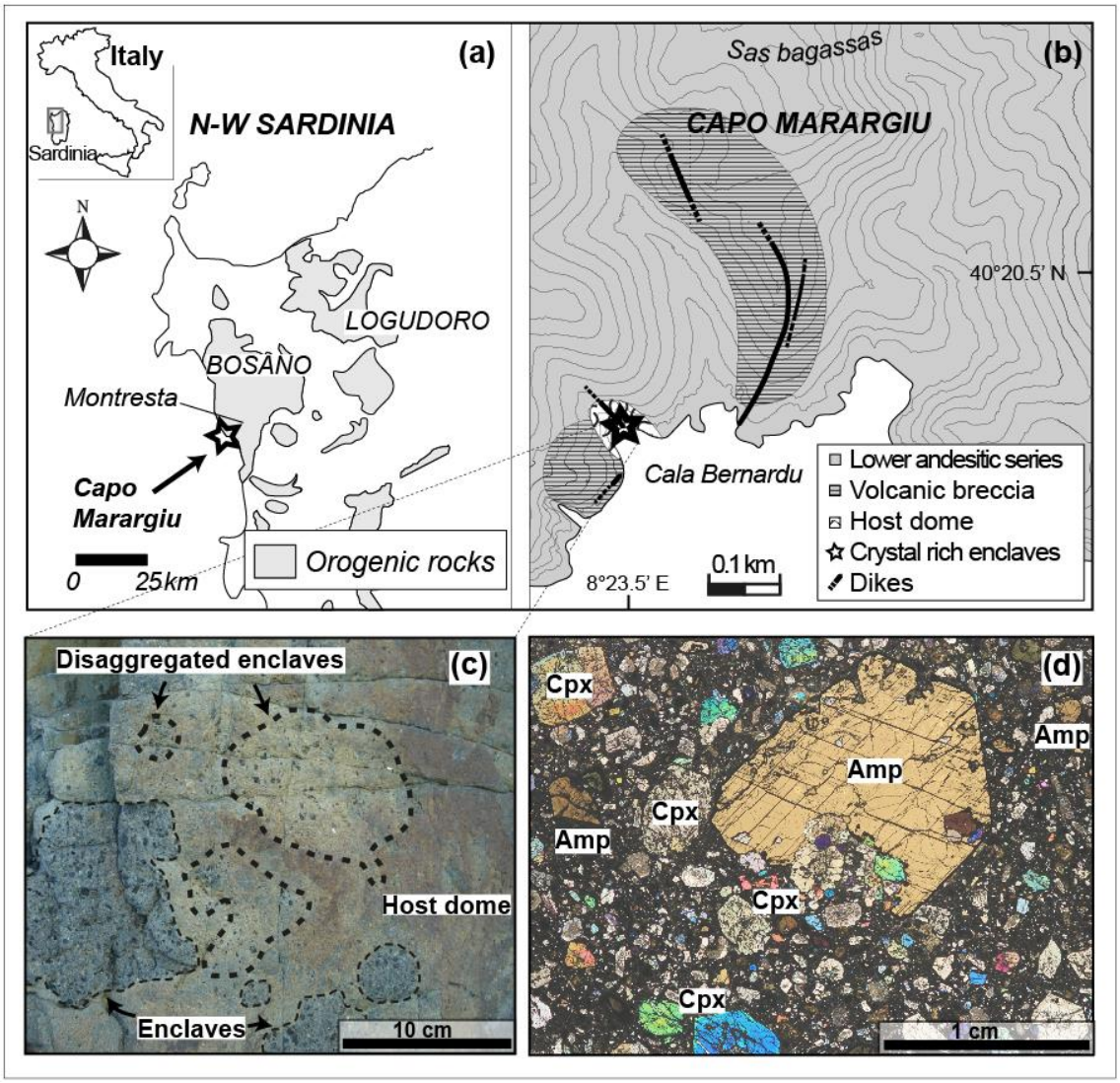

Fig. 1. Schematic maps showing the Capo Marargiu Volcanic District (i.e., CMVD) located at about 10 km south-westward of Montresta (Sardinia, Italy) (a) and the sampling area of the volcanic dome on the coast of Cala Bernardu (b). The studied rocks are enclaves, host dome, dikes and crystal clots. The dome appears as a yellowish, porphyritic rock, whereas the dark-grey enclaves are centimetre-to-metre-sized rounded blocks (c). Some portions of the dome are also enriched in crystals produced by enclave disaggregation in the surrounding magma (c). The enclaves are crystal-rich, porphyritic rocks containing ~40-50% of coarse-grained clinopyroxene + amphibole + plagioclase + olivine + titanomagnetite/ilmenite ± Cr-spinel (d). Clinopyroxene (i.e., Cpx) and amphibole (i.e., Amp) are the most abundant minerals.

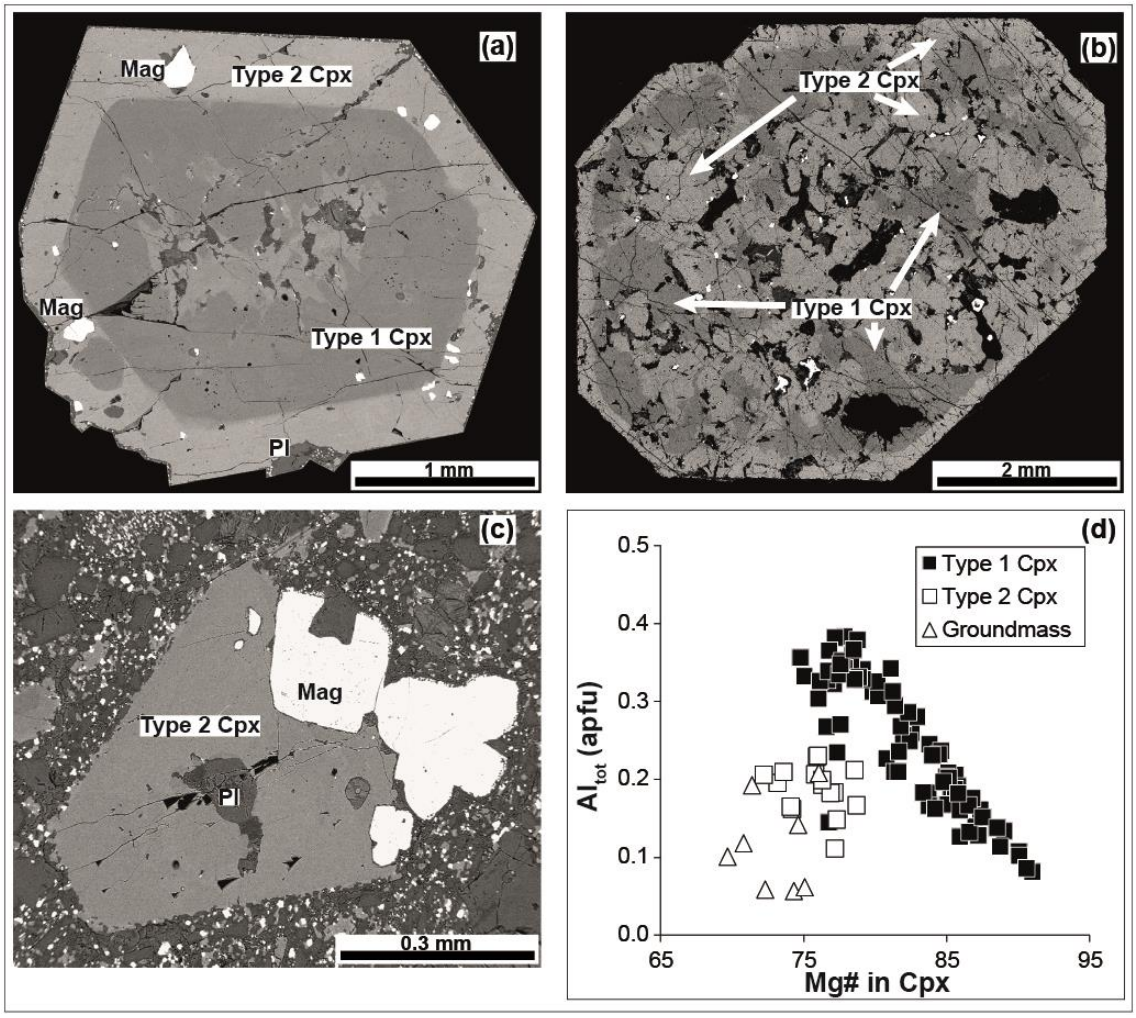

Fig. 2. Textural characteristics of Type 1 and Type 2 clinopyroxenes from enclaves. Type 2 crystals are observed to overgrow on Type 1 clinopyroxenes (a). Dissolution reaction phenomena form spongy cellular texture and patchy zoning (b). Heavy chemical species (more primitive portions of Type 1) backscatter electrons better than light elements (more evolved portions of Type 2). Type 2 grains occur also as millimetre-sized glomerocrysts together with plagioclase and titanomagnetite (c). Type 1 crystals are generally more primitive than Type 2 clinopyroxenes and groundmass microlites (d). Error bars are within the symbols.

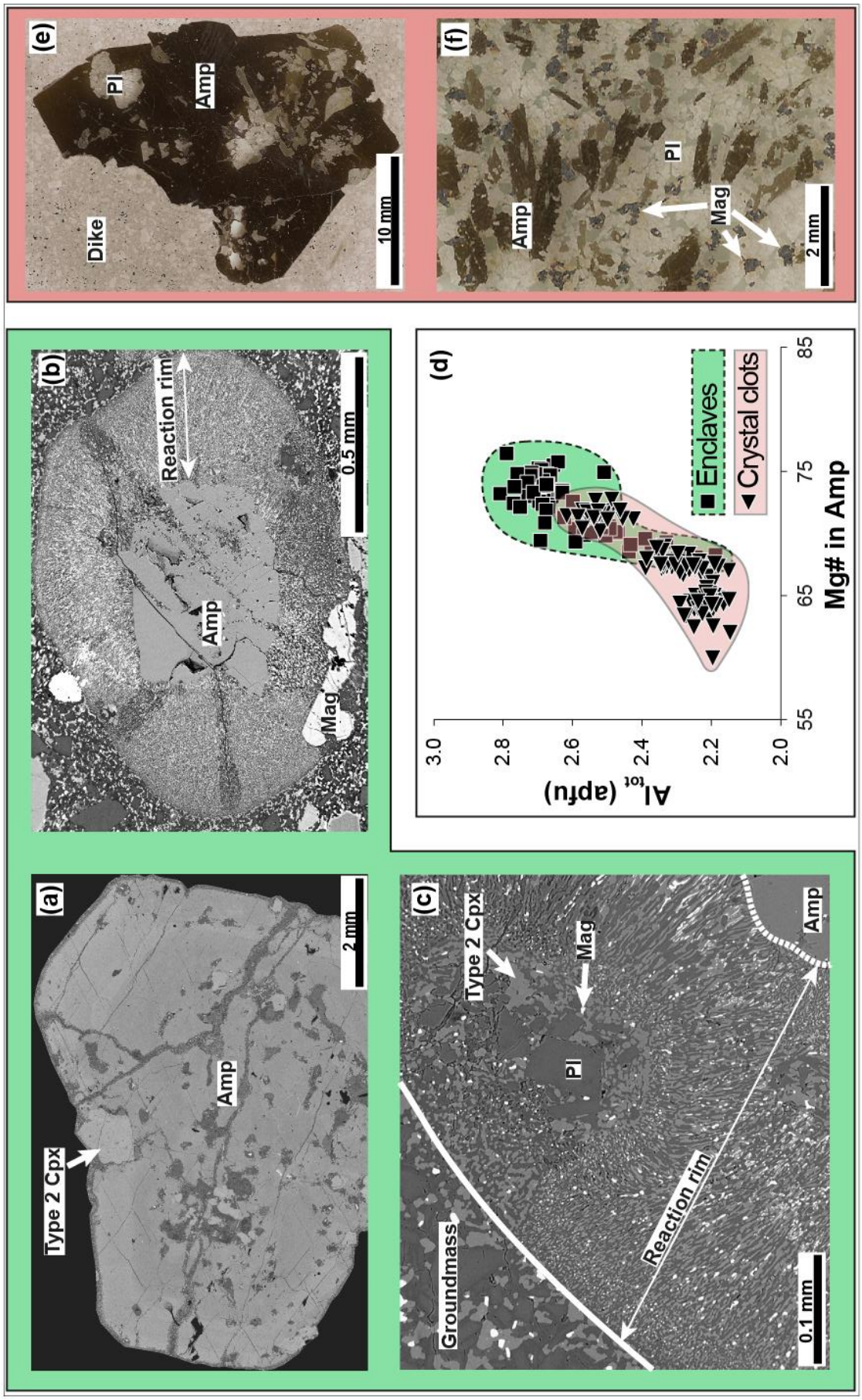
(a)
Type 2 Cpx
Amp
2 mm
(b)
Reaction rim
Amp
Mag
0.5 mm
(c)
Type 2 Cpx
Mag
Pl
Amp
Groundmass
Reaction rim
0.1 mm
(d)
Enclaves
Crystal clots
Al_{tot} (apfu)
Mg# in Amp
3.0
2.8
2.6
2.4
2.2
2.0
55
65
75
85
(e)
Pl
Amp
Dike
10 mm
(f)
Amp
Pl
Mag
2 mm

Fig. 3. Textural characteristics of amphiboles from enclaves and crystal clots. Amphibole are millimetre-to-centimetre sized crystals characterised by spongy cellular texture (a) with fine-grained reaction rims including groundmass minerals of clinopyroxene + plagioclase + titanomagnetite/ ilmenite ± low-Ca pyroxene (b and c). The composition of amphibole from enclaves is magnesiohastingsite and most of the analytical dataset is restricted to a nearly constant value of Al_{tot} between 2.6 and 2.8 apfu (d). These data partially overlap with those of amphibole from crystal clots, which however are mostly evolved and restricted to values of Al_{tot} between 2.2 and 2.4 apfu (error bars within the symbols). Coarse-grained clots are characterised by centimetre-sized, texturally homogeneous amphibole crystals (e). Plagioclase is scarce in the coarse-grained clots (e), whereas its abundance increases in the medium-grained samples up to levels comparable to the amphibole contents (f).

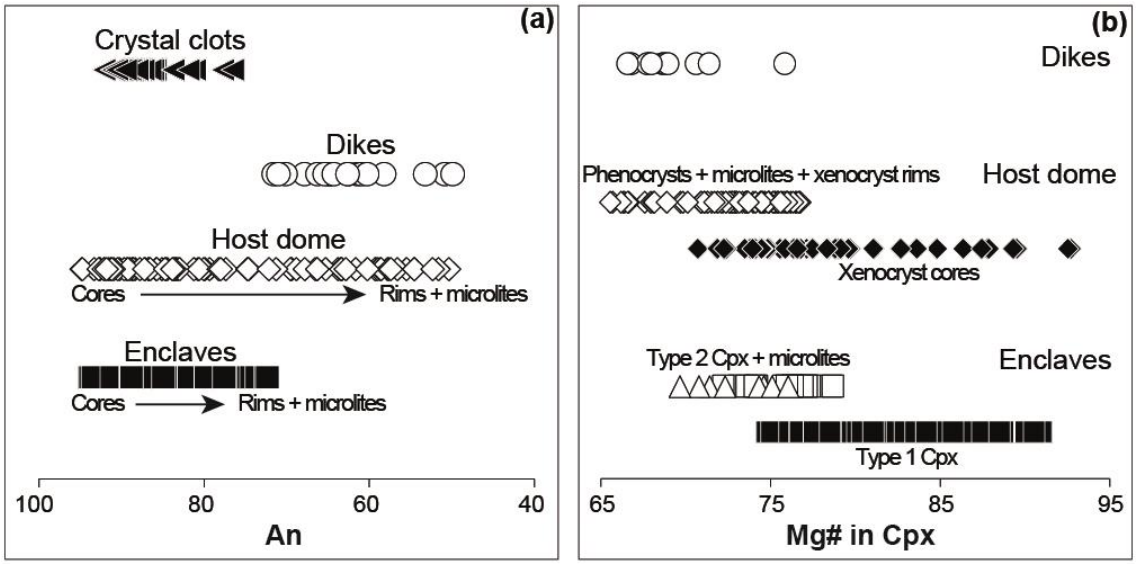

Fig. 4. Compositional variations of plagioclase (a) and clinopyroxene (b) crystals from the studied rocks (error bars within the symbols). An is anorthite in plagioclase. Mg# is Mg-number [i.e., 100 · Mg/(Mg + Fe_{tot})] in clinopyroxene.

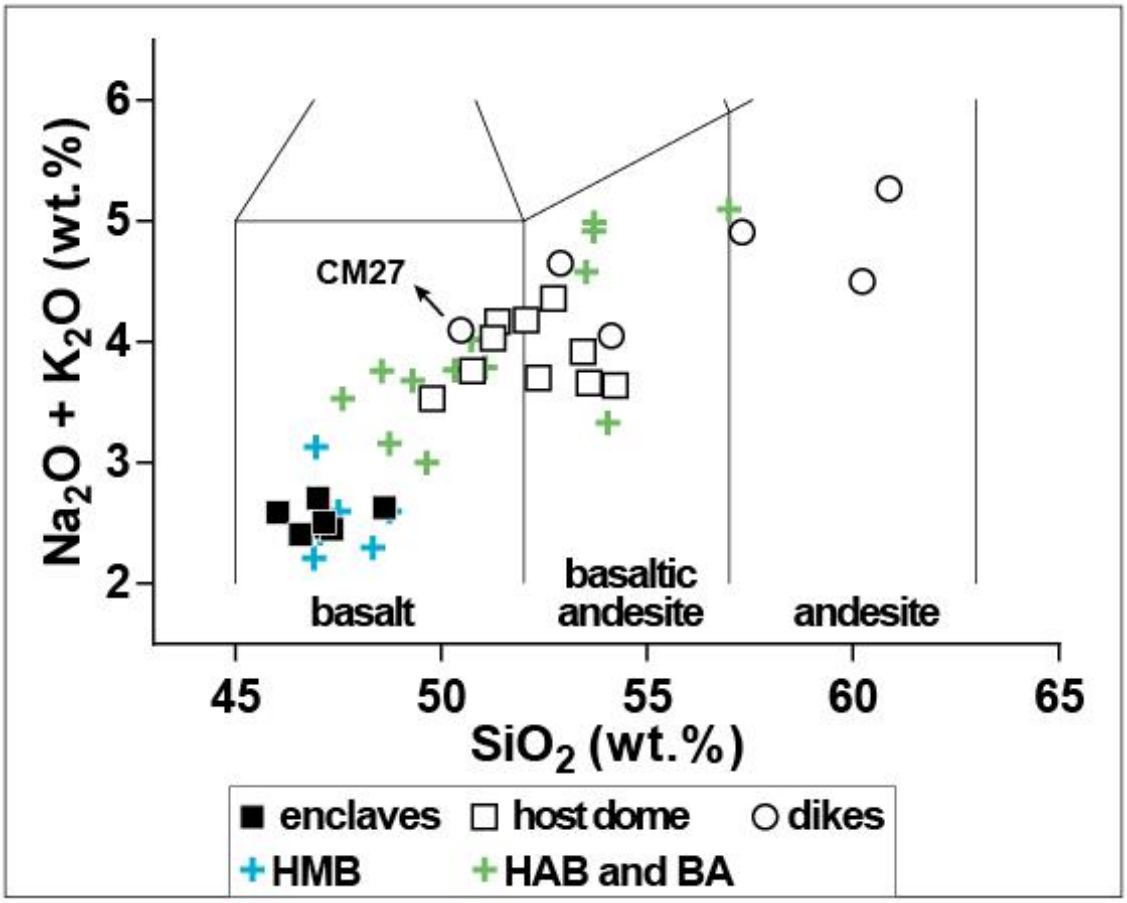

Fig. 5. Bulk-rock compositions of products from the CMVD are plotted in the TAS (total alkali vs. silica) diagram of Le Bas et al. (1986). Data from this study are also compared with the Montresta compositions reported by Morra et al. (1997), i.e., high-Mg basalts (HMB), more differentiated high-Al basalts (HAB), and basaltic andesites (BA). Error bars are within the symbols.

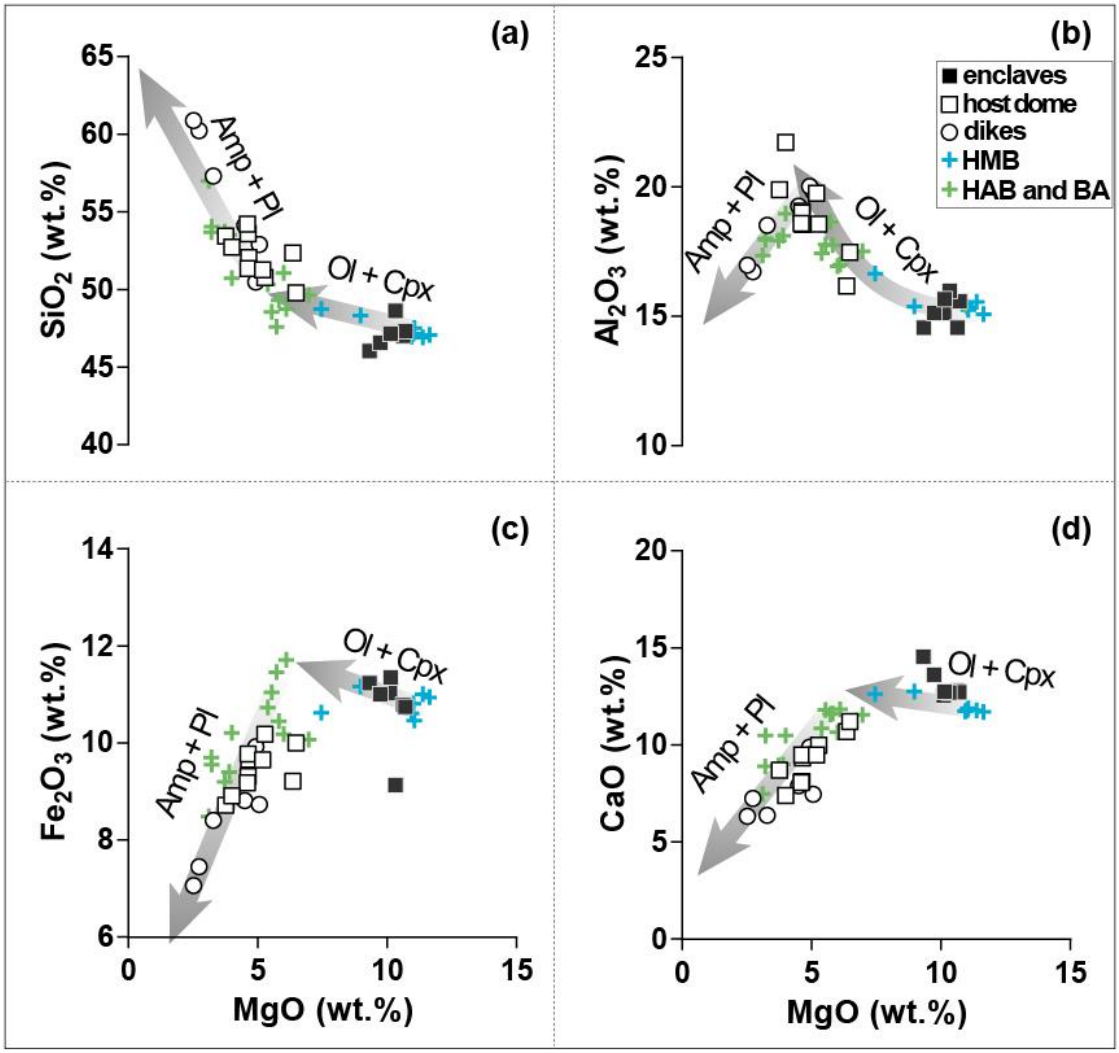

Fig. 6. Bulk-rock compositions of products from the CMVD are plotted in the MgO vs. SiO_2 (a), Al_2O_3 (b), Fe_2O_3 (c), and CaO (d) diagram (error bars within the symbols). Arrows indicate the prevalent fractionation of Fo-rich olivine (Ol) + Type 1 clinopyroxene (Cpx) and amphibole (Amp) + An-rich plagioclase (Pl). Data from this study are also compared with the Montresta compositions reported by Morra et al. (1997), i.e., high-Mg basalts (HMB), more differentiated high-Al basalts (HAB), and basaltic andesites (BA).

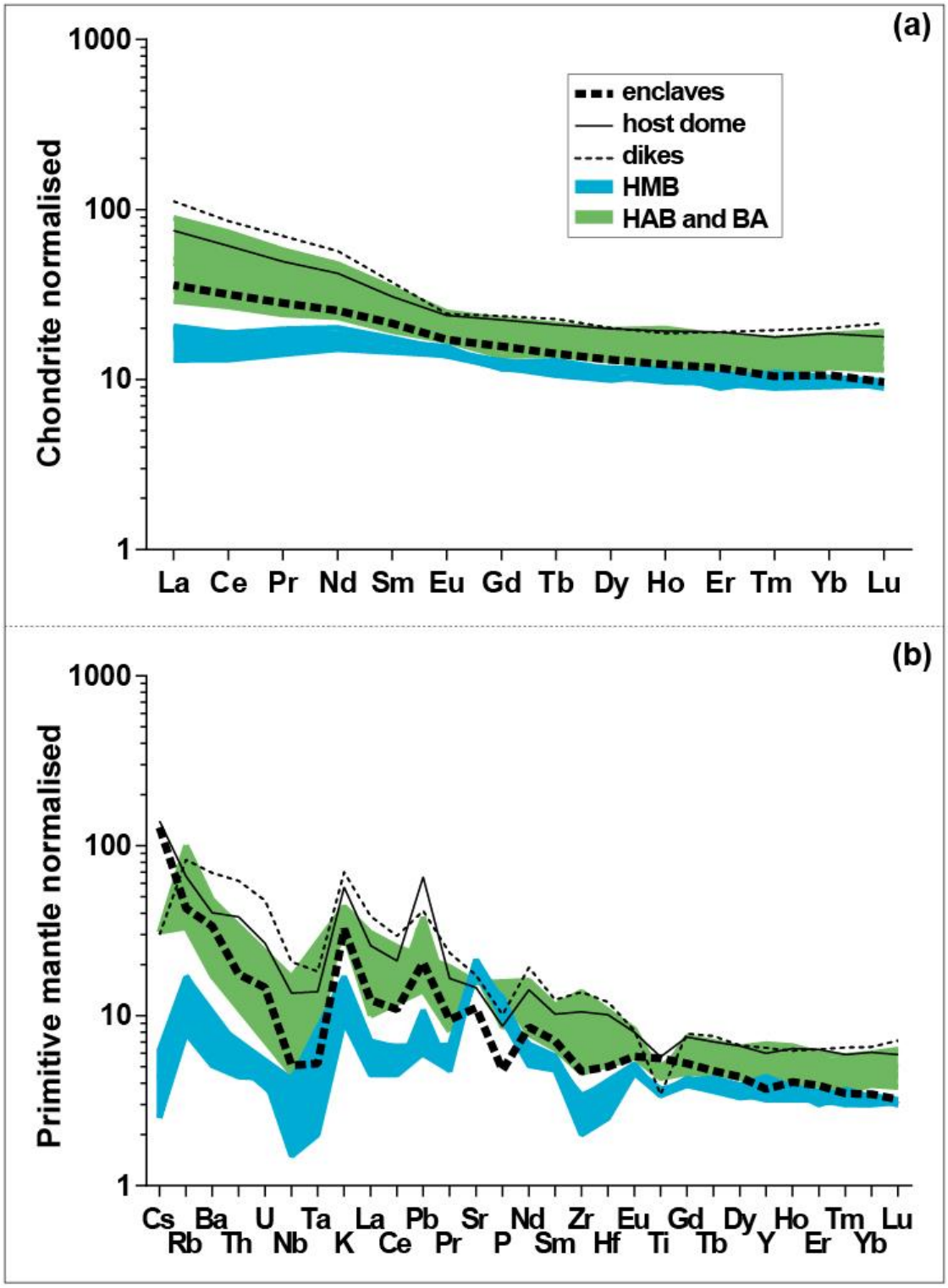

Fig. 7. Chondrite-normalised patterns of Rare Earth Elements (REE) (a) and primitive mantle-normalised trace element patterns (b). Data from this study (error bars within the symbols) are also compared with the Montresta compositions reported by Morra et al. (1997), i.e., high-Mg basalts (HMB), more differentiated high-Al basalts (HAB), and basaltic andesites (BA).

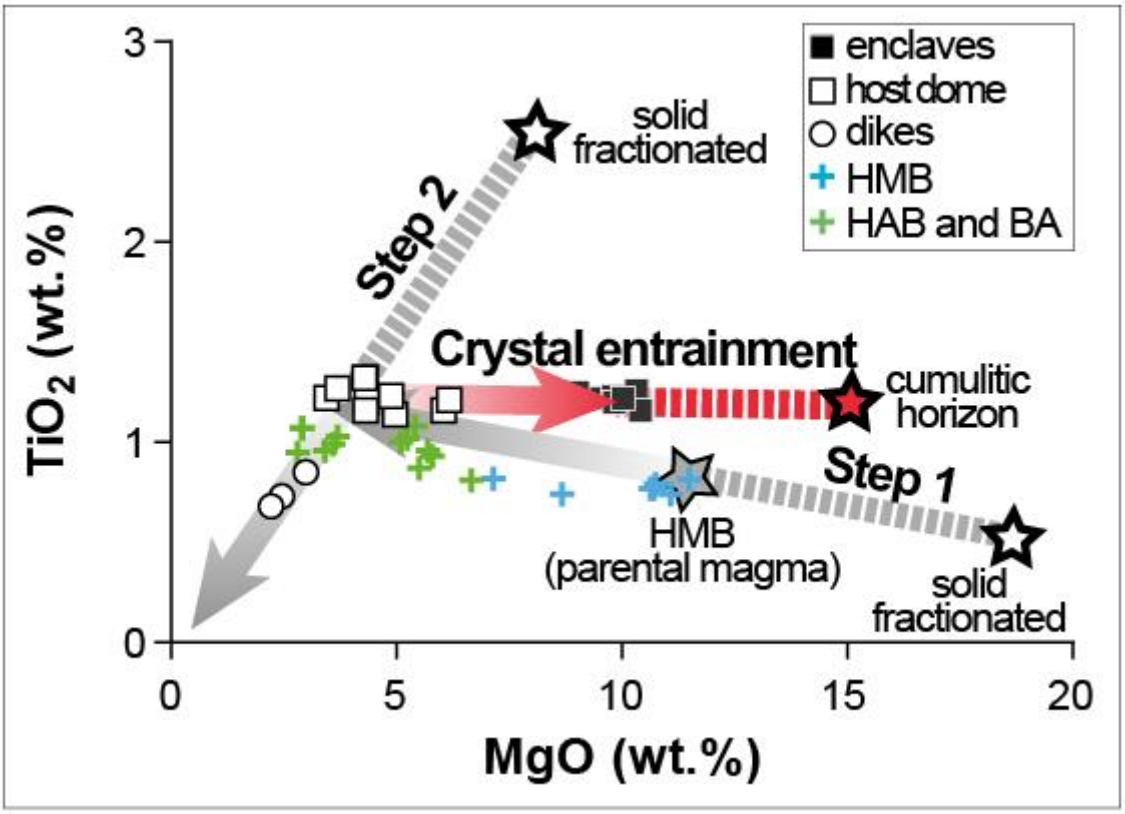

Fig. 8. MgO vs. TiO_2 diagram from modelling data in Table A8 (error bars within the symbols). A two-step calculation has been performed by subtracting 1) the enclave coarse-grained paragenesis (i.e., Fo_{86} olivine + $Mg\#_{87}$ Type 1 clinopyroxene + $Mg\#_{73}$ amphibole + An_{91} plagioclase + Usp_5 titanomagnetite) to the composition of HMB, and 2) the crystal clot paragenesis (i.e., $Mg\#_{67}$ amphibole + An_{90} plagioclase + Usp_{30} titanomagnetite) to the residual melt derived by step 1. The host dome composition is fairly reproduced (SSR = 0.44) by the crystallisation of olivine (~11%) + Type 1 clinopyroxene (~16%) + amphibole (~12%) + plagioclase (~11%) + titanomagnetite (~3%). For the case of step 2, the dike composition is also adequately reconstructed (SSR = 0.13) by subtraction of amphibole (~23%) + plagioclase (~16%) + titanomagnetite (~3%). The enclave compositions are well reproduced (SSR = 0.02-0.04) by the addition of Fo_{86} olivine (3-4%), $Mg\#_{87}$ Type 1 clinopyroxene (20-21%), $Mg\#_{73}$ amphibole (20-21%), An_{91} plagioclase (5-6%) and Usp_5 titanomagnetite (2-3%) to the basaltic andesitic magma.

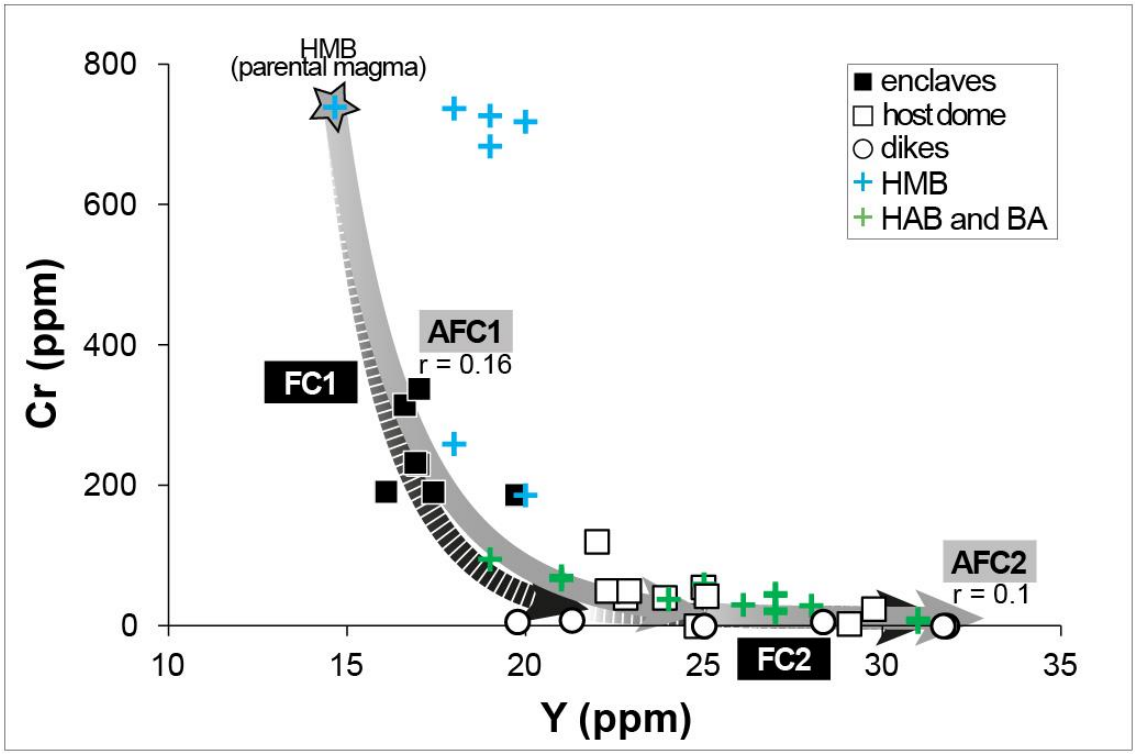

Fig. 9. Y vs. Cr diagram from fractional crystallisation (FC) and assimilation and fractional crystallisation (AFC) calculations (error bars within the symbols). Two distinct vectors are calculated accounting for the prevalent fractionation of Fo-rich olivine + Type 1 clinopyroxene (i.e., FC1 and AFC1) and $Mg\#_{67}$ amphibole + An_{90} plagioclase (i.e., FC2 and AFC2). The assimilant composition comes from Tommasini et al. (1995) and corresponds to the Hercynian granite from Sardinian-Corsan Batholith. Input and output data concerning FC and AFC modelling are listed in Table A9, together with the values of partition coefficients derived for calc-alkaline magmas.

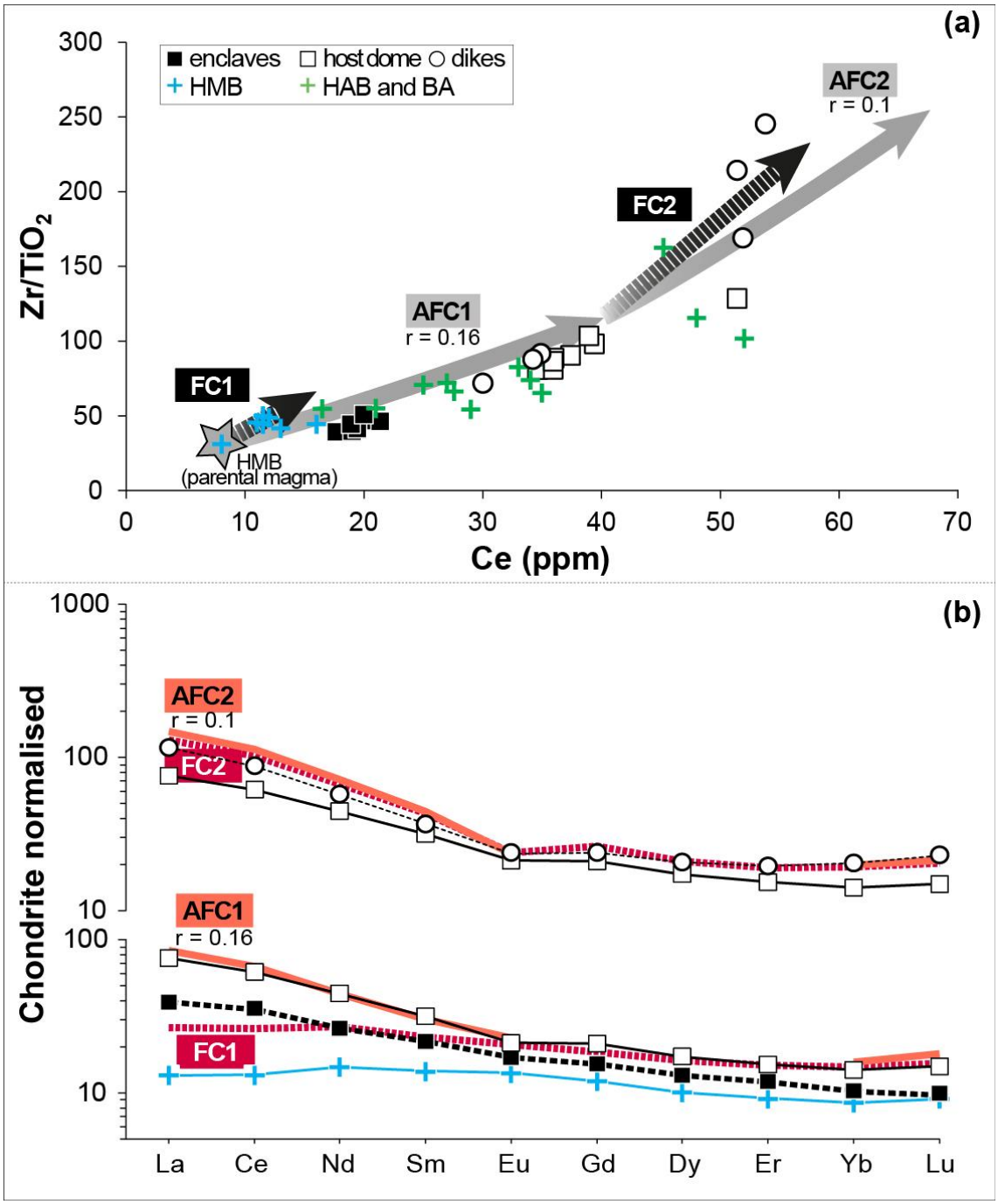

Fig. 10. Ce vs. Zr/TiO_2 ratio from fractional crystallisation (FC) and assimilation and fractional crystallisation (AFC) calculations (a). Two distinct vectors account for the prevalent fractionation of Fo-rich olivine + Type 1 clinopyroxene (i.e., FC1 and AFC1) and $Mg\#_{67}$ amphibole + An_{90} plagioclase (i.e., FC2 and AFC2). See Table A9 for further details. The FC1 vector cannot reproduce in full the transition from HMB magmas to basaltic andesites. This geochemical evolution is captured only by the AFC1 vector when the ratio of the assimilation rate to the crystallisation rate is $r = 0.16$. Both FC2 and AFC2 trajectories describe plausible differentiation paths for the basaltic andesitic magmas. The AFC2 vector denotes

lower degrees of contamination for the more differentiated products with $r = 0.1$. REE patterns from the same calculations described above confirm that crustal contribution is more effective during step 1, producing strong LREE enrichments in the basaltic andesitic melt (b). Error bars are within the symbols.

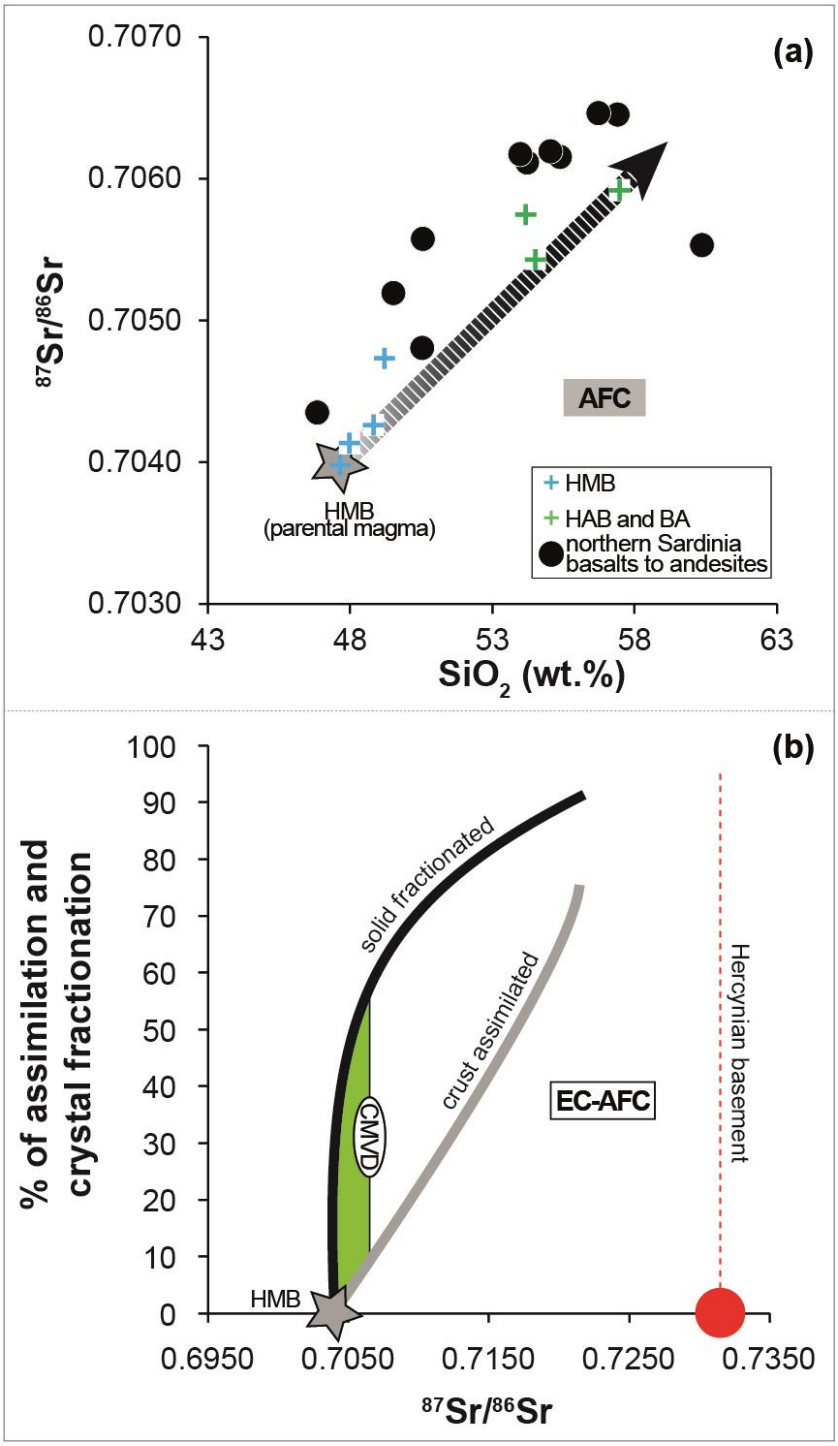

Fig. 11. SiO_2 vs. $^{87}Sr/^{86}Sr$ ratio (error bars within the symbols) of Montresta and northern Sardinia products (a). Modelling data (Tab. A10) from DePaolo (1981) indicate that the parental HMB magma ($^{87}Sr/^{86}Sr$ = 0.7039) differentiated towards the andesitic rocks ($^{87}Sr/^{86}Sr$ = 0.7062-0.7068) by assimilation of the Hercynian crust ($^{87}Sr/^{86}Sr$ = 0.732). The energy-constrained assimilation–fractional crystallisation (EC-AFC) formulation of Spera and Bohrson (2001) points out that the highest $^{87}Sr/^{86}Sr$ ratio measured for HMB products is related to a maximum crustal assimilation of 10% and fractional crystallisation of 55% (b).

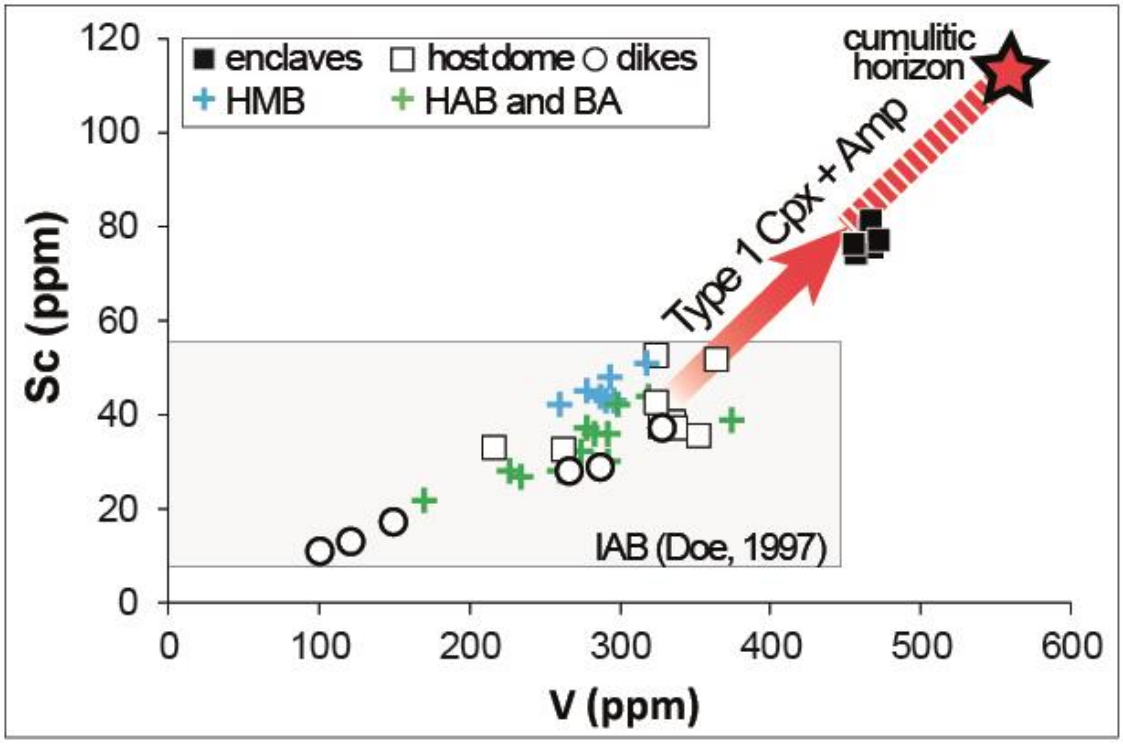

Fig. 12. V vs. Sc diagram showing as the trace element contents measured for the enclaves (error bars within the symbols) are intriguingly higher than transition elements typically measured for Island Arc Basalts (i.e., IAB; cf. Doe, 1997). The vector accounts for the entrainment of Type 1 clinopyroxene and amphibole within the basaltic andesitic host dome. The concentrations of V and Sc in Type 1 clinopyroxene and amphibole crystals come from equilibrium partitioning calculations performed on HMB (sample KBLF) and HAB (sample CM43) compositions (further details are given in Table A11). Enclaves lie on a mixing trajectory resulting from entrainment of Type 1 clinopyroxene (51%) and amphibole (49%) in the basaltic andesitic magma (the mineral content corresponds to mass balance data normalised to 100).

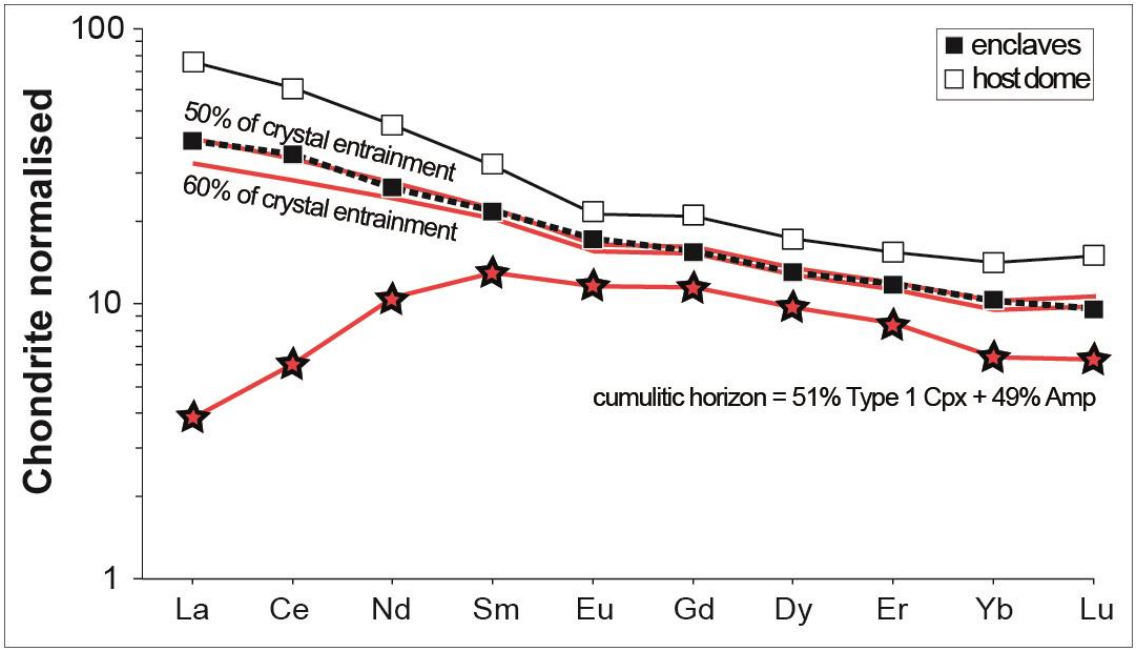

Fig. 13. Mixing calculations for REE attest that enclave compositions (error bars within the symbols) are associated with hybridisation phenomena due to entrainment of a solid fraction (50-60%) of Type 1 clinopyroxene and $Mg\#_{71-76}$ amphibole into the original basaltic andesitic magma. See Table A11 for further details.

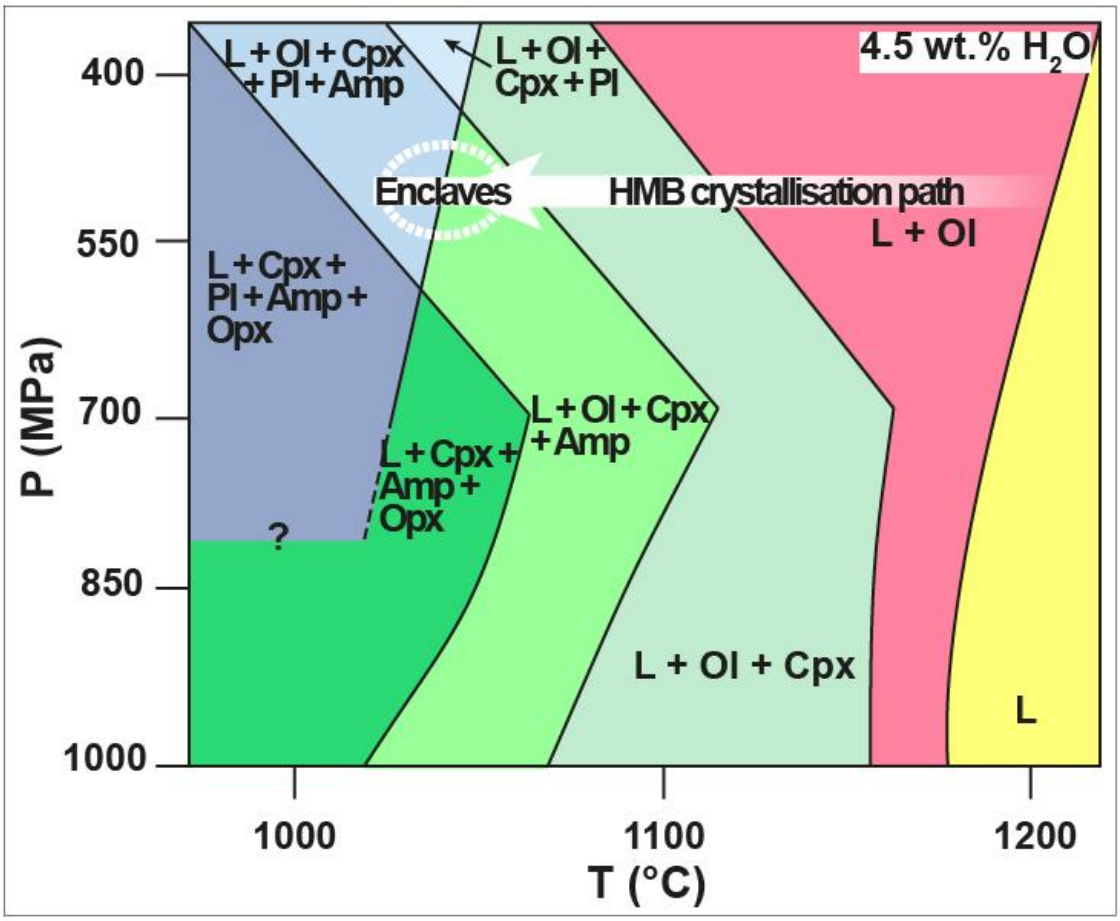

Fig. 14. Phase relations for a calc-alkaline high-Mg basalt equilibrated at *P* = 400-1000 MPa, *T* = 1000-1200 °C, H_2O = 4.5 wt.%, and fO_2 = NNO-NNO+4. (cf. Pichavant and Macdonald, 2007; Melekhova et al., 2015). Abbreviations indicate: Ol, olivine; Cpx, clinopyroxene; Opx, orthopyroxene; Amp, amphibole; Pl, plagioclase; L, liquid. Amphibole saturates the primitive basaltic liquid after the crystallisation of olivine, Cr-spinel, and clinopyroxene but before the onset of plagioclase at *P* > 400 MPa and *T* > 1030 °C.

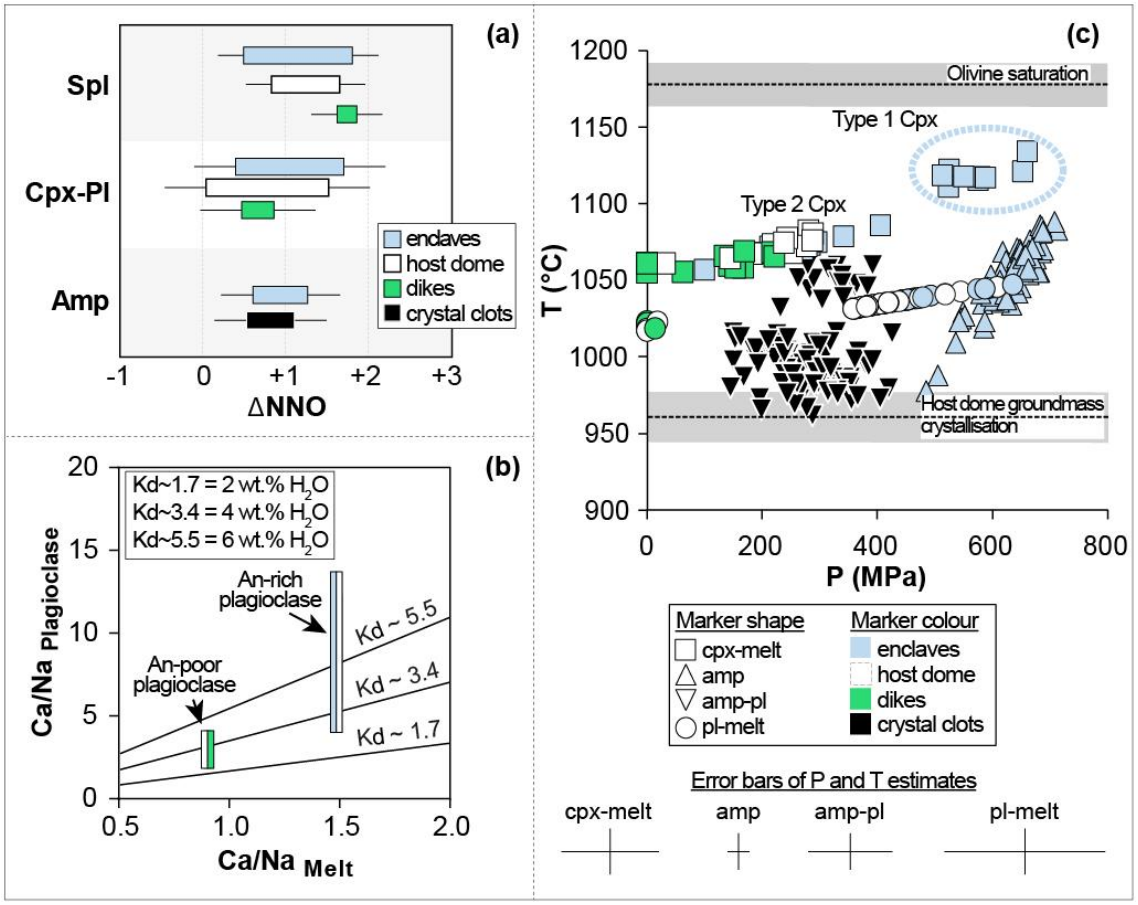

Fig. 15. Modelling data for the *P*-*T*-H_2O-fO_2 path of the system. The redox state of enclaves, host dome, dikes, and crystal clots (a) has been measured through the equations of Ariskin and Nikolaev (1996), France et al. (2010), and Ridolfi et al. (2010) based on spinel-melt (error of ±0.3 log unit), clinopyroxene-plagioclase (error of ±0.5 log unit), and amphibole-melt equilibria (error of ±0.4 log unit), respectively. The amount of H_2O in equilibrium with plagioclase has been determined through the Ca-Na exchange experimentally-derived by Sisson and Grove (1993) (b). Straight lines represent Ca-Na exchange partition coefficients derived by anhydrous ($^{pl\text{-}melt}Kd_{Ca–Na}$ = 1.1) to H_2O-saturated ($^{pl\text{-}melt}Kd_{Ca–Na}$ = 5.5) experiments. Bars represent the range of $^{pl\text{-}melt}Kd_{Ca–Na}$ measured for natural plagioclase from enclaves (light blue), host dome (white), and dikes (green). The saturation temperature of $Fo_{84\text{-}87}$ olivines from enclaves (c) has been estimated with the thermometer (error of ±29 °C) of Putirka et al. (2007). The crystallisation pressure and temperature of clinopyroxene have been calculated integrating the barometer (error of ±140 MPa) of Neave and Putirka (2017) with the P-independent thermometer (error of ±27 °C) of Putirka et al. (1996). The crystallisation conditions of plagioclase have been constrained with the model

(errors of ±240 MPa and ±26 °C) of Putirka (2005). Conversely, the formulations of Ridolfi et al. (2010) and Ridolfi and Renzulli (2012) have been adopted to retrieve, respectively, the saturation temperature (error of ±22 °C) and pressure (error of ±37 MPa) of amphibole. For the specific case of crystal clots, the barometer (error of ±150 MPa) of Molina et al. (2015) has been employed.

Chapter 2

Snapshots of primitive arc magma evolution recorded by clinopyroxene textural and compositional variations: The case study of hybrid crystal-rich enclaves from Capo Marargiu Volcanic District (Sardinia, Italy)

Vanni Tecchiato[a], Mario Gaeta[a], Silvio Mollo[a], Olivier Bachmann[b], Albrecht von Quadt[b], Piergiorgio Scarlato[c]

[a] Dipartimento di Scienze della Terra, Sapienza-Università di Roma, Piazzale Aldo Moro 5, 00185 Roma, Italy

[b] Institute of Geochemistry and Petrology, ETH Zürich, Clausiusstrasse 25, 8092 Zürich, Switzerland

[c] Istituto Nazionale di Geofisica e Vulcanologia, Via di Vigna Murata 605, 00143 Roma, Italy

Abstract

Capo Marargiu Volcanic District (CMVD) is an Oligo-Miocene calc-alkaline complex located in north-western Sardinia (Italy) and characterised by the widespread occurrence of basaltic to andesitic domes. One of these domes hosts abundant crystal-rich enclaves with millimetre-to-centimetre-sized clinopyroxenes showing intriguing textural features due to complex magma dynamics. With the aim to better understand the mechanisms governing the early evolution of the CMVD magmatic system, such clinopyroxene phenocrysts have been investigated in terms of their major, trace element and isotopic compositions. Three distinct clinopyroxene populations have been identified, i.e., Type 1, Type 2, and Type 3. Type 1 appears as the sub-rounded cores of clinopyroxenes with overgrowth textures corresponding to Type 2 and Type 3. These latter populations may also occur as single isolated crystals, i.e., Type 2 exhibits oscillatory zoning and spongy cellular textures with Type 3 overgrowths, whereas Type 3 are polycrystalline glomerocrysts with occasional Type 2 overgrowths. The crystal overgrowths are striking evidence of magma recharge dynamics. Type 1 ($^{cpx}Mg\#_{83\text{-}92}$), Type 2 ($^{cpx}Mg\#_{75\text{-}82}$), and Type 3 ($^{cpx}Mg\#_{72\text{-}79}$) are, respectively, in equilibrium with Sardinian mantle-derived high-Mg basalts (HMB with $^{melt}Mg\#_{56\text{-}73}$), more primitive (PBA with $^{melt}Mg\#_{45\text{-}56}$), and more evolved (EBA with $^{melt}Mg\#_{41\text{-}50}$) basaltic andesites. Type 1 and Type 2 are diopsidic phenocrysts evolving along a similar geochemical path (i.e., linear increase of Al, Ti, La, and Hf contents, as well as negligible Eu-anomaly) controlled by to olivine + clinopyroxene + amphibole fractionation. This differentiation path is addressed to phenocryst crystallisation from hydrous HMB and PBA magmas stalling at moderate crustal pressures. The occurrence of globular sulphides within Type 1 suggests saturation of the HMB magma with a sulphide liquid under relatively low redox conditions. Moreover, Type 1 isotopic systematics denote variable $^{87}Sr/^{86}Sr$ ratios ascribable either to assimilation of crustal material by HMB magma or a mantle source variably contaminated by crustal components. In contrast, Type 3 are augitic phenocrysts recording the effect (i.e., low Al and Ti contents associated with high La and Hf concentrations, as well as important Eu-anomaly) of plagioclase and titanomagnetite fractionation from more degassed EBA magmas ponding at shallow depths. Rare titanite associated to Type 3 and titanomagnetite crystals point to high oxidising conditions for EBA magmas. On

the other hand, the $^{87}Sr/^{86}Sr$ ratios of both Type 2 and Type 3 are almost constant, accounting for a limited interaction of PBA and EBA magmas with the country rock. The overall textural and compositional features of Type 1, Type 2, and Type 3 clinopyroxene phenocrysts lead to the conclusion that CMVD is characterised by a polybaric plumbing system where geochemically distinct magmas crystallise and mix under variable environmental conditions.

2.1. Introduction

Igneous rocks crystallised from arc magmas may show complex textural and compositional features that potentially reflect the intricate processes controlling the solidification path of the system. For example, during ascent of magma from the deep source region to a shallow storage reservoir, puzzling phenocryst textures and zoning patterns may result from resorption and remobilisation phenomena (Pyle et al., 1988; Turner et al., 2003; Dungan and Davidson, 2004), as well as from convection in a thermally and chemically zoned magma chamber (Singer et al., 1995). In arc environments, the labyrinthine architecture of the volcanic plumbing system can exert a primary control on magma evolution, implying that different magma bodies evolve separately and then eventually interact via mingling and mixing processes (e.g. Anderson, 1976; Eichelberger, 1980; Clynne, 1999). The mineral texture of hybrid products will ultimately depend on the degree of interaction between the two end-member magmas, responding to the effect of melt viscosity (e.g. Sparks and Marshall, 1986; Jellinek et al., 1999), bulk composition (Sparks and Marshall, 1986), and involved melt volume (Nakagawa et al., 2002; Streck et al., 2002; Humphreys et al., 2013). However, recharge events in shallow magma reservoirs may be cryptic and difficult to detect accounting for only the information retrieved from bulk rock analyses (e.g., Streck et al., 2002; Humphreys et al., 2006). In contrast, mineral textural and compositional variations can faithfully document the magmatic history of the system (e.g., D'Lemos, 1996; Humphreys et al., 2006; Frey and Lange, 2011). Among all the most common mineral phases, clinopyroxene nucleates and grows under a wide spectrum of crystallisation conditions, recording the pressure (Putirka, 2008; Neave and Putirka, 2017), temperature (Putirka et al., 2003; Putirka, 2008), melt-water content (Armienti et al., 2013; Perinelli et al., 2016), and oxygen fugacity (France et al., 2010) of the system. This is especially true for the case of mafic to intermediate arc magmas, where the clinopyroxene-in temperature shifts from the liquidus of high-pressure basaltic/picritic melts (e.g., Melekhova et al., 2015) to the sub-aerial solidus of the volcanic rocks (e.g., Baker and Eggler, 1987; Grove and Juster, 1989). In this framework, major and trace element zoning patterns, as well as stable and radiogenic isotope concentration in clinopyroxene are used to retrieve important information on: (i) the mantle source of primitive arc products (e.g., Sas et al., 2017), (ii) mixing processes

between compositionally distinct magmas (e.g., Nakagawa et al., 2002; Streck et al., 2002), (iii) crystal mush remobilisation phenomena (e.g., Forni et al., 2016), and (iv) extensive assimilation of the country rock by magma (e.g., Gaeta et al., 2009; Di Rocco et al., 2012).

The Capo Marargiu Volcanic District (CMVD) is a calc-alkaline complex located in north-western Sardinia (Italy) and is characterised by the occurrence of basaltic to andesitic domes and dikes. Magma dynamics at CMVD were controlled by fractional crystallisation, country rock assimilation, and crystal recycling in polybaric environments (Tecchiato et al. 2017). In this study, we present results from major, trace element and isotopic compositions of millimetre-to-centimetre-sized clinopyroxene phenocrysts from crystal-rich enclaves found in the lava domes at CMVD. The intriguing zoning patterns and complex geochemical variations of clinopyroxenes provide new insights on the mechanisms governing the early evolution of the magmatic system and evidence a complex interplay between Sardinian magmas and the continental crust stretched by back-arc tectonics.

2.2. Geological setting

The late Mesozoic-Cainozoic eastward to southward migration of the Apennine-Maghrebide fold-and-thrust belt (Carminati et al., 2012; Lustrino et al., 2004, 2009), at the subduction-collisional boundary between the upper European and the lower Ionian and Adria plates, caused (i) the back-arc stretching and boudinage of the European margin, (ii) the formation of a series of V-shaped basins and (iii) the ultimate isolation of lithospheric ribbons in the middle of Central-Western Mediterranean area (Carminati et al., 2012, and references therein). In this context, the islands of Sardinia and Corsica represent a thin slice of the European continental block between the Ligurian-Provençal and Tyrrhenian oceanic basins, left behind after a ~55-60° counter-clockwise rotation lasted from Late Oligocene to Early Miocene (Cherchi et al., 2008; Dieni et al., 2008, and references therein). Rationally, during the time span between Late Eocene - Early Miocene (Lustrino et al., 2009), the geodynamic evolution was accompanied by the widespread production of subduction-related magmas with both tholeiitic and calc-alkaline affinities. The earliest manifestation of this magmatic phase (~38 Ma) corresponded to the microdioritic body of Calabona

(north-western Sardinia), interpreted as the result of anatexis phenomena within the Hercynian lower crust (Lustrino et al., 2009). This event was chronologically isolated from the acme of productivity (22-18 Ma) recorded by the thick volcanic sequences erupted throughout the north-south Fossa Sarda graben (Lecca et al., 1997; Lustrino et al., 2004, 2009). According to the extensional structures (Lecca et al., 1997), such intense magmatism was triggered and fed by processes of mantle hydration via slab-derived fluids (Franciosi et al., 2003; Lustrino et al., 2013) coupled with adiabatic upwelling of asthenosphere (Carminati et al., 2012; Franciosi et al., 2003; Mattioli et al., 2000). Indeed, incompatible trace element variations in tholeiitic and calc-alkaline basalts to rhyolites denote the typical subduction-related geochemical signature of arc magmas (e.g., Avanzinelli et al., 2009; Duggen et al., 2005; Lustrino et al., 2011), with chondrite-normalised patterns showing LREE-enrichments and HREE-flattening, due to a metasomatised spinel-bearing mantle source (Brotzu et al., 1997b; Downes et al., 2001; Franciosi et al., 2003; Lustrino et al., 2009; Morra et al., 1997). The variation of Nd-Sr isotopes relative to SiO_2 has been interpreted to reflect three main processes: (1) interaction between mantle magmas and crustal material (Morra et al., 1997; Franciosi et al., 2003; Lustrino et al., 2013), (2) re-melting of early underplated and solidified mafic rocks (Lustrino et al., 2013), and (3) mixing between crustal-contaminated and anatectic magmas (Lustrino et al., 2013).

At the scale of a single volcanic district, such as Sarroch (Conte et al., 1997), Sant'Antioco (Conte et al., 2010), Narcao (Brotzu et al., 1997a), Arcuentu (Brotzu et al., 1997b), Sindia (Lonis et al., 1997), and Montresta (Morra et al., 1997), mafic to intermediate products almost ubiquitously delineate multiple differentiation trends. These geochemical variations have been greatly justified by the segregation of either "dry" or "wet" solid assemblages from compositionally heterogeneous progenitors crystallising in polybaric environments (e.g., Brotzu et al., 1997a; Brotzu et al., 1997b; Conte et al., 1997; Lonis et al., 1997). A similar scenario conforms to the syntectonic character of the magmatic system interacting with a crustal environment affected by extensive structural deformation (Lecca et al., 1997; Mattioli et al., 2000). Additionally, the finding of xenocrystic materials, plutonic textured enclaves, and cognate polycrystalline aggregates in the eruptive products confirms that fractional crystallisation is the principal mechanism driving Sardinian magmatism.

In north-western Sardinia (i.e., Logudoro-Bosano domain; Fig. 1a) four eruptive sequences were identified: lower andesitic, lower ignimbritic, upper andesitic, and upper ignimbritic series (Coulon and Baque, 1973; Coulon et al., 1978; Deriu, 1964). The volcanic succession is therefore structured as alternating units of bimodal compositions, corresponding to either basalt/andesite (andesitic series) or dacite/rhyolite (ignimbritic series). In addition, rare high-Mg basaltic terms, representing the most primitive products of the island (Morra et al., 1997), are also found at Montresta (Fig. 1a), ~10 km northeast of CMVD. Geochronological studies conducted with the K-Ar method constrain the four eruptive sequences between 24 ± 1.2 Ma (Montigny et al., 1981) and 16.3 ± 1.0 Ma (Coulon et al., 1974). The CMVD stratigraphy is dominated by the lower andesitic series (Fig. 1b), as large volumes of basaltic andesitic domes and andesitic autoclastic lava flows (cf. Deriu, 1964; Lecca et al., 1997). Late stage andesitic dikes and sills pervasively intrude these formations. Importantly, on the coast of Cala Bernardu (Fig. 1b), a cliff exposes the inner part of a basaltic andesitic dome hosting abundant crystal-rich enclaves (Figs. 1c). The dome appears as a yellowish, porphyritic rock with ~15% of phenocrysts, whereas the dark-grey enclaves are centimetre-to-metre-sized rounded blocks with ~50% of coarse-grained crystals (Fig. 1d). From a mineralogical, petrological, and geochemical point of view, the crystal-rich enclaves, basaltic andesitic domes, and andesitic dikes have been described in detail by Tecchiato et al. (2017) and, therefore, they are only briefly summarised in this study.

2.3. Summary of enclave petrology

Enclaves are crystal-rich, porphyritic rocks containing ~40-50% of coarse grained diopsidic to augitic clinopyroxene + Mg-hastingsitic amphibole + anorthitic to bytownitic plagioclase + Fo_{66-87} olivine + titanomagnetite ± Cr-spinel (in order of abundance). The millimetre-to-centimetre-sized minerals are dispersed in a microcrystalline groundmass of bytownitic to andesinic plagioclase + augitic clinopyroxene + titanomagnetite ± low-Ca pyroxene ± titanite. Coarse-grained diopside and Mg-hastingsite show complex textures (i.e., dissolution features and reaction rims) that reflect sharp disequilibrium effects due to open-system magma dynamics ascribable to entrainment of early-formed crystals in a compositionally distinct melt (Tecchiato et al., 2017). While olivine (Fo_{84-87}) and

clinopyroxene ($Mg\#_{83-92}$) phenocryst cores equilibrated with a high-Mg basaltic magma ($Mg\#_{64-65}$) progenitor of the CMVD stratigraphic succession, the groundmass crystallisation was controlled by the input of basaltic andesitic to andesitic magmas compositionally similar to lava domes and dikes (Tecchiato et al., 2017).

The hybrid nature of crystal-rich enclaves is also confirmed by bulk rock chemical data. Enclaves are high-Mg basalts (9.3–10.7 wt.% MgO and 46.0–48.6 wt.% SiO_2) with low Cr (186-338 ppm) and Ni (26-133 ppm) contents and high Sc (74-81 ppm) and V (457-470 ppm) concentrations in conflict with the typical mantle derived products erupted in Sardinia (i.e., Cr = 186-739 ppm, Ni = 47-226 ppm, Sc = 42-51 ppm, V = 261-318 ppm; cf. Morra et al., 1997). Moreover, primordial mantle-normalised incompatible trace element patterns of enclaves (e.g., La_N = 11.7-13.5, Ba_N = 27.3-55.5, Nb_N = 3.5-5.8) closely match with those (i.e., La_N = 10.0-27.7, Ba_N = 17.2-36.1, Nb_N = 4.5-14.0; cf. Morra et al., 1997) of more evolved basaltic to basaltic andesitic rocks erupted at Montresta (Fig. 1a).

In this framework, major and trace element modelling reveals that the coarse-grained assemblage of enclaves corresponds to the cumulitic horizon segregated during magma differentiation of the high-Mg basaltic progenitor to produce basaltic andesitic compositions (Tecchiato et al., 2017). Contextually to the emplacement of the basaltic andesitic dome, further melt infiltrated, disaggregated and reacted within the cumulate horizon, carrying ~50% of the early-formed material (Tecchiato et al., 2017).

2.4. Methods

Enclaves specimens were crushed to centimetre-sized fragments using a mechanic mill and then further disaggregated through a high voltage pulse power system. The resulting natural shaped clinopyroxenes and clinopyroxene fragments were hand-picked and set in 1-inch epoxy mounts for polishing.

Major element analyses of clinopyroxene (Tabs. B1-B3) were carried out with a Jeol-JXA8200 electron probe micro analyser (EPMA) installed at the HPHT Laboratory of Experimental Volcanology and Geophysics of the Istituto Nazionale di Geofisica e Vulcanologia (INGV) in Rome, Italy. The accelerating voltage and beam current were 15 kV and 10 nA, respectively. The beam size was 5 μm with a counting time of 20 and 10 s on peaks and background, respectively. The

following standards have been adopted for the various chemical elements: wollastonite (Si and Ca), jadeite (Na), corundum (Al), forsterite (Mg), andradite (Fe), rutile (Ti), orthoclase (K), spessartine (Mn) and chromite (Cr). The precision of the microprobe was measured through the analysis of well-characterised synthetic oxides and minerals. Data quality was ensured by analysing these test materials as unknowns following Iezzi et al. (2014).

Images were collected at the INGV using the backscattered electron (BSE) mode of a field emission gun-scanning electron microscopy (FE-SEM) Jeol 6500F equipped with an energy-dispersive spectrometer (EDS) detector.

Trace element concentrations in clinopyroxene were determined by laser ablation inductively coupled plasma mass spectrometry (LA-ICPMS) using a 193 nm Resonetics ArF excimer laser coupled with a Thermo Element XR ICP mass spectrometer at the Institute of Geochemistry and Petrology, ETH Zürich. The following geochemical groups were analysed: (i) rare earth elements (REE), including light rare earth elements (LREE; i.e., La, Ce, Pr, Nd), middle rare earth elements (MREE; i.e., Sm, Eu, Gd, Tb, Dy), and heavy rare earth elements (HREE; i.e., Ho, Er, Tm, Yb, Lu, Y), (ii) large ion lithophile elements (LILE; i.e., K, Rb, Sr, Cs, Ba), and (iii) high field strength elements (HFSE; i.e., Zr, Nb, Hf, Ta). The spot size was 29 μm and the output energy of the laser beam was typically ~3.5 J/cm^2. The MATLAB-based program SILLS (Guillong et al., 2008) was employed to calculate element concentration ratios using signal intensities obtained from NIST612/NIST610 silicate glasses as external standards measured twice every 25-30 spots to correct for drift. For each data point, the resulting ratios were converted to absolute concentrations using the internal standard of CaO content previously acquired from EPMA analyses. USGS reference glass GSD-1G was used as secondary standard to monitor the accuracy of the instrument. The precision of a single spot analysis is difficult to quantify, but replicate analyses of a homogeneous mineral or glass give precisions for element concentrations ≫LOD (limit of detection) better than 5% of the value.

Selected crystals were cut along the boundary between adjacent chemical zones using the 193 nm Resonetics ArF excimer laser. The spot size and the output energy of the laser beam adopted were 73 μm and ~4.5 J/cm^2, respectively. Prior to cutting, thick (~300-400 μm) sections of the epoxy mounts

were prepared with the aim of regularising crystal geometry and exerting an accurate control on zoning pattern propagation in the inner of crystal. This improved the precision of our technique by lowering the probability that undesired remnants of a chemical zone remained embedded in the adjacent portion after cutting. Clinopyroxene portions were sufficiently large (>$6 \cdot 10^{-2}$ mm^3) and rich in Sr (~20-25 ppm) to ensure a minimum quantity of ~3 ng of Sr (cf. Ramos and Tepley, 2008) necessary for $^{87}Sr/^{86}Sr$ measurements by thermal ionisation mass spectrometry (TIMS). Crystals were digested with a concentrated HF/HNO_3 mixture for 3 days. After evaporation, the material was re-dissolved in 2.5 N HNO_3, followed by Sr separation in PP ion exchange columns with Sr-spec resin, according to the chromatography technique of Pin et al. (1994). Strontium isotope ratios were measured on a Thermo TRITON Plus multicollector TIMS at ETH Zürich in static mode. The Sr isotope ratios are mass fractionation corrected to $^{88}Sr/^{86}Sr = 8.375209$. The NBS 987 standard measurements returned $^{87}Sr/^{86}Sr = 0.7102460 \pm 0.0000034$ (2 se; n = 14) during the period of analysis.

2.5. Clinopyroxene zoning patterns

Mineral textural (Figs. 2, 3, and 4) and compositional (Tabs. B1-B3) features discriminate three distinct clinopyroxene populations, i.e., Type 1, Type 2, and Type 3. Type 1 appears as the core of large (> 1 mm in size) clinopyroxenes with overgrowth textures corresponding to Type 2 and Type 3 populations (Fig. 2) that, however, may also occur as single isolated crystals. Type 1 shows disequilibrium dissolution features (Fig. 2a and b), predominantly sub-rounded edges (Fig. 2a), and rare spongy cellular textures associated with patchy zoning (cf. Tecchiato et al., 2017). These crystals usually contain globular inclusions of Fe + Ni + Co sulphides, that likely represent drops of an immiscible liquid (Fig. 2c). Type 2 occurs as millimetre-sized crystals with a weak reverse oscillatory zoning (Fig. 3a and c) or, alternatively, a spongy cellular texture associated with thick (0.1 - 0.5 mm) Type 3 overgrowths (Fig. 3b). In some cases, Fo_{75-79} olivine is included in Type 2 that, in turn, may be entrapped by large amphibole crystals with $Mg\#_{73-76}$ (Fig. 3c). Type 3 is typically found as millimetre-sized glomerocrysts together with plagioclase (An_{88-93}), titanomagnetite (Usp_{20-40}) and rare Fo_{66-67} olivine (Fig. 4a and b). These clinopyroxenes occasionally show Type 2 overgrowths (Fig. 4c).

According to Morimoto (1988), Type 1 and Type 2 are diopside (Wo_{44-47}-En_{44-50}-Fs_{5-9} and Wo_{45-48}-En_{40-44}-Fs_{9-14}, respectively), whereas Type 3 is augite (Wo_{41-45}-En_{41-45}-Fs_{12-16}). The Al_{tot} vs. Mg-number [Mg# = 100 · Mg/(Mg + Fe_{tot})] and Ti diagrams (Fig. 5) show that Type 1 and Type 2 evolve along a similar path controlled by olivine + clinopyroxene + amphibole fractionation (Fig. 3c and d). As a consequence, Al_{tot} and Ti increase, respectively, from 0.081 to 0.383 apfu and from 0.006 to 0.037 apfu, whereas Mg# decreases from 93 to 75. Differently, Type 3 appears as an isolated group of data recording the effect of plagioclase fractionation (Fig. 4a and b). The more evolved character of the magma causes that Al_{tot} and Mg# in Type 3 reach minimum values of 0.111 apfu and 72, respectively. This observation is also confirmed by the Zn vs Eu/Eu* (Eu_N/[$\sqrt{(Sm_N)} \times \sqrt{(Gd_N)}$]) diagram (Fig. 6a), evidencing high (0.71–0.82) and low (0.80–1.01) Eu anomalies for Type 3 and for Type 1 + Type 2, respectively. Similarly, the Y vs. Zr diagram (Fig. 6b) shows that Type 3 (plagioclase-dominated environment) is characterised by the highest concentrations of incompatible trace elements relative to Type 1 + Type 2 (olivine + clinopyroxene + amphibole - dominated environment). The REE chondrite-normalised patterns (Fig. 7) for Type 1, Type 2 and Type 3 are bell-shaped, depicting relative depletions in both LREE and HREE with respect to MREE. The REE concentrations increase from Type 1 + Type 2 to Type 3, according to the more differentiated character of the magma. The Sr isotopic composition of Type 1 evidences highly variable $^{87}Sr/^{86}Sr$ ratios (0.705815-0.707344) at the early stage of magma differentiation controlled by olivine + clinopyroxene fractionation (Fig. 8). Differently, the $^{87}Sr/^{86}Sr$ ratios remain almost constant for Type 2 and Type 3 (0.706825-0.707286), at the late stage of magmatic evolution.

2.6. Discussion

2.6.1. Magma differentiation processes

According to a number of studies (Dobosi, 1989; Simonetti et al., 1996; Cioni et al., 1998; Mollo et al., 2010; Morgan et al., 2004; Forni et al. 2017), the compositional variation of clinopyroxene closely reflect the physicochemical changes of the magmatic reservoir under the effects of both closed- and open-system processes (i.e., magma mixing/mingling, mush rejuvenation, and crust assimilation). In this context, major and trace element analyses of Type 1, Type

2, and Type 3 are potential sources of information on the mechanisms driving the differentiation of CMVD magmas in different *P*-*T*-*X*-H_2O environments.

As a first approach, the compositions of the melts hypothetically in equilibrium with the distinct clinopyroxene populations have been derived by applying the clinopyroxene-melt Fe-Mg exchange reaction [$^{cpx\text{-}melt}Kd_{Fe–Mg} = (Fe^{cpx} / Fe^{melt}) \times (Mg^{melt} / Mg^{cpx})$] proposed by Putirka (2008). This model is based on the global regression fit of equilibrium clinopyroxene-melt pairs obtained in laboratory, showing values that are not perfectly invariant and, consequently, exhibit a weak temperature dependency. Under such circumstances, the early equilibrium interval of 0.27 ± 0.03 (Putirka et al., 2003) extends to 0.28 ± 0.08 (Putirka, 2008). However, if a conservative equilibrium interval of 0.27 ± 0.03 is arbitrarily assumed, results from calculations suggest the attainment of equilibrium crystallisation between Type 1 ($^{cpx}Mg\#_{83\text{-}92}$) and mantle-derived high-Mg basalts (HMB with $^{melt}Mg\#_{56\text{-}73}$ from Montresta, Arcuentu, and Marmilla), Type 2 ($^{cpx}Mg\#_{75\text{-}82}$) and primitive basaltic andesites (PBA with $^{melt}Mg\#_{45\text{-}56}$ from Arcuentu and Sarroch), and Type 3 ($^{cpx}Mg\#_{72\text{-}79}$) and more evolved basaltic andesites (EBA with $^{melt}Mg\#_{41\text{-}50}$ from Montresta, Sindia, and Sant'Antioco). These mineral-melt equilibria evidence that the coexistence of Type 1, Type 2, and Type 3 from crystal-rich enclaves reflect open-system pre-eruptive crystallisation conditions, as well as they indicate that magma differentiation and magma mixing were the most important mechanisms contributing to the geochemical evolution of the plumbing system, as typically observed for a variety of subduction-related arc settings with calc-alkaline affinity (cf. Scarlato et al., 2017 and references therein).

The linear increase of Al_{tot} from Type 1 to Type 2 (Fig. 5) is related to the differentiation of HMB towards PBA, responding to the fractionation of mafic mineral phases. This is consistent with the low Eu-anomaly of Type 1 + Type 2 (0.80–1.01) coupled with the low concentrations of Zn (14-41 ppm; Fig. 6). Previous experimental studies (Pichavant and Macdonald, 2007; Melekhova et al., 2015) have recognised that, under high pressure and hydrous conditions, the differentiation of primitive arc magmas (i.e., HMB) located at the base of the crust is mostly driven by olivine + clinopyroxene + amphibole segregation, whereas plagioclase crystallisation is suppressed. Importantly, Type 2 compositions (6.2-8.6 wt.% Al_2O_3) have been experimentally derived by Melekhova et al. (2015) for clinopyroxenes (4.2-8.1 wt.% Al_2O_3) formed from high-Al basaltic melts (14.6-

17.9 wt.% Al_2O_3) equilibrated at P = 0.7-1.0 GPa, T = 1030-1150 °C, H_2O = 5.3-9.7 wt.%, and fO_2 = NNO – NNO+4. Coherently, barometric, thermometric, hygrometric, and oxygen barometric estimates conducted on the CMVD products by Tecchiato et al. (2017) provide constraints on the crystallisation of high-Mg basaltic to basaltic andesitic magmas at 0.5-0.7 GPa, 1030-1180 °C, 5-6 wt.% H_2O, and NNO – NNO+2. Large amphibole crystals associated with Type 2 clinopyroxenes (Fig. 3d) and olivines (Fig. 3c) testify to H_2O-rich environments where plagioclase crystallisation is delayed and possibly suppressed. From Type 1 to Type 2, the significant decrease of transition elements (i.e., Cr = 11-4628 ppm) with increasing the concentrations of incompatible elements (i.e., Zr = 0.4-27.7 ppm) suggests early and extensive crystallisation of mafic minerals (e.g., Cr-spinel + clinopyroxene + amphibole) in which Cr is prevalently incorporated (Tabs. B1-B3). In contrast, the low Al_{tot} content (Fig. 5), the evident Eu-anomaly and the high Zn concentration (Fig. 6) of Type 3 reflect clinopyroxene and plagioclase cosaturation from EBA magmas (Figs. 4a and b). Specifically, the incorporation of zincous into clinopyroxene structure is highly influenced by the activity of calcium in the melt (Gori et al., 2015). This implies that Ca fully occupies clinopyroxene M2 site, forcing Zn to enter the M1 site in six-fold coordination. Since Zn preferentially assumes a four-fold coordination (Neumann, 1949), it readily enters the M2 site becoming strongly compatible into clinopyroxene as soon as Ca-activity in the melt decreases and calcium is unable to buffer this site. In this position, zincous is accepted in the more appropriate four-fold coordination when the structural deformation is easily accommodated by the highly flexible M2 site (Gori et al., 2015). Rationally, the onset of plagioclase crystallisation indirectly lowers the Ca-activity of the melt, favouring Zn incorporation into the Type 3 crystal lattice.

The Fe_{tot}^{+2} vs. ΣTs (Ca-Tschermak + CaFe-Tschermack + CaTi-Tschermak) diagram (Fig. 9) shows that Type 1 + Type 2 describe a positive trend, as the result of HMB differentiation towards PBA magmas along an increasing water path. Indeed, Dolfi and Trigila (1978) have experimentally investigated the compositional effect produced by water dissolved in the melt on clinopyroxene, obtaining that ΣTs and Fe linearly increase (from 0.22 to 0.27 and from 0.29 to 0.41, respectively) when the melt Si-activity and Fe^{+2}/Fe^{+3} ratio get lowered under increasingly hydrous conditions (from 2.2 to 3.5 wt.% H_2O). High water contents

are known to (1) depress the saturation surface of plagioclase, expanding the stability field of olivine, clinopyroxene, and amphibole (Sisson and Grove, 1993; Melekhova et al., 2015), and (2) shift the crystallisation temperature of spinel close to the liquidus of basaltic magmas (Berndt et al., 2005). In this context, Type 1 + Type 2 clinopyroxenes with Ca-Al-rich, Fe-poor compositions preferentially crystallise from HMB + PBA magmas, accounting for the lack of plagioclase and the early fractionation of spinel. Conversely, Type 3 and plagioclase cosaturation characterise the more degassed EBA magmas, likely ponding in upper crustal reservoirs. Tecchiato et al. (2017) have estimated that Type 3 clinopyroxenes equilibrate at *P* and H_2O conditions (i.e., 0.1-0.4 GPa and 1-3 wt.%, respectively) remarkably lower than those of Type 1 + Type 2 (i.e., 0.7-1.0 GPa and 5.3-9.7 wt.%, respectively). The same finding can be extended to other volcanic districts in Sardinia (Fig. 9), according to the similar compositional features shared by Type 3 clinopyroxenes and the natural phenocrysts found in basaltic to andesitic products from Sarroch (Conte et al., 1997), Narcao (Brotzu et al., 1997a), Arcuentu (Brotzu et al., 1997b) and Sindia (Lonis et al., 1997).

The Al^{IV} vs. La and Hf diagrams (Fig. 10) confirm that Type 1 + Type 2 evolve along an almost linear path, depicting the progressive differentiation of HMB to PBA magmas. It has been greatly documented in literature that the incorporation of REE (+3 cations) into clinopyroxene structure is positively correlated with Al^{IV}, responding to the increased ease of locally balancing the excess charge at M2 site as the number of surrounding tetrahedral Al atoms increases (Hill et al., 2000; Wood and Blundy, 2001; Wood and Trigila, 2001; Tuff and Gibson, 2007; Sun and Liang, 2012; Mollo et al., 2013a, 2016, 2017; Bedard, 2014; Scarlato et al., 2014). This conforms to the differentiation of Type 1 + Type 2 that is mostly controlled by the exchange equilibria between Ca-Tschermak (CaTs) and Dipside + Hedenbergite (DiHd), where the volume changes for the solution of CaTs into DiHd are significantly low, leading to a temperature-dependent reaction (Putirka et al., 1996; Putirka, 2008; Mollo et al., 2013b). Consequently, as the temperature of the system decreases driving melt differentiation, REE contents in clinopyroxene increases through the exchange of ^{M2}Mg with ^{M1}Al coupled with the substitution of Si with Al in the tetrahedral site to form CaTs (Fig. 10). Similarly, HFSE (+4 and +5 cations) are more easily accepted into clinopyroxene crystal lattice when this coupled substitution causes a charge deficiency in the

tetrahedral site and the increase of M1 site average charge (Hill et al., 2000; Wood and Trigila, 2001; Marks et al., 2004; Mollo et al., 2013a, 2016, 2017). In this framework, Type 3 forms an isolated group of data characterised by low Al^{IV} and high Hf and La concentrations (Fig. 10) due to clinopyroxene crystallisation from a geochemically distinct magma that equilibrated at shallow and more degassed conditions in a plagioclase-dominated environment (Fig. 6).

2.6.2. Magma redox state

Textural evidence directly ascribable to magma redox conditions account for fO_2 variations from HMB + PBA to EBA magmas. The occurrence of globular sulphides within Type 1 (Fig. 2c) suggests saturation of HMB melt with a sulphide liquid (cf. Hattori, 1996). Depending on magma fO_2 conditions, sulphur is found either as S^{2-} (with minor HS^-) or as $(SO_4)^{2-}$ (Katsura and Nagashima, 1974; Carroll and Rutherford, 1988). According to Carroll and Rutherford (1988), the redox boundary of dissolved sulphur species is one log fO_2 unit above the NNO buffer. Therefore, globular sulphides within Type 1 indicates that S^{2-} is the predominant sulphur species dissolved in the HMB, testifying to oxygen fugacity below NNO+1 (e.g., Parat et al., 2011). These estimates match with those provided by Morra et al. (1997) for Montresta HMB (NNO – NNO+1) and by Tecchiato et al. (2017) for amphibole crystals in equilibrium with Type 2 clinopyroxenes from PBA magmas (NNO+0.7 and NNO+1.1). Conversely, rare titanite crystals occur in the groundmass of the enclaves together with Type 3 + plagioclase + titanomagnetite, perhaps indicating slightly higher oxidising conditions for the EBA products. For example, it has been reported in literature that magnetite and titanite coexist in intermediate to silicic magmas under the effect of increasing buffering conditions from NNO+1 to NNO+2 (Lipman, 1971; Nakada, 1991; Verhoogen, 1962; Wones, 1981).

2.6.3. Magma recharge dynamics and crustal contamination

The textural and compositional changes of clinopyroxenes from crystal-rich enclaves found at CMVD are clear evidence of polybaric crystallisation events that took place in geochemically distinct magmas ascending along the plumbing system of the volcano. On one hand, hydrous and poorly differentiated HMB + PBA magmas crystallised olivine + clinopyroxene + amphibole at relatively high

pressures under the effect of more reduced oxygen fugacity conditions. On the second hand, degassed and highly differentiated EBA magmas ponded at shallow crustal levels, favouring clinopyroxene + plagioclase formation in a more oxidised environment. The crystal cargo from enclaves is characterised by overgrowth features (e.g., Figs. 2, 3a and b, 4c) that are striking evidence of magma recharge dynamics. Rationally, oscillatory zoned Type 2 (Figs. 3a and c) testifies to multiple injections of new PBA magma batches, segregating from the mafic HMB system after an early fractionation stage of Fo_{84-87} olivine + Cr-spinel + Type 1. In this view, Type 1 represents antecrystic material transported and dispersed in the main PBA magma body, where partial resorption phenomena took place (Fig. 2b). Differently, Type 3 corresponds to the final crystallisation stage of EBA magmas, carrying Type 1 + Type 2 xenocrysts (Figs. 2a, 3a and b) while ascending towards the upper parts of the plumbing system. Note that the rare Type 2 overgrowths surrounding Type 3 (Fig. 4c) account also for the input of EBA into the marginal regions of the PBA magma body.

While the negative trend depicted by the $^{87}Sr/^{86}Sr$ vs. Mg# diagram (Fig. 8) may potentially suggest assimilation of crustal material by HMB magma during Type 1 crystallisation, the less pronounced variation observed for Type 2 and Type 3 is consistent with negligible PBA and EBA interaction with the country rock. This scenario agrees with the AFC (Assimilation and Fractional Crystallisation) modelling data derived by Tecchiato et al. (2017), denoting as the ratio of the assimilation rate to the crystallisation rate decreases from 0.16 to 0.10 along the overall differentiation path of magma. The broad scattering ($^{87}Sr/^{86}Sr$ = 0.70595-0.70681) of the most primitive (>$Mg\#_{90}$) Type 1 can be plausibly inherited from a mantle source variably contaminated by crustal components. In this view, bulk rock isotopic data from literature (cf. Franciosi et al., 2003; Franciosi et al., 2003; Lustrino et al., 2009) reveal that Sardinian HMB magmas are compositionally heterogeneous ($^{87}Sr/^{86}Sr$ = 0.70399 – 0.70631 and $^{206}Pb/^{204}Pb$ = 18.609 – 18.707) due to the distinctive addition of fluids from both oceanic crust (0.1-0.5%; $^{87}Sr/^{86}Sr$ = 0.70450 and $^{206}Pb/^{204}Pb$ = 18.300) and pelagic sediments (0.035-0.08%; $^{87}Sr/^{86}Sr$ = 0.71985 and $^{206}Pb/^{204}Pb$ = 18.985) to a depleted spinel-bearing mantle wedge ($^{87}Sr/^{86}Sr$ = 0.70250 and $^{206}Pb/^{204}Pb$ = 18.100).

2.7. Conclusive remarks

Clinopyroxene phenocrysts found in crystal-rich enclaves from a basaltic andesitic dome at CMVD have been the object of the present study. Results from detailed petrographic and geochemical analyses lead to the following conclusions:

1. Type 1 + Type 2 clinopyroxenes formed during the differentiation of a HMB parental magma towards PBA compositions by olivine + clinopyroxene + amphibole fractionation under high *P*-H_2O and low-fO_2 conditions;
2. Type 3 clinopyroxene + plagioclase + titanomagnetite cosaturation occurred in a degassed and more evolved EBA magma ponding at shallow crustal level under oxidised buffering conditions;
3. Type 1 + Type 2 clinopyroxenes represent the xenocrystic cargo entrained in the EBA magma during ascent towards the surface;
4. Type 1 isotopic compositions reflect assimilation of crustal material at the early stage of HMB crystallisation, whereas Type 2 and Type 3 account for limited to negligible interaction of PBA and EBA magmas with the country rock;
5. Scattering of Type 1 isotopic data for clinopyroxene phenocrysts with Mg#>90 testify to the presence of a heterogeneous mantle source.

Acknowledgments

This work was supported by the “CRYSTMAG” project, “#000047 Avvio alla Ricerca” project and doctoral scholarship at Sapienza - Università di Roma. F. Forni, D. Szymanowski, B. Ellis, M. Guillong, J. Sliwinski, Y. Buret, S. Large, and M. Nazzari are acknowledged for their valuable help, suggestions, and assistance during sample preparation and analytical work. A. Parmigiani is also acknowledged for the logistical support provided during V.T. staying at ETH Zürich.

References

Anderson, A. T., 1976. Magma mixing: petrological process and volcanological tool. Journal of Volcanology and Geothermal Research 1, 3–33.

Armienti, P., Perinelli, C., Putirka, K.D., 2013. A new model to estimate deep-level magma ascent rates, with applications to Mt. Etna (Sicily, Italy). J. Petrol. 54, 795–813. doi:10.1093/petrology/egs085

Avanzinelli, R., Lustrino, M., Mattei, M., Melluso, L., Conticelli, S., 2009. Potassic and ultrapotassic magmatism in the circum-Tyrrhenian region: Significance of carbonated pelitic vs. pelitic sediment recycling at destructive plate margins. Lithos 113, 213–227. doi:10.1016/j.lithos.2009.03.029

Baker, D. R., Eggler, D. H., 1987. Compositions of anhydrous and hydrous melts coexisting with plagioclase, augite, and olivine or low-Ca pyroxene from 1 atm to 8 kbar; application to the Aleutian volcanic center of Atka. American Mineralogist, 72(1-2), 12-28.

Bédard, J.H., 2014. Parameterizations of calcic clinopyroxene-melt trace element partition coefficients. Geochemistry, Geophysics, Geosystems 15, 303–336. https://doi.org/10.1002/2013GC005112

Berndt, J., Koepke, J., Holtz, F., 2004. An experimental investigation of the influence of water and oxygen fugacity on differentiation of MORB at 200 MPa. Journal of Petrology, 46(1), 135-167.

Brotzu, P., Callegari, E., Morra, V., Ruffini, R., 1997a. The orogenic basalt-andesite suites from the Tertiary volcanic complex of Narcao, SW-Sardinia (Italy): petrology, geochemistry and Sr-isotope characteristics. Period. di Mineral. 66, 101–150.

Brotzu, P., Lonis, R., Melluso, L., Morbidelli, L., Traversa, G., Franciosi, L., 1997b. Petrology and evolution of calcalkaline magmas from the Arcuentu volcanic complex (SW Sardinia, Italy). Period. di Mineral. 66, 151–184.

Carminati, E., Lustrino, M., Doglioni, C., 2012. Geodynamic evolution of the central and western Mediterranean: Tectonics vs. igneous petrology constraints. Tectonophysics 579, 173–192. doi:10.1016/j.tecto.2012.01.026

Carroll, M. R., Rutherford, M. J., 1988. Sulfur speciation in hydrous experimental glasses of varying oxidation state: results from measured wavelength shifts of sulfur X-rays. American Mineralogist 73, 845–849.

Cherchi, A., Mancin, N., Montadert, L., Murru, M., Putzu, M.T., Schiavinotto, F., Verrubbi, V., 2008. The stratigraphic response to the Oligo-Miocene extension in

the western Mediterranean from observations on the Sardinia graben system (Italy). Bull. la Société géologique Fr. 179, 267–287.

Cioni, R., Marianelli, P., Santacroce, R., 1998. Thermal and compositional evolution of the shallow magma chambers of Vesuvius: evidence from pyroxene phenocrysts and melt inclusions, Journal Geophys. Res., 103, 277-18, 294.

Clynne, M.A., 1999. A complex magma mixing origin for rocks erupted in 1915, Lassen Peak, California. J. Petrol. 40, 105–132. doi:10.1093/petroj/40.1.105

Conte, A., 1997. Petrology and geochemistry of Tertiary calcalkaline magmatic rocks from the Sarroch district (Sardinia, Italy). Period. di Mineral. 66, 63–100.

Conte, A.M., Palladino, D.M., Perinelli, C., Argenti, E., 2010. Petrogenesis of the high-alumina basalt-andesite suite from Sant'Antioco Island, SW Sardinia, Italy. Period. di Mineral. 79, 27–55. doi:10.2451/2010PM0002

Coulon, C., Baque, L., 1973. Les andésites cénozoïques et les laves associées en Sardaigne Nord-Occidentale (Provinces du Logudoro et du Bosano) - Caractères minéralogiques et chimiques. Contrib. to Mineral. Petrol. doi:10.1007/BF00371502

Coulon, C., Demant, A., & Bellon, H., 1974. Premières datations par la méthode K/Ar de quelques laves cénozoïques et quaternaires de Sardaigne Nord-Occidentale. Tectonophysics, 22(1-2), 41-57.

Coulon, C., Dostal, J., Dupuy, C., 1978. Petrology and geochemistry of the ignimbrites and associated lava domes from N.W. Sardinia. Contrib. Miner. Pet. 68, 89–98.

D'Lemos, R. S., 1996. Mixing between granitic and dioritic crystal mushes, Guernsey, Channel Islands, UK. Lithos 38, 233–257.

Deriu, M., 1964. Notizie sulla costituzione geologica del Bosano, della Planargia e del Montiferro settentrionale e occidentale. Tipografia Bernardi.

Di Rocco, T., Freda, C., Gaeta, M., Mollo, S., Dallai, L., 2012. Magma chambers emplaced in carbonate substrate: petrogenesis of skarn and cumulate rocks and implications for CO2 degassing in volcanic areas. Journal of Petrology, 53(11), 2307-2332.

Dieni, I., Massari, F., Médus, J., 2008. Age, depositional environment and stratigraphic value of the Cuccuru 'e Flores Conglomerate: insight into the Palaeogene to Early Miocene geodynamic evolution of Sardinia. Bull. la Société Géologique Fr. 179(1), 51-72.

Dobosi, G., 1989. Clinopyroxene zoning patterns in the young alkali basalts of Hungary and their petrogenetic significance, Contrib. Mineral. Petrol., 101, 112-121.

Dolfi, D., Trigila, R., 1978. The role of water in the 1944 Vesuvius eruption. Contrib. to Mineral. Petrol. 67, 297–304.

Downes, H., Thirlwall, M. F., Trayhorn, S. C., 2001. Miocene subduction-related magmatism in southern Sardinia: Sr–Nd-and oxygen isotopic evidence for mantle source enrichment. Journal of Volcanology and Geothermal Research, 106(1), 1-22.

Duggen, S., Hoernle, K., van den Bogaard, P., Garbe-Schönberg, D., 2005. Post-collisional transition from subduction-to intraplate-type magmatism in the westernmost Mediterranean: Evidence for continental-edge delamination of subcontinental lithosphere. J. Petrol. doi:10.1093/petrology/egi013

Dungan, M.A., Davidson, J., 2004. Partial assimilative recycling of the mafic plutonic roots of arc volcanoes: an example from the Chilean Andes. Geology 32, 773–776. doi:10.1130/G20735.1

Eichelberger, J. C., 1980. Vesiculation of mafic magma during replenishment of silicic magma reservoirs. Nature, 288(5790), 446-450.

Foden, J.D., Green, D.H., 1992. Possible role of amphibole in the origin of andesite: some experimental and natural evidence. Contrib. to Mineral. Petrol. 109, 479–493. doi:10.1007/BF00306551

Forni, F., Bachmann, O., Mollo, S., De Astis, G., 2016. The origin of a zoned ignimbrite: insights into the Campanian Ignimbrite magma chamber (Campi Flegrei, Italy). Earth Planet. Sci. Lett. 449, 259–271. doi:10.1016/j.epsl.2016.06.003

France, L., Ildefonse, B., Koepke, J., Bech, F., 2010. A new method to estimate the oxidation state of basaltic series from microprobe analyses. J. Volcanol. Geotherm. Res. 189, 340–346. doi:10.1016/j.jvolgeores.2009.11.023

Franciosi, L., Lustrino, M., Melluso, L., Morra, V., D'Antonio, M., 2003. Geochemical characteristics and mantle sources of the Oligo-Miocene primitive basalts from Sardinia: The role of subduction components. Ofioliti 28, 105–114.

Frey, H.M., Lange, R.A., 2011. Phenocryst complexity in andesites and dacites from the Tequila volcanic field, Mexico: Resolving the effects of degassing vs. magma mixing. Contrib. to Mineral. Petrol. 162, 415–445. doi:10.1007/s00410-010-0604-1

Gaeta, M., Di Rocco, T., Freda, C., 2009. Carbonate assimilation in open magmatic systems: the role of melt-bearing skarns and cumulate-forming processes. Journal of Petrology, 50(2), 361-385.

Gori, C., Tribaudino, M., Mantovani, L., Delmonte, D., Mezzadri, F., Gilioli, E., Calestani, G., 2015. Ca-Zn solid solutions in C2/c pyroxenes: Synthesis, crystal structure, and implications for Zn geochemistry. American Mineralogist, 100(10), 2209-2218.

Grove, T.L., Juster, T.C., 1989. Experimental investigations of low-Ca pyroxene stability and olivine-pyroxene-liquid equilibria at 1-atm in natural basaltic and andesitic liquids. Contrib. to Mineral. Petrol. 103, 287–305. doi:10.1007/BF00402916

Guillong, M., Meier, D.L., Allan, M.M., Heinrich, C.A., Yardley, B.W.D., 2008. SILLS: aMATLAB-based program for the reduction of laser ablation ICP-MS data of homogeneous materials and inclusions. Short Course Notes -Geol. Assoc. Can.40, 328–333.

Hattori, K., 1996. Occurrence and origin of sulfide and sulfate in the 1991 Mount Pinatubo eruption products. Fire and Mud: Eruptions and Lahars of Mount Pinatubo, Philippines, 807-824.

Hill, E., Wood, B. J., Blundy, J. D., 2000. The effect of Ca-Tschermaks component on trace element partitioning between clinopyroxene and silicate melt. Lithos, 53(3), 203-215. https://doi.org/10.1016/S0024-4937(00)00025-6

Humphreys, M.C.S., Blundy, J.D., Sparks, R.S.J., 2006. Magma evolution and open-system processes at Shiveluch Volcano: Insights from phenocryst zoning. J. Petrol. 47, 2303–2334. doi:10.1093/petrology/egl045

Humphreys, M.C.S., Edmonds, M., Plail, M., Barclay, J., Parkes, D., Christopher, T., 2013. A new method to quantify the real supply of mafic components to a hybrid andesite. Contrib. to Mineral. Petrol. 165, 191–215. doi:10.1007/s00410-012-0805-x

Iezzi, G., Mollo, S., Shahini, E., Cavallo, A., Scarlato, P., 2014. The cooling kinetics of plagioclase feldspar as revealed by electron-microprobe mapping. Am. Mineral. 99, 898–907. doi:10.2138/am.2014.4626

Jellinek, A. M., Kerr, R. C. & Griffiths, R. W., 1999. Mixing and compositional stratification produced by natural convection. 1. Experiments and their application to Earth's core and mantle. Journal of Geophysical Research 104(B4), 7183–7201.

Katsura, T., Nagashima, S., 1974. Solubility of sulfur in some magmas at 1 atmosphere. Geochimica et Cosmochimica Acta, 38(4), 517-531.

Lecca, L., Lonis, R., Luxoro, S., Melis, E., Secchi, F., Brotzu, P., 1997. Oligo-Miocene volcanic sequences and rifting stages in Sardinia: a review. Period. di Mineral. 66, 7–61.

Lipman, P. W., 1971. Iron-titanium oxide phenocrysts in compositionally zoned ash-flow sheets from southern Nevada. The Journal of Geology, 79(4), 438-456.

Lonis, R., Morra, V., Lustrino, M., Melluso, L., Secchi, F., 1997. Plagioclase textures, mineralogy and petrology of Tertiary orogenic volcanic rocks from Sindia (central Sardinia). Period. di Mineral. 66, 185–210.

Lustrino, M., Duggen, S., Rosenberg, C.L., 2011. The Central-Western Mediterranean: Anomalous igneous activity in an anomalous collisional tectonic setting. Earth-Science Rev. doi:10.1016/j.earscirev.2010.08.002

Lustrino, M., Fedele, L., Melluso, L., Morra, V., Ronga, F., Geldmacher, J., Duggen, S., Agostini, S., Cucciniello, C., Franciosi, L., Meisel, T., 2013. Origin and evolution of Cenozoic magmatism of Sardinia (Italy). A combined isotopic (Sr-Nd-Pb-O-Hf-Os) and petrological view. Lithos 180–181, 138–158. doi:10.1016/j.lithos.2013.08.022

Lustrino, M., Morra, V., Fedele, L., Franciosi, L., 2009. Beginning of the Apennine subduction system in central western Mediterranean: Constraints from Cenozoic

"orogenic" magmatic activity of Sardinia, Italy. Tectonics 28, 1–23. doi:10.1029/2008TC002419

Lustrino, M., Morra, V., Melluso, L., Brotzu, P., D'Amelio, F., Fedele, L., Franciosi, L., Lonis, R., Lieberckнecht, A.M.P., 2004. The Cenozoic igneous activity of Sardinia. Period. di Mineral. 73, 105–134.

Marks, M., Halama, R., Wenzel, T., Markl, G., 2004. Trace element variations in clinopyroxene and amphibole from alkaline to peralkaline syenites and granites: Implications for mineral-melt trace-element partitioning. Chem. Geol. 211, 185–215. https://doi.org/10.1016/j.chemgeo.2004.06.032

Mattioli, M., Guerrera, F., Tramontana, M., Raffaelli, G., D'Atri, M., 2000. High-Mg Tertiary basalts in Southern Sardinia (Italy). Earth Planet. Sci. Lett. 179, 1–7. doi:10.1016/S0012-821X(00)00103-5

McDonough, W. F., Sun, S. S., 1995. The composition of the Earth. Chemical geology, 120(3-4), 223-253.

Melekhova, E., Blundy, J., Robertson, R., Humphreys, M.C.S., 2015. Experimental evidence for polybaric differentiation of primitive arc basalt beneath St. Vincent, Lesser Antilles. J. Petrol. 56, 161–192. doi:10.1093/petrology/egu074

Mollo, S., Blundy, J.D., Giacomoni, P., Nazzari, M., Scarlato, P., Coltorti, M., Langone, A., Andronico, D., 2017. Clinopyroxene-melt element partitioning during interaction between trachybasaltic magma and siliceous crust: Clues from quartzite enclaves at Mt. Etna volcano. Lithos 284–285, 447–461. https://doi.org/10.1016/j.lithos.2017.05.003.

Mollo, S., Forni, F., Bachmann, O., Blundy, J.D., De Astis, G., Scarlato, P., 2016. Trace element partitioning between clinopyroxene and trachy-phonolitic melts: A case study from the Campanian ignimbrite (Campi Flegrei, Italy). Lithos 252–253, 160–172. doi:10.1016/j.lithos.2016.02.024.

Mollo, S., Blundy, J. D., Iezzi, G., Scarlato, P., Langone, A., 2013a. The partitioning of trace elements between clinopyroxene and trachybasaltic melt during rapid cooling and crystal growth. Contributions to Mineralogy and Petrology, 166(6), 1633-1654.

Mollo, S., Putirka, K., Misiti, V., Soligo, M., Scarlato, P., 2013b. A new test for equilibrium based on clinopyroxene-melt pairs: Clues on the solidification temperatures of Etnean alkaline melts at post-eruptive conditions. Chemical Geology 352, 92-100. doi: 10.1016/j.chemgeo.2013.05.026.

Mollo, S., Gaeta, M., Freda, C., Di Rocco, T., Misiti, V., Scarlato, P., 2010. Carbonate assimilation in magmas: a reappraisal based on experimental petrology. Lithos, 114(3), 503-514.

Montigny, R., Edel, J.B., Thuizat, R., 1981. Oligo-Miocene rotation of Sardinia: K-Ar ages and paleomagnetic data of Tertiary volcanics. Earth Planet. Sci. Lett. 54, 261–271. doi:10.1016/0012-821X(81)90009-1

Morgan, D. J., Blake, S., Rogers, N. W., DeVivo, B., Rolandi, G., Macdonald, R., Hawkesworth, C. J., 2004. Time scales of crystal residence and magma chamber volume from modelling of diffusion profiles in phenocrysts: Vesuvius 1944. Earth and Planetary Science Letters, 222(3), 933-946.

Morimoto, N., 1988. Nomenclature of Pyroxenes. Mineral. Petrol. 39, 55–76. doi:10.1007/BF01226262

Morra, V., Secchi, F. a. G., Melluso, L., Franciosi, L., 1997. High-Mg subduction-related Tertiary basalts in Sardinia, Italy. Lithos 40, 69–91. doi:10.1016/S0024-4937(96)00028-X

Nakada, S., 1991. Magmatic processes in titanite-bearing dacites, central Andes of Chile and Bolivia. American Mineralogist 76, 548-560.

Nakagawa, M., Wada, K., Wood, C.P., 2002. Mixed Magmas, Mush Chambers and Eruption Triggers: Evidence from Zoned Clinopyroxene Phenocrysts in Andesitic Scoria from the 1995 Eruptions of Ruapehu Volcano, New Zealand. J. Petrol. 43, 2279–2303. doi:10.1093/petrology/43.12.2279

Neave, D. A., & Putirka, K. D., 2017. A new clinopyroxene-liquid barometer, and implications for magma storage pressures under Icelandic rift zones. American Mineralogist, 102(4), 777-794.

Neumann, H., 1949. Notes on the mineralogy and geochemistry of zinc. Mineral. Mag, 28, 575-581.

Parat, F., Holtz, F., Streck, M. J., 2011. Sulfur-bearing magmatic accessory minerals. Reviews in Mineralogy and Geochemistry, 73(1), 285-314.

Perinelli, C., Mollo, S., Gaeta, M., De Cristofaro, S. P., Palladino, D. M., Armienti, P., Scarlato, P., Putirka, K. D., 2016. An improved clinopyroxene-based hygrometer for Etnean magmas and implications for eruption triggering mechanisms. American Mineralogist, 101(12), 2774-2777.

Pichavant, M., Macdonald, R., 2007. Crystallization of primitive basaltic magmas at crustal pressures and genesis of the calc-alkaline igneous suite: Experimental evidence from St Vincent, Lesser Antilles arc. Contrib. to Mineral. Petrol. 154, 535–558. doi:10.1007/s00410-007-0208-6

Pin, C., Briot, D., Bassin, C., Poitrasson, F., 1994. Concomitant separation of strontium and samarium-neodymium for isotopic analysis in silicate samples, based on specific extraction chromatography. Anal Chim Acta 298:209–217. doi:10.1016/0003-2670(94)00274-6

Putirka, K., Johnson, M., Kinzler, R., Longhi, J., Walker, D., 1996. Thermobarometry of mafic igneous rocks based on clinopyroxene-liquid equilibria, 0-30 kbar. Contrib. to Mineral. Petrol. 123, 92–108. https://doi.org/10.1007/s004100050145

Putirka, K.D., 2008. Thermometers and Barometers for Volcanic Systems. Rev. Mineral. Geochemistry 69, 61–120. doi:10.2138/rmg.2008.69.3

Putirka, K.D., Mikaelian, H., Ryerson, F., Shaw, H., 2003. New clinopyroxene-liquid thermobarometers for mafic, evolved, and volatile-bearing lava compositions, with applications to lavas from Tibet and the Snake River Plain, Idaho. Am. Mineral. 88, 1542–1554. doi:10.2138/am.2005.431

Pyle, D. M., Ivanovich, M., Sparks, R. S. J., 1988. Magma–cumulate mixing identified by U–Th disequilibrium dating. Nature 331, 157–159.

Ramos, F. C., Tepley, F. J., 2008. Inter-and intracrystalline isotopic disequilibria: techniques and applications. Reviews in Mineralogy and Geochemistry, 69(1), 403-443.

Sas, M., Debari, S. M., Clynne, M. A., Rusk, B. G., 2017. Using mineral geochemistry to decipher slab, mantle, and crustal input in the generation of high-

Mg andesites and basaltic andesites from the northern Cascade Arc. American Mineralogist, 102(5), 948-965.

Scarlato, P., Mollo, S., Del Bello, E., Von Quadt, A., Richard, J.B., Gutierrez, E., Martinez-Hackert, B., Papale, P., 2017. The 2013 eruption of Chaparrastique volcano (El Salvador): Effects of magma storage, mixing, and decompression. Chemical Geology 448, 110-122, http://dx.doi.org/10.1016/j.chemgeo.2016.11.015.

Scarlato, P., Mollo, S., Blundy, J.D., Iezzi, G., Tiepolo, M., 2014. The role of natural solidification paths on REE partitioning between clinopyroxene and melt. Bull. Volcanol. 76, 1–4. https://doi.org/10.1007/s00445-014-0810-1

Simonetti, A., Shore, M., Bell, K, 1996. Diopside phenocrysts from nephelinite lavas, Napak volcano eastern Uganda: evidence for magma mixing, Can. Mineral., 34, 411-421.

Singer, B.S., Dungan, M.A., Layne, G.D., 1995. Textures and Sr, Ba, Mg, Fe, K, and Ti compositional profiles in volcanic plagioclase: clues to the dynamics of calc-alkaline magma chambers. Am. Mineral. 80, 776–798. doi:10.2138/am-1995-7-815

Sparks, R. S. J., Marshall, L. A., 1986. Thermal and mechanical constraints on mixing between mafic and silicic magmas. Journal of Volcanology and Geothermal Research 29, 99–124.

Streck, M.J., Dungan, M.A., Malavassi, E., Reagan, M.K., Bussy, F., 2002. The role of basalt replenishment in the generation of basaltic andesites of the ongoing activity at Arenal volcano, Costa Rica: Evidence from clinopyroxene and spinel. Bull. Volcanol. 64, 316–327. doi:10.1007/s00445-002-0209-2

Sun, C., Liang, Y., 2012. Distribution of REE between clinopyroxene and basaltic melt along a mantle adiabat: Effects of major element composition, water, and temperature. Contrib. to Mineral. Petrol. 163, 807–823. https://doi.org/10.1007/s00410-011-0700-x

Tecchiato, V., Gaeta, M., Mollo, S., Scarlato, P., Bachmann, O., Perinelli, C., 2017. Petrological constraints on the high-Mg basalts from Capo Marargiu (Sardinia, Italy): Evidence of cryptic amphibole fractionation in polybaric environments. Journal of Volcanology and Geothermal Research.

Tuff, J., Gibson, S.A., 2007. Trace-element partitioning between garnet, clinopyroxene and Fe-rich picritic melts at 3 to 7 GPa. Contrib. to Mineral. Petrol. 153, 369–387. https://doi.org/10.1007/s00410-006-0152-x

Turner, S., George, R., Jerram, D. A., Carpenter, N., Hawkesworth, C., 2003. Case studies of plagioclase growth and residence times in island arc lavas from Tonga and the Lesser Antilles, and a model to reconcile discordant age information. Earth and Planetary Science Letters 214, 279–294.

Verhoogen, J., 1962. Distribution of titanium between silicates and oxides in igneous rocks. American Journal of Science, 260(3), 211-220.

Wones, D. R., 1981. Mafic silicates as indicators of intensive variables in granitic magmas. Mining Geology, 31(168), 191-212.

Wood, B.J., Blundy, J.D., 2001. The effect of cation charge on crystal–melt partitioning of trace elements. Earth Planet. Sci. Lett. 188, 59–71. https://doi.org/10.1016/S0012-821X(01)00294-1

Wood, B.J., Trigila, R., 2001. Experimental determination of aluminous clinopyroxene-melt partition coefficients for potassic liquids, with application to the evolution of the Roman province potassic magmas. Chem. Geol. 172, 213–223. https://doi.org/10.1016/S0009-2541(00)00259-X

Chapter 2: Figures

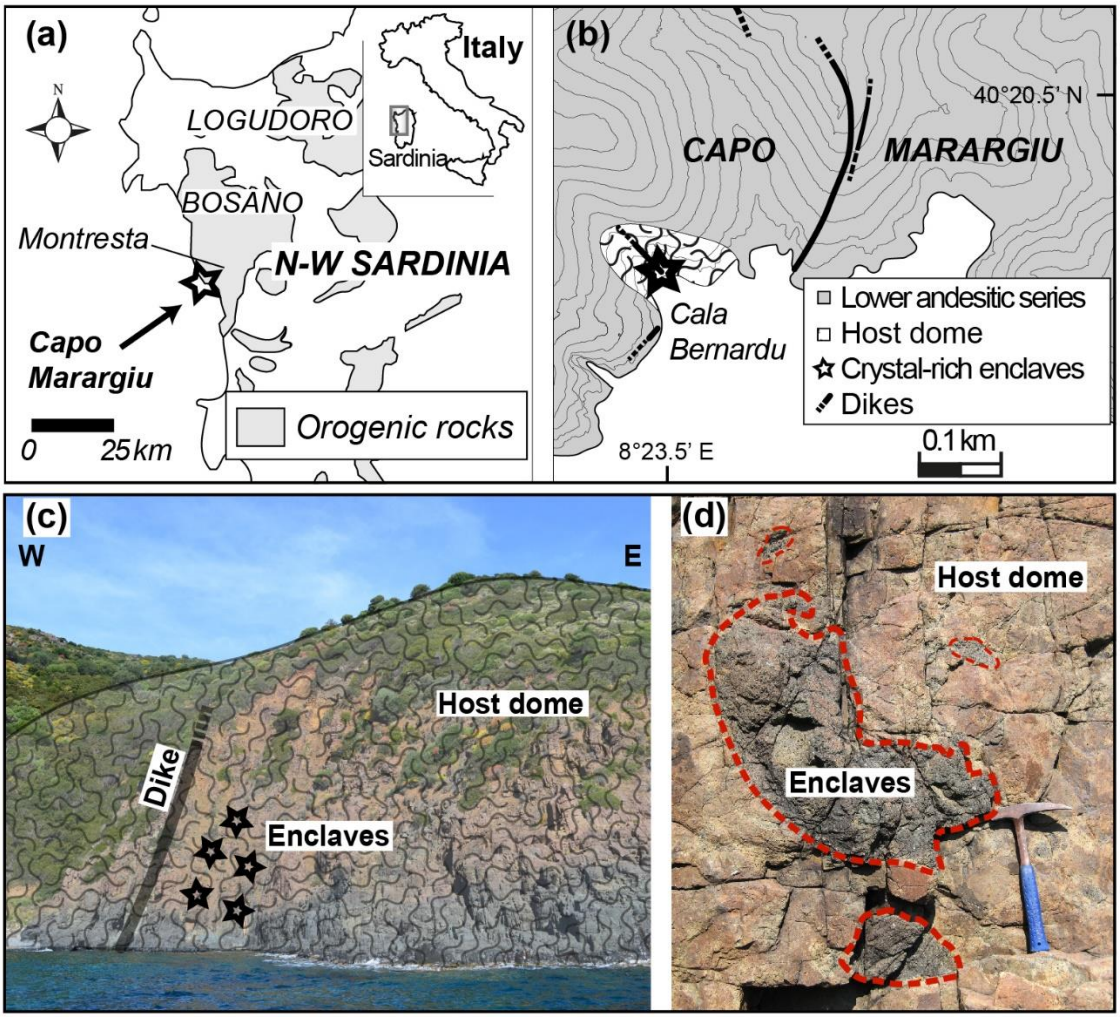

Figure 1. Schematic maps showing the Capo Marargiu Volcanic District (i.e., CMVD), located at about 10 km south-westward of Montresta (a), and the sampling area of the lava dome on the coast of Cala Bernardu (b). A cliff exposes the inner part of a basaltic andesitic dome hosting abundant crystal-rich enclaves (c). The dome appears as a yellowish, porphyritic rock, whereas the dark-grey enclaves are centimetre-to-metre-sized rounded blocks of crystal-rich material (d).

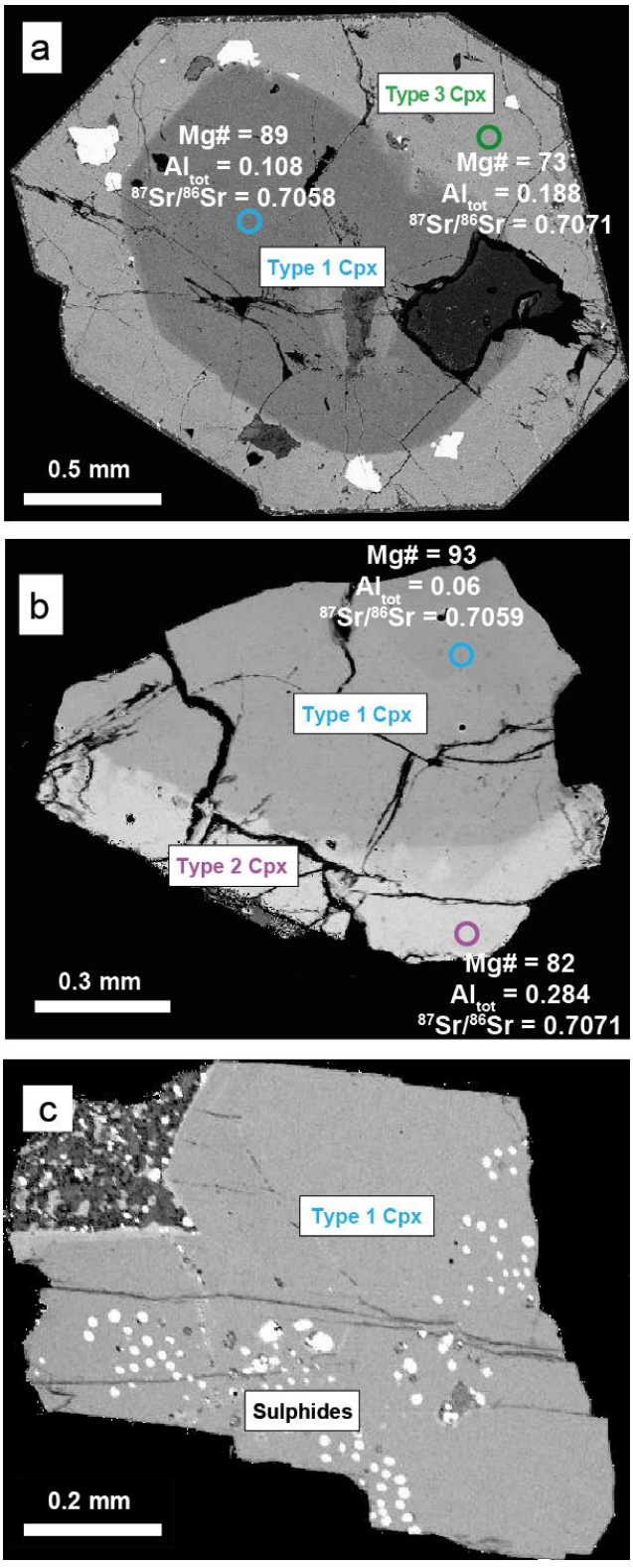

Figure 2. Textural characteristics of Type 1 clinopyroxene. Type 1 appears as the core of large clinopyroxenes, showing disequilibrium dissolution features predominantly at the sub-rounded edges. Sharp overgrowth textures correspond to Type 3 (a) and Type 2 (b). Type 1 crystals usually contain globular inclusions of Fe + Ni + Co sulphides, that likely represent drops of an immiscible liquid (c).

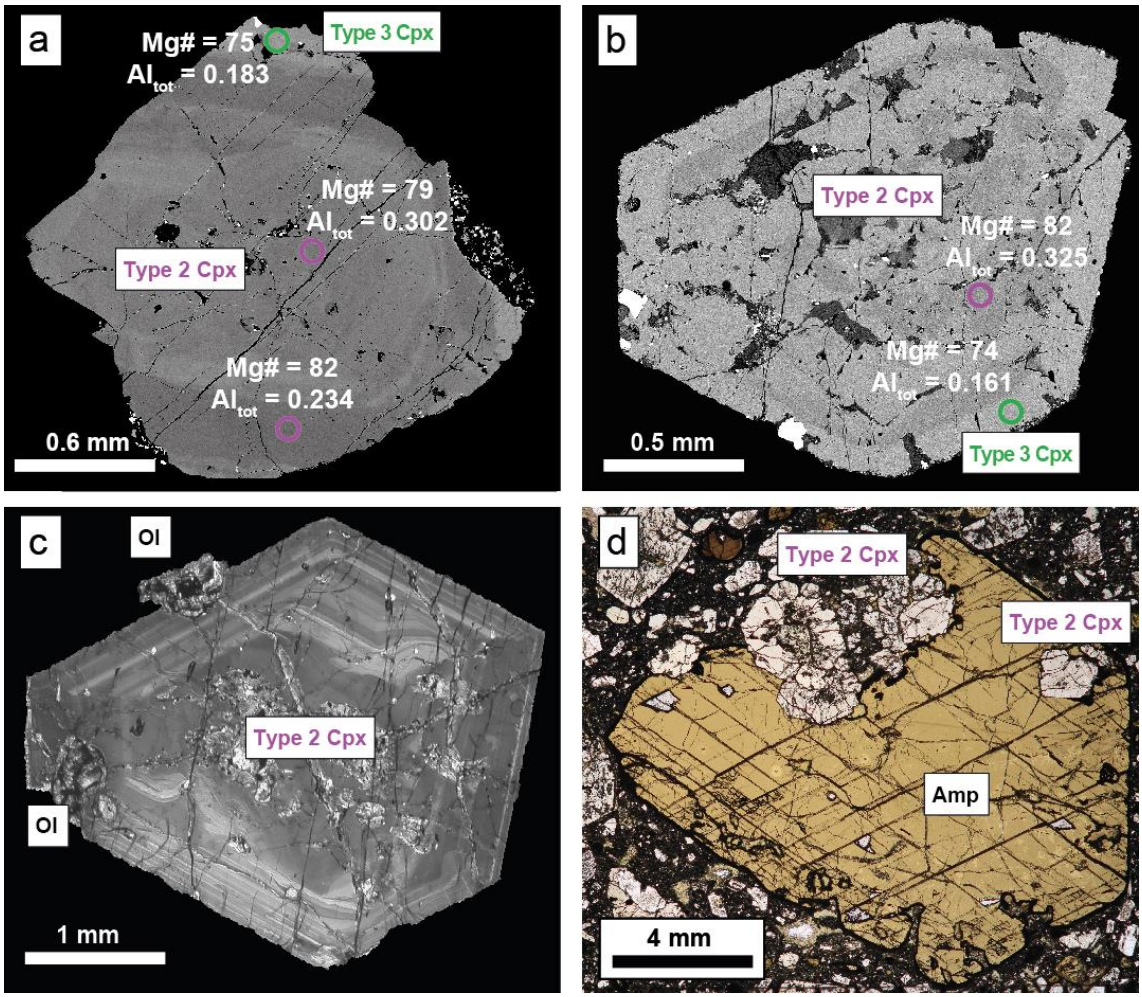

Figure 3. Textural characteristics of Type 2 clinopyroxene. Type 2 occurs as millimetre-sized crystals with a weak reverse oscillatory zoning (a) or a spongy cellular texture associated with thick Type 3 overgrowths (b). In some cases, olivine is included in Type 2 crystals (c) that, in turn, may be entrapped by large amphiboles (d).

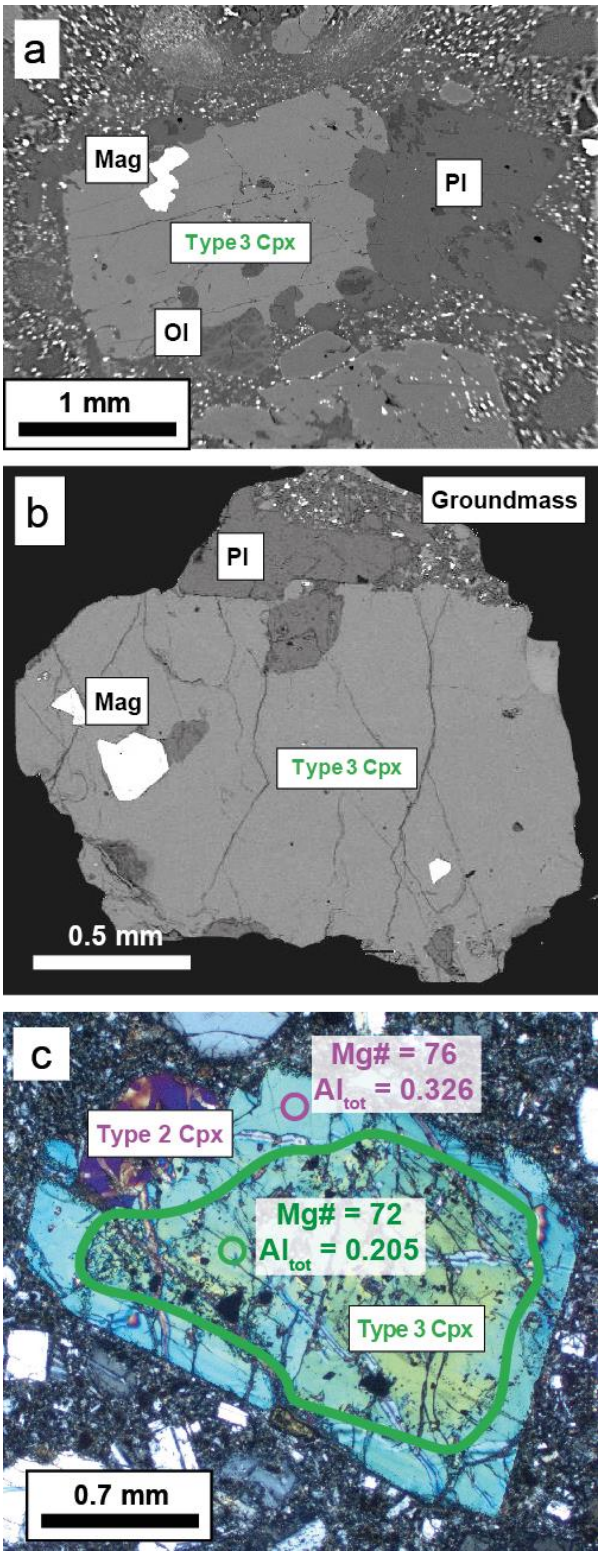

Figure 4. Textural characteristics of Type 3 clinopyroxene. Type 3 is typically found as millimetre-sized glomerocrysts together with plagioclase, titanomagnetite, and rare olivine (a and b). These clinopyroxenes occasionally show Type 2 overgrowths (c).

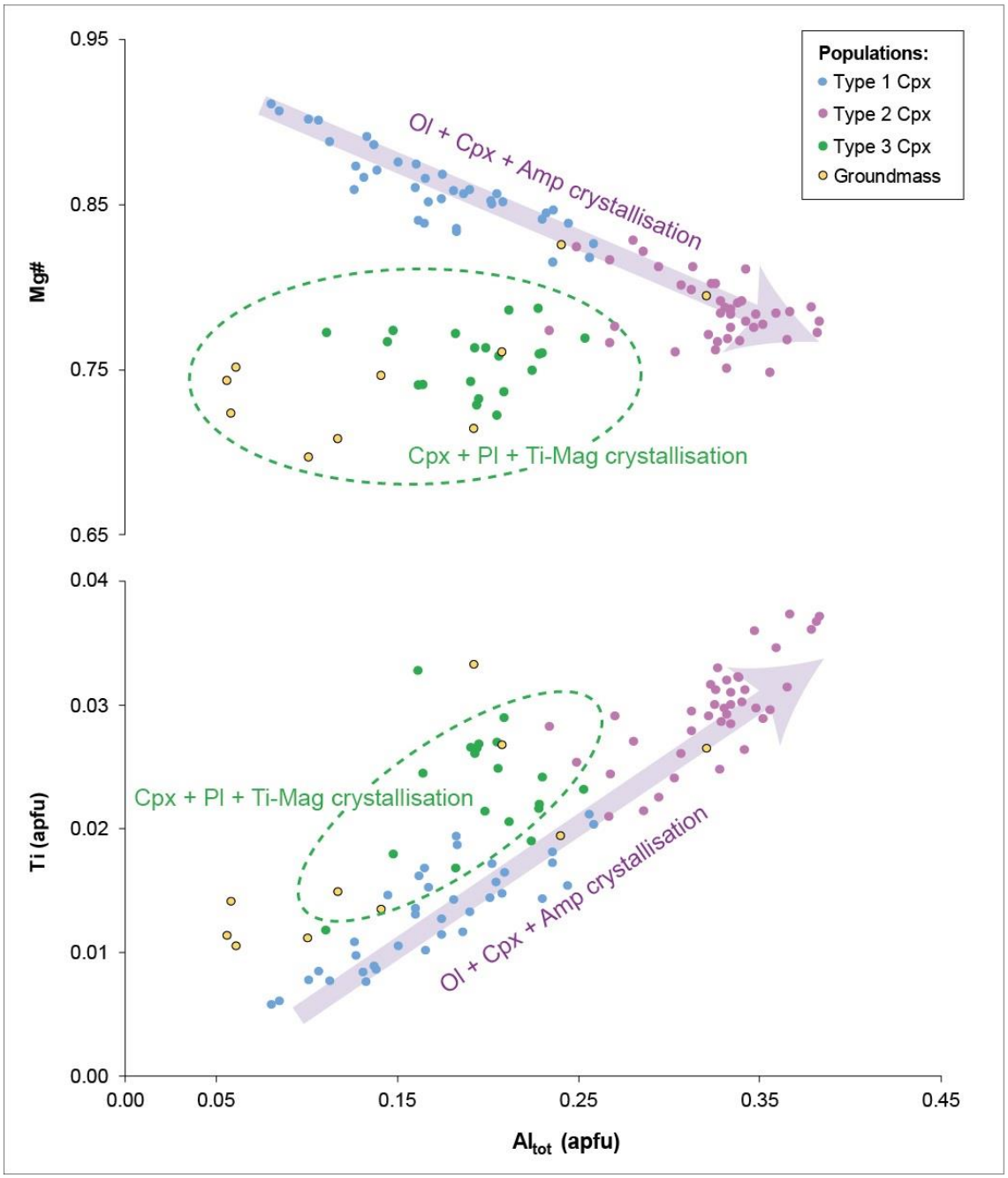

Figure 5. Clinopyroxene major element compositions. The Al_{tot} vs. Mg-number and Ti diagrams show that Type 1 and Type 2 evolve along the same path controlled by olivine + clinopyroxene + amphibole fractionation, whereas Type 3 appears as an isolated group of data recording the effect of plagioclase fractionation.

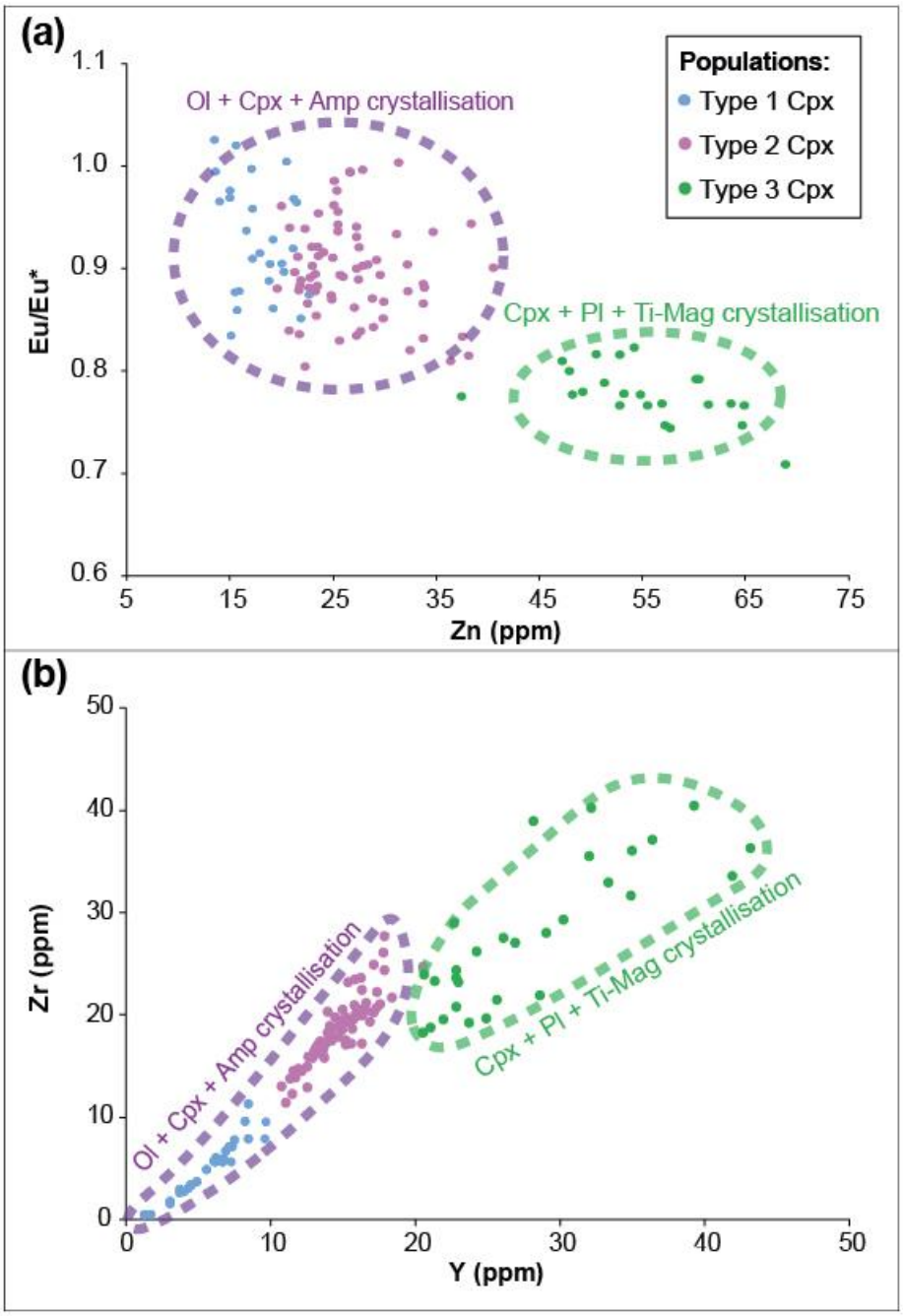

Figure 6. Clinopyroxene trace element composition. The Zn vs Eu/Eu* diagram (a) evidences high and low Eu anomalies, respectively, for Type 3 and Type 1 + Type 2. The Y vs. Zr diagram (b) shows that Type 3 (plagioclase-dominated environment) is characterised by the highest concentrations of incompatible trace elements relative to Type 1 + Type 2 (olivine + clinopyroxene + amphibole - dominated environment).

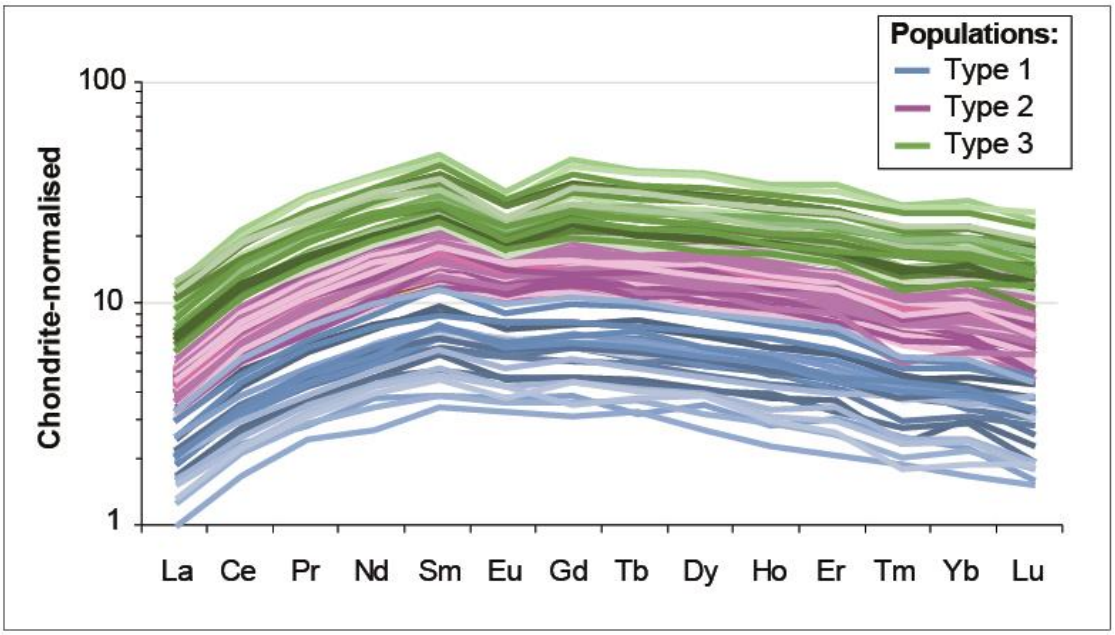

Figure 7. REE chondrite-normalised (McDonough and Sun, 1995) patterns of clinopyroxenes are bell-shaped, depicting relative depletions in both LREE and HREE with respect to MREE. The REE concentrations increase from Type 1 + Type 2 to Type 3, according to the more differentiated character of the magma.

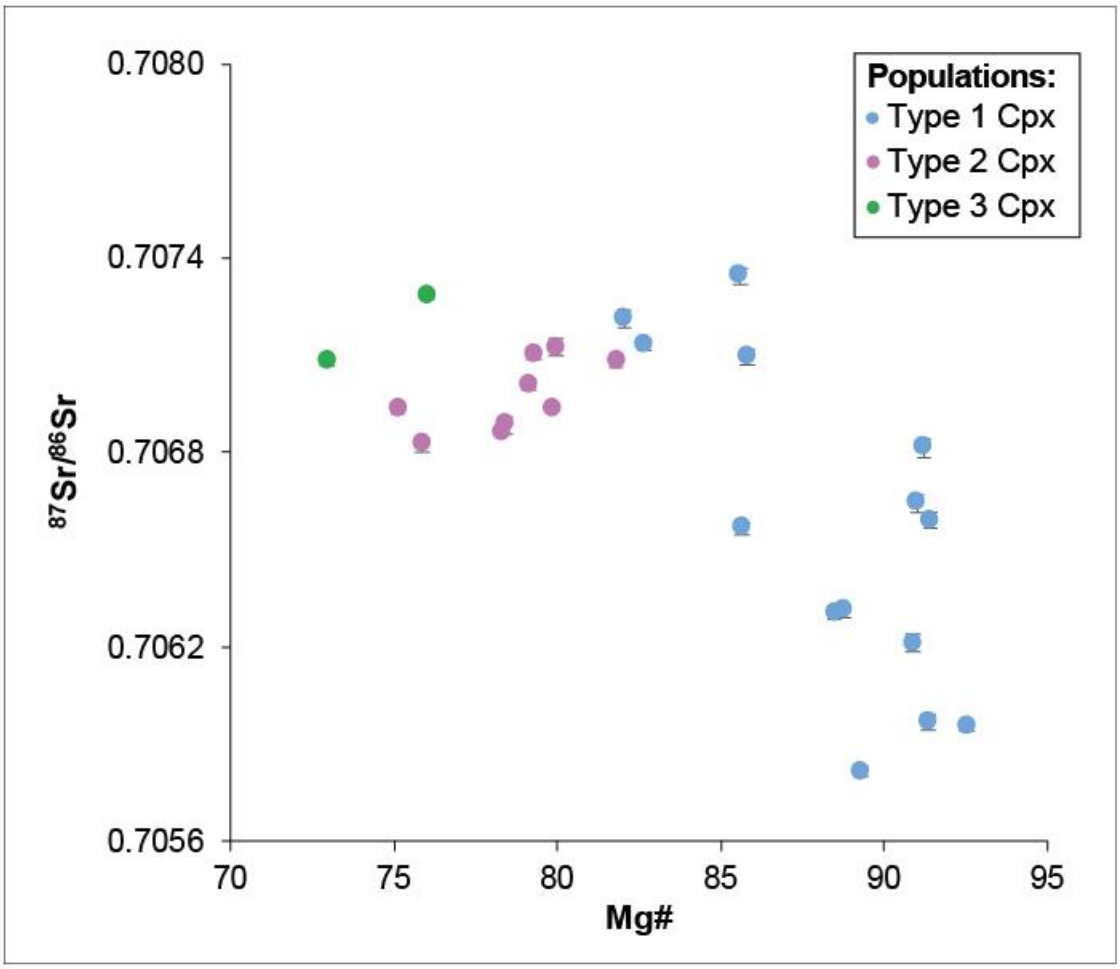

Figure 8. The $^{87}Sr/^{86}Sr$ vs. Mg# diagram shows that Type 1 isotopic composition is highly variable at the early stage of magma differentiation when both crystal fractionation and assimilation of crustal material occur. Differently, the $^{87}Sr/^{86}Sr$ ratios of Type 2 and Type 3 do not show significant variations, accounting for limited to negligible interaction of PBA and EBA magmas with the country rock.

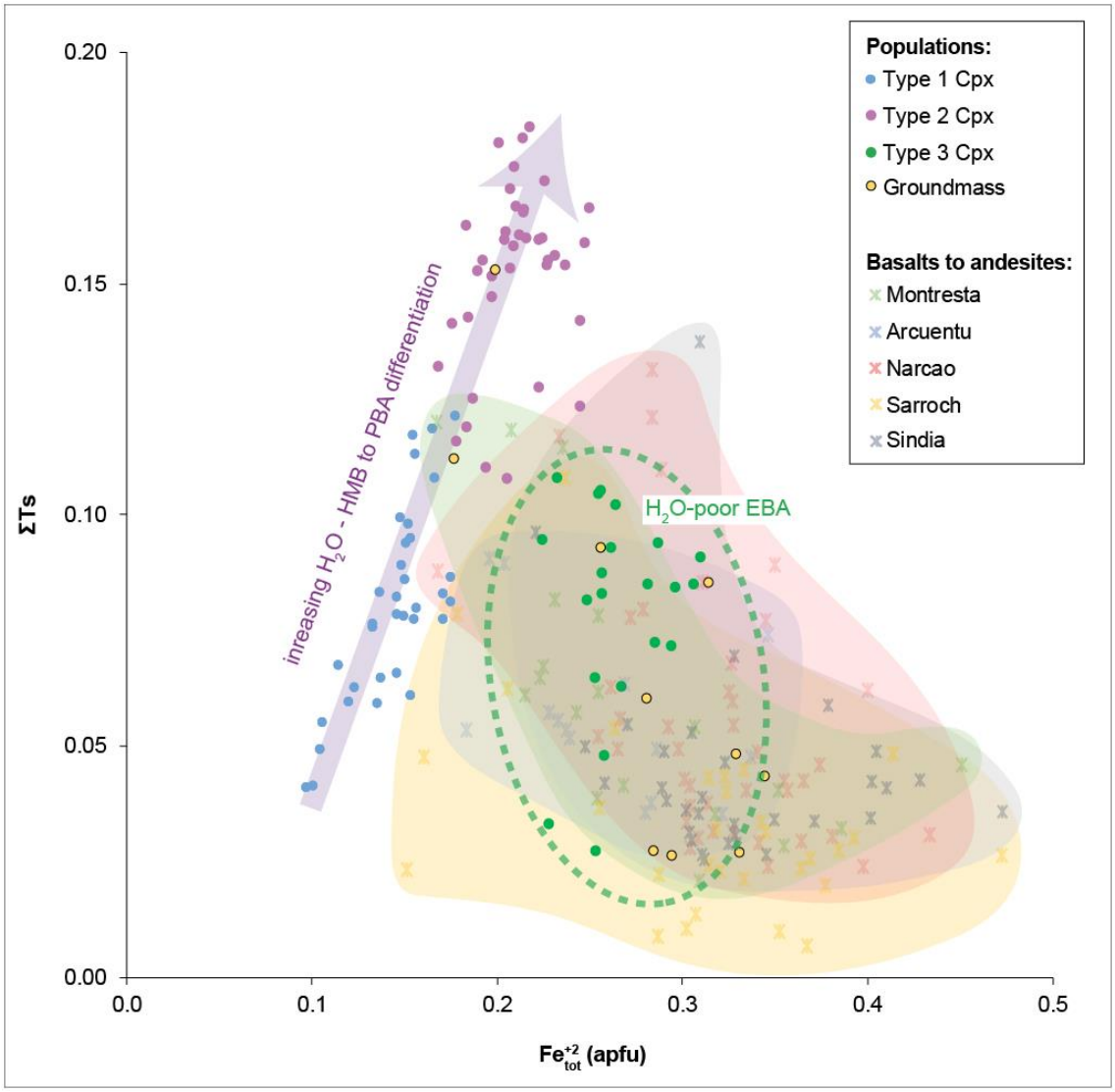

Figure 9. The Fe_{tot}^{+2} vs. ΣTs (Ca-Tschermak + Ca-Ti-Tschermak) diagram shows that Type 1 + Type 2 describe a positive linear trend due to crystallisation from HMB + PBA magmas in water-rich environment (e.g., Dolfi and Trigila, 1978). Conversely, Type 3 clinopyroxene and plagioclase cosaturation occur in the degassed EBA magmas, ponding at shallow crustal levels. This feature resembles that observed for clinopyroxenes from other volcanic districts in Sardinia where minerals crystallised at relatively low *P*-H_2O conditions.

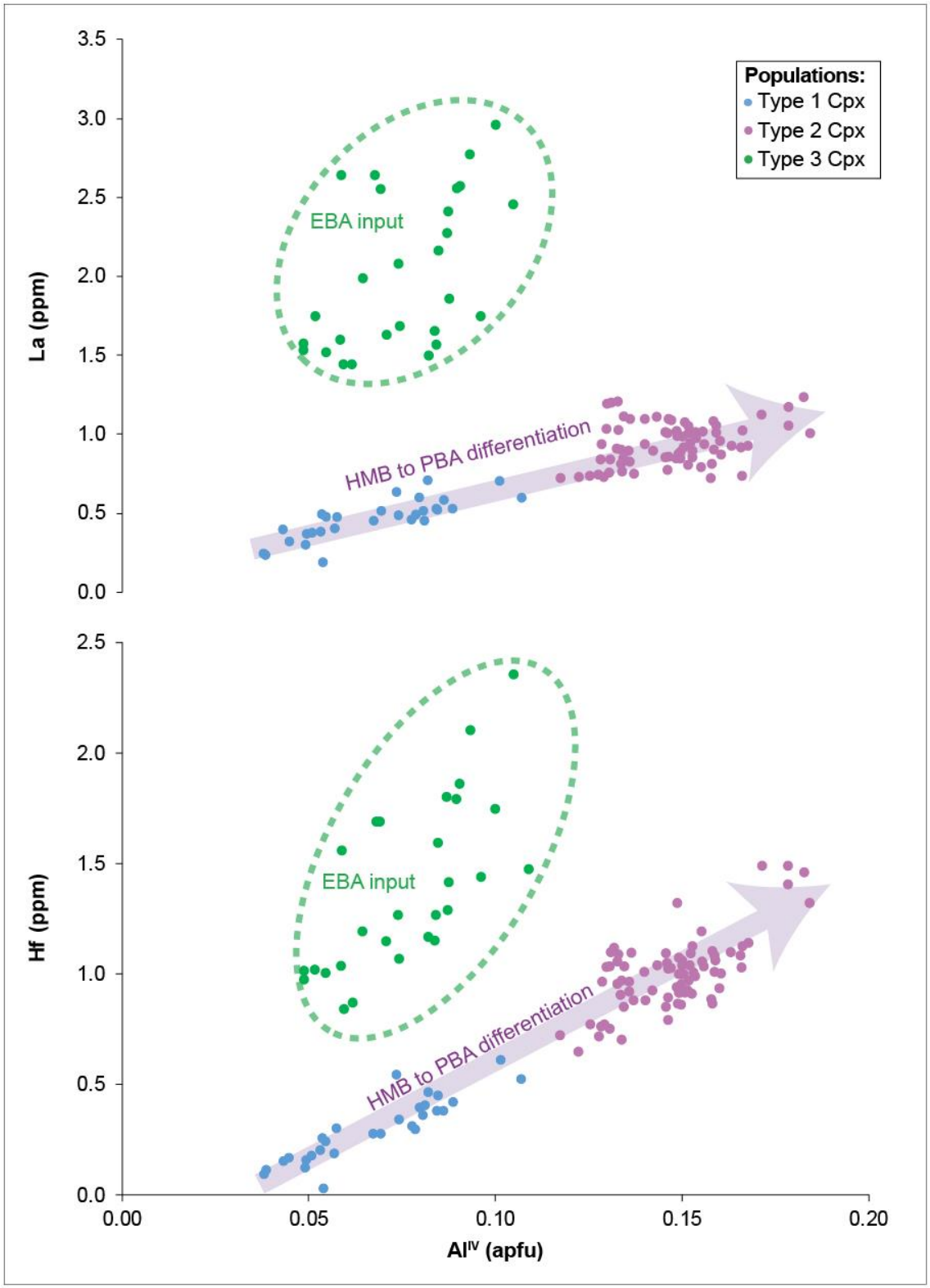

Figure 10. The Al^{IV} vs. Hf and La diagrams show that Type 1 + Type 2 evolve along similar linear paths, accounting for the progressive differentiation of HMB into PBA, whereas Type 3 forms an isolated group of data where low Al^{IV} and high Hf and La concentrations indicate crystallisation from a compositionally distinct magma under the effect of different environmental conditions.

Chapter 3

Experimental constraints on amphibole stability in primitive alkaline and calc-alkaline magmas

Barbara Bonechi[a], Cristina Perinelli[a], Mario Gaeta[a], Vanni Tecchiato[a], Serena F. Granati[a]

[a] Dipartimento di Scienze della Terra, Sapienza-Università di Roma, Piazzale Aldo Moro 5, 00185 Roma, Italy

Published in Periodico di Mineralogia 86, 231-285.

Abstract

Equilibrium crystallisation experiments were carried out on two primitive basaltic rocks (APR16: Na_2O+K_2O = 4.40 wt.%; CM42: Na_2O+K_2O = 2.59 wt.%) with the aim to investigate the amphibole stability in the differentiation processes at deep crustal level, of primitive alkaline (APR16) and calc-alkaline (CM42) magmas. The experiments were performed with different initial H_2O contents (0-5 wt.%), at pressure of 800 MPa, in the temperature range of 975-1225 °C. For the explored conditions, amphibole crystallisation occurs in both compositions at H_2O in the melt >7wt.% while the temperature of their occurrence is lower in the alkaline composition (<1050 °C in APR16 and ≥1050 °C in CM42). Moreover, amphibole crystallisation seems to be influenced by the Na_2O/K_2O ratio rather than the absolute Na_2O content in the melt. This is evident when experimental results on the APR16 and CM42 are compared with experimental data obtained from a primitive ultrapotassic composition (leucite-basanite: Na_2O+K_2O = 4.58 wt.%) and with thermodynamic modelling by the Rhyolite-MELTS algorithm. The comparison shows that amphibole never saturates the leucite-basanite at any of the investigated/modelled conditions, even when an extended crystallisation increases the Na_2O of melts up to contents like those of calc-alkaline experimental glasses. We conclude that, at pressure of 800 MPa and hydrous conditions, only primitive liquids with Na_2O/K_2O ratio ≥0.9 are more prone to crystallise amphibole.

Keywords: Experimental petrology; Rhyolite-MELTS modelling; Calcic amphibole; Calc-alkaline melts; Alkaline melts; Na_2O/K_2O ratio.

3.1. Introduction

At the vast majority of volcanic arcs, the dominant erupted magma type is usually too evolved to have equilibrated directly with a mantle peridotite source at depth, suggesting that primary melts undergo significant differentiation at the roots of continental crust (Grove et al., 2003; Melekhova et al., 2015 and references therein). In this environment, high pressure and hydrous conditions favour significant amphibole crystallisation, with remarkable effects on arc magmas evolution (Cawthorn et al., 1976; Hilyard et al., 2000; Müntener and Ulmer, 2006; Davidson et al., 2007; Nandedkar et al., 2014). Experimental studies have shown that amphibole crystallises under hydrous conditions from a wide variety of liquids at crustal pressures - i.e. dacitic and andesitic magmas (Allen and Boettcher, 1983; Rutherford and Devine, 1988; Grove et al., 1997; Prouteau and Scaillet, 2003; Alonso-Perez et al., 2009; Masotta and Keppler, 2015), tholeiitic basalts (Holloway and Burnham, 1972; Helz, 1973; Anderson, 1980) and primitive magmas of arc systems (Moore and Carmichael, 1998; Blatter and Carmichael, 1998; Pichavant and Macdonald, 2007).

Factors that primarily control amphibole crystallisation are (i) magma water content (Holloway and Burnham, 1972; Anderson, 1980; Medard and Grove, 2008; Krawczynski et al., 2012), (ii) oxygen fugacity (i.e., ΔNNO between -0.51 and +3; Helz, 1973, 1976; Barclay and Carmichael, 2004; Krawczynski et al., 2012; Melekhova et al., 2015) and (iii) alkali content (Cawthorn and O'Hara, 1976; Nandedkar et al., 2014). Cawthorn and O'Hara (1976) and Nandedkar et al. (2014) denote that calc-alkaline liquids achieve amphibole saturation for Na_2O >3 wt.%. Amphibole has been synthesised experimentally from a wide range of starting materials over a pressure range of 1-23 kbar and 400-1150 °C and therefore, it can be a considerable indicator of crystallisation conditions, both as a geothermometer and geobarometer. Holland and Richardson (1979) examined equilibria among the end-member species glaucophane, edenite, tremolite, and hornblende in assemblages with chlorite, epidote, albite, quartz and H_2O in order to explain zoning profiles in amphibole as *P*-*T*-time indicators; Graham and Powell (1984) have formulated a garnet-amphibole thermometer for application to amphibolite grade metamorphic rocks; Hammarstrom and Zen (1986) and Hollister et al. (1987) have proposed an empirical amphibole geobarometer for use with granitoid rocks. Nabelek and Lindsley (1985) proposed a preliminary

empirical calibration of a hornblende-plagioclase thermometer while Ridolfi et al. (2010) and Ridolfi and Renzulli (2012), relying on a large number of experimental and natural data, proposed a model requiring only the amphibole compositions to estimate the physico-chemical parameters (*P*, *T*, fO_2 and the amount of H_2O dissolved in the melt) of calcic amphibole crystallisation from calc-alkaline and alkaline melts. In order to explore the influence of alkali in primitive melts on amphibole stability at deep-crustal level, we report the results of new phase equilibria experiments performed at *P* = 800 MPa, *T* = 975-1225 °C, on two primitive (Mg# = $Mg/(Mg+Fe_{tot})$ = 0.64-0.69; with total Fe as Fe^{2+}) basaltic compositions APR16 and CM42 characterised by different amount of alkali (Na_2O+K_2O = 4.40 and 2.59 wt.%, respectively) and alkali ratio (Na_2O/K_2O = 1.89 and 2.08 wt.%, respectively). We also compare the experimental phase relations with those calculated by means of the Rhyolite-MELTS software (Ghiorso and Sack, 1995; Asimow and Ghiorso, 1998; Gualda et al., 2012) and those obtained experimentally on primitive ultrapotassic basalt by Conte et al. (2009) to discuss the stability of amphibole in primitive alkaline and subalkaline magmas.

3.2. Experimental and thermodynamic approach

3.2.1. Starting material

We selected two samples of primitive basalts with different alkali contents (Table C1) as starting material for equilibrium experiments. APR16 is a lithic lava clast (D'Antonio et al., 1999) occurring in the deposit of the Solchiaro hydromagmatic centre located in the Procida island belonging to the Phlegraean Volcanic District (South Italy; Figure 1a). It consists in a primitive alkaline basalt (Mg# = 0.64, Na_2O+K_2O = 4.40 wt.%, L.O.I. = 0.61 wt.%; Figure 2) with 12 vol.% of forsteritic olivine and diopsidic clinopyroxene phenocrysts in a groundmass of olivine, clinopyroxene, plagioclase, Ti-magnetite, alkali feldspar and glass (D'Antonio et al., 1999). Inclusions of Cr-spinel can be found within olivine phenocrysts. CM42 is a mafic enclave occurring in the calc-alkaline hypabyssal rocks of the Capo Marargiu Volcanic District (Tecchiato et al., 2015; Figure 1b-c). The sample is a primitive calc-alkaline basalt (Mg# = 0.69, Na_2O+K_2O = 2.59 wt.%, L.O.I. = 2.50 wt.%) with ~50 vol.% of clinopyroxene, amphibole, plagioclase, olivine and magnetite phenocrysts in a groundmass of plagioclase, clinopyroxene, low-Ca pyroxene and magnetite (Tecchiato et al., 2015).

Centimetre-sized fragments of the APR16 and CM42 samples without weathering evidences were crushed in an agate shatterbox and subsequently by hand, under acetone, in an agate mortar. We obtain a final grain-size <60 μm (as estimated through the SEM images).

3.2.2. Experimental procedures

We carried out experiments with different initial H_2O contents (from 0 to 5 wt.%), at pressure of 800 MPa and temperatures from 975 to 1225 °C, using an end-loaded piston cylinder apparatus installed at the HP-HT Laboratory of the Earth Science Department, Sapienza - University of Rome (Figure 3a). This device is a solid medium press equipped with a ½ inch pressure vessel (Figure 3b) capable of attaining pressure of 3.5 GPa and temperature of 1500 °C. We load Au_{75}-Pd_{25} alloy capsules (7 mm of length and 2.8 mm of diameter) with the starting material and appropriate amounts of water (using a microsyringe) before sealing the capsule tip by arc welding.

We use an assembly as described in Figure 3d, whose components are: a) a fluorite cylinder (CaF_2), which converts from uniaxial to hydrostatic pressure; b) a graphite cylinder that acts as a heating furnace; c) two cylindrical supports of workable magnesia (MgO) bored to allow the insert of the thermocouple; d) a ceramic sleeve placed between the magnesia supports to prevent capsule and thermocouple to be at direct contact. The assembly is prepared placing the capsule into the MgO supports and filling the spaces with pyrophyllite powder. Pyrophyllite prevents undesired capsule movements during pressurization as well as hydrogen loss produced by water dissociation and hydrogen permeation through the capsule alloy during experimental runs. Before placing the assembly into the pressure vessel, it is wrapped in a lead foil; the lead foil has the function of lubricant between the assembly and the pressure vessel walls. We therefore position into the pressure vessel (i.e., above the assembly) a stainless-steel plug surrounded by a pyrophyllite ring; the plug acts as an electric conductor ensuring energy supply to the graphite furnace. We finally set the pressure vessel in the piston cylinder apparatus. We used an insulating Mylar foil and a Plexiglas support to hold the thermocouple plate above the pressure vessel. We insert a type D thermocouple (W_{97}-Re_3- W_{75}-Re_{25}) on the upper side of the plate, within a groove accurately designed for this purpose. This thermocouple allows to monitor

temperature in the isothermal zone of the assembly with accuracy of ±5 °C. At the beginning of each experiment, we achieve the working conditions of pressure and temperature using the “hot piston out” technique. This consists in (i) applying an overpressure >10% of the run pressure, (ii) gradually increasing the temperature, and (iii) correcting for pressure drops due to stress relaxation within the assembly during heating. We terminate the experimental runs after 3-6 hours; the isobaric quench was made by turning off the power.

Finally, all the runs were self-buffered; we attempt to estimate fO_2 through the equation of Kress and Carmichael (1991) using the liquid Fe^{3+}/Fe_{tot} mole ratios from $^{Ol\text{-}melt}Kd_{Fe\text{-}Mg}$ calculated according to Toplis (2005). This procedure yielded fO_2 values of ΔNNO +0.2 to +1.1, in agreement with those estimated for similar furnace assemblages (Conte et al., 2009; Weaver et al., 2013).

3.2.3. Analytical methods

After each experiment, we recover and mount the product in epoxy resin for polishing and carbon coating. We characterise textures and phase assemblages by Scanning Electron Microscopy (SEM) using a FEI quanta 400 equipped for microanalysis with an EDAX Genesis system at the Earth Science Department, Sapienza - University of Rome. We estimate the modal proportion of each phase in the experimental products by detailed image analysis using ImageJ freeware (http:// imagej.nih.gov/ij/) following the procedure described by Philpotts and Ague (2009). The ease to threshold the experimental phases from SEM images yielded a good estimate of their modal abundance. We analyse phase compositions by Electron Probe Micro-Analysis (EPMA) using a Cameca SX50 equipped with five-wavelength dispersive spectrometer (WDS). The EPMA facility belongs to CNR Istituto di Geologia Ambientale e Geoingegneria (Rome). A 15 kV accelerating voltage, 15 nA beam current and the following standards are used: metals for Mn and Cr, jadeite for Na, wollastonite for Si and Ca, orthoclase for K, corundum for Al, magnetite for Fe, rutile for Ti and periclase for Mg. Raw data are corrected using the ZAF method. We analyse minerals using a beam diameter of 1 μm, and glasses with a defocused beam from 10 to 15 μm of diameter to minimize the alkali loss. Water contents of experimental glasses are estimated according to the by difference method (Devine et al., 1995).

3.2.4. Thermodynamic approach

We constrain phase equilibria at high pressure for APR16 and CM42 on a thermodynamic base using Rhyolite-MELTS (Ghiorso and Sack, 1995; Asimow and Ghiorso, 1998; Gualda et al., 2012). Similarly, we model the crystallisation of a leucite-basanite (MF: Mg# = 0.75, Na_2O+K_2O = 4.58, L.O.I. = 0.65 wt.%; Table 1) from Montefiascone centre (Vulsini Volcanic District, Central Italy). This latter has been object of a previous experimental study by Conte et al. (2009). For APR16 and CM42, Rhyolite-MELTS calculations are performed at isobaric conditions (800 MPa), consistently with our phase equilibria experiments. Conversely, MF crystallisation is modelled at 1000 MPa to match the experimental pressure conditions of Conte et al. (2009). Isobaric cooling simulations start at superliquidus temperatures and initial water content (H_2O_i) ranging from 0 to 7 wt.%. According to the experimental study, we constrain the redox conditions of magma at the Ni-NiO (NNO) buffer.

3.3. Experimental and thermodynamic modelling

3.3.1. Experimental results

The phase assemblages of the run products are presented in Table 1. Experiments are always below the liquidus temperatures and, according to the occurrence of euhedral minerals, are characterised by the equilibrium between the melt and crystalline phases (Figure 4).

As regards APR16, clinopyroxene is the mineral crystallised from the NWA (no water added) run at the highest temperature (1225 °C). Olivine (Ol), oxide (Ox) and plagioclase (Plg) are obtained at 1000 °C, and K-feldspar (KFld) crystallises at 975 °C (i.e., NWA run solidus). In the hydrous experiments (~5 wt.% H_2O_i), APR16 crystallises (i) Cpx + Ol + orthopyroxene (Opx) + Ox at 1050 °C, and (ii) Cpx + Opx + amphibole (Amph) + Ox at 1000 °C (Table 1). Remarkably, Plg never crystallises under hydrous conditions, whereas Ol is absent at low temperature.

As regards CM42, the mineral assemblage resulting from the damp run (~2 wt.% H_2O_i) at 1110 °C is Cpx + Ol + Opx + Plg + Ox. In turn, that from the wet run (~5 wt.% H_2O_i) at 1050 °C is Cpx + Ol + Amph + Ox (Table 1). Notably, high water contents suppress Opx and Plg crystallisation.

Phase compositions

The compositions of minerals and glasses are reported in Table C2-C7. However, both the small size of K-feldspar and of most oxides, as well as the paucity of residual glass in some runs (i.e., APR16-2C), prevent the accurate acquisition of electron microprobe analyses on these phases.

Olivines

Forsterite (Fo) content of APR16 experimental olivines in the NWA runs does not change with the decrease of temperature (Fo_{67}) while the Ol composition at hydrous conditions is Fo_{85} (Table C2). Olivines from CM42 have compositions Fo_{81} and Fo_{79} for the 2 wt.% and 5 wt.% H_2O_i runs, respectively (Table C2).

Pyroxenes

Clinopyroxenes in APR16 experimental sample are diopsides ($Wo_{45-48}En_{39-48}Fs_{7-13}$; Figure 5) according to the classification scheme of Morimoto et al. (1988). In the NWA runs, the Mg# decreases from 0.87 to 0.76 with temperature, whereas TiO_2 increases from 0.67 wt.% at 1225 °C to 1.89 wt.% at 975 °C (Table C3). In comparison, Cpx from the hydrous runs (5 wt.% H_2O_i) at 1050-1000 °C shows higher Mg-number ($Mg\#_{0.81-0.82}$) and lower TiO_2 contents (1.35-1.31 wt.%; Table C3). Opx is classified as clinoenstatite ($Wo_5En_{81}Fs_{14}$; Figure 5).

Experimental clinopyroxenes from CM42 runs are diopsides ($Wo4_{3-47}En_{40-47}Fs_{7-14}$; Table C3). Cpx compositions from the wet run (~5 wt.% H_2O_i) show lower Al_2O_3 and higher FeO contents than Cpx crystallised from the damp run (~2 wt.% H_2O_i). Interestingly, the initial H_2O content of starting material does not influence Cpx Mg-number ($Mg\#_{0.81}$ and $Mg\#_{0.82}$ from the wet and damp run, respectively). Opx are clinoenstatites ($Wo_3En_{73}Fs_{24}$; Figure 5).

Clinopyroxene-liquid Fe-Mg exchange coefficient have been calculated by using the formula $(FeO/MgO)^{Cpx}/(FeO/MgO)^{Liq}$; the average value is 0.31 ± 0.05 for APR16 and 0.29 ± 0.01 for CM42 runs, taking into account FeO as FeO_{tot}. APR16 Kd values are in agreement with experimental data for hydrous basaltic compositions (0.27 ± 0.06, Pichavant et al., 2014; 0.26-0.31, Sisson and Grove, 1993; 0.29 ± 0.08, Pichavant and Macdonald, 2007). Even orthopyroxene-liquid Fe-Mg exchange coefficient has been calculated using the formula $(FeO/MgO)^{Opx}/(FeO/MgO)^{Liq}$; the average value is 0.27 ± 0.01 for APR16 and 0.26 for CM42.

Plagioclases

Plagioclase compositions are plotted in the albite-orthoclase- anorthite ternary diagram (Figure 6). Plg from APR16 runs shows decreasing anorthite (An) content from 71 (bytownite) to 66 (labradorite) with temperature decreasing from 1000 °C to 975 °C (Table C4). Plg from the CM42 damp run is bytownite (An_{84}).

Amphiboles

In both APR16 and CM42 experiments, amphibole crystallises when H_2O_i = 5 wt.%. According to the classification scheme of Hawthorne and Oberti (2007) the amphiboles are pargasites (APR16-W13, 1000 °C run) and magnesiohastingsites (CM42-2, 1050 °C run). Pargasites are characterised by $Mg\#_{0.75}$ and 1.11 wt.% K_2O, whereas magnesiohastingsite shows $Mg\#_{0.70}$ and 0.67 wt.% K_2O (Table C5).

Oxides

Oxides in APR16 experiments vary in composition from Cr-rich spinel [Cr# = 0.46-0.44 calculated as $Cr^{3+}/(Cr^{3+} + Al^{3+})$] to Ti-magnetite with 24-28 mol.% of ulvöspinel content (Usp; Table C6). Similarly, oxides from CM42 products correspond to Usp_{28-32} Ti-magnetites showing a negative correlation between Usp and H_2O_i: Usp increasing from 28 to 32 with H_2O_i decreasing from 5 to 2 wt.%.

Glass

In the Total Alkali-Silica (TAS) diagram (Figure 7) the composition of residual glass (Table C7) in APR16 experiments evolves from basalt to trachybasalt with Mg# = 0.62 and Na_2O/K_2O = 1.85 in the NWA run at 1225 °C, to shoshonite with Mg# = 0.56 and Na_2O/K_2O = 1.63 in the hydrous run at 1050 °C. In turn, the chemical composition of residual glass in CM42 experiments varies from basaltic with Mg# = 0.52, Na_2O/K_2O = 1.81 and H_2O_f (final water content) ≈7 wt.% in the hydrous run, to basaltic andesite with Mg# = 0.45, Na_2O/K_2O = 0.88 and H_2O_f ≈5 wt.% in the damp run.

The important crystallisation of plagioclase (~22 vol.%) in the damp run is responsible for the relative enrichment of K_2O over Na_2O in the melt, reflected by

the striking decrease of Na_2O/K_2O ratio (from 2.08 of starting material to 0.88 wt.%).

3.3.2. Rhyolite-MELTS results

The phase equilibria predicted by Rhyolite-MELTS for APR16, CM42 and MF are shown in the *T*-H_2O diagrams of Figure 8.

The anhydrous liquidus of APR16 is calculated at 1320 °C and decreases to 1148 °C with increasing water content to 7 wt.% H_2O_i (Figure 8a). Clinopyroxene is the liquidus phase at 0-3 wt.% H_2O_i, followed by oxide, orthopyroxene and plagioclase at lower temperatures. This mineral assemblage represents the stable paragenesis at H_2O contents in the residual melt lower than ~6 wt.%. Olivine is the first mineral to crystallise at >3 wt.% H_2O_i (Figure 8a), followed by clinopyroxene and oxides. The Ol + Cpx + Ox paragenesis is stable until, at peritectic, olivine starts to react with the melt to form orthopyroxene (Figure 8a). Amphibole crystallisation is predicted by Rhyolite-MELTS calculations at temperatures <970 °C and with >5 wt.% H_2O in the residual melt. Phlogopite is the last mineral to crystallise at temperatures ≤900 °C and H_2O_f ≥6 wt.%. Under such conditions, the stable paragenesis consists of Gl + Opx + Cpx + Amph + Phlog + Ox (Figure 8a).

As regards CM42 composition, the liquidus temperature at anhydrous conditions is found to be at 1340 °C and rationally decreases at 1180 °C with increasing of water content to 6 wt.% H_2O_i (Figure 8b). Orthopyroxene represents the liquidus phase at <3 wt.% H_2O_i, followed by clinopyroxene, oxide and plagioclase at lower temperatures. Gl + Cpx + Plg corresponds to the stable paragenesis at H_2O contents in the residual melt lower than ~4 wt.%. Olivine is the first mineral to crystallise at ≥3 wt.% H_2O_i, followed by clinopyroxene and oxides. The Ol + Cpx + Ox paragenesis is stable until the onset of olivine-melt peritectic reaction to produce orthopyroxene, comparably to results from APR16 simulations previously described. Amphibole crystallisation is retrieved by Rhyolite-MELTS at temperatures <960 °C and with H_2O contents in the residual melt between 11 and 14 wt.%. At such conditions, the stable mineral assemblage consists of Opx + Cpx + Ox + Amph.

The MF anhydrous liquidus is predicted at temperature of 1385 °C and it decreases to 1250 °C with increasing water content to 7 wt.% H_2O_i (Figure 8c).

Clinopyroxene is the liquidus phase at 0-1 wt.% H_2O_i, followed by olivine, spinel and leucite during cooling and crystallisation (H_2O_f = 0-3.5 wt.%). The modelled crystallisation sequence at >1 wt.% H_2O_i is Ol → Ol + Cpx → Ol + Cpx + Ox → Ol + Cpx + Ox + phlogopite (Phlog). The onset of phlogopite occurs at temperatures <1150 °C and with >3 wt.% H_2O in the residual melt. Garnet (Gt) also crystallises and coexists with Cpx + Ox + Phlog at temperatures ≤1035 °C and ≥3.5 wt.% H_2O_f.

3.4. Discussion

In the following section, we discuss the phase relations of primitive subalkaline to alkaline APR16, CM42 and MF compositions combining the results of the Rhyolite-MELTS simulations with those of experiments from both this study and literature (i.e., Conte et al., 2009). We therefore address the effect of alkali content, in particular of the Na_2O/K_2O ratio, on the stability of amphibole and phlogopite.

3.4.1. Phase relations in the APR16, CM42 and MF composition

We find that results from Rhyolite-MELTS modelling on the alkaline basalt APR16 are in substantial harmony with experimental phase equilibria. Indeed, we observe a good correspondence between predicted models and observed phase relations from both the NWA experiment at 1225 °C (APR16-20 run) and the hydrous (~5 wt.% H_2O_i) experiment at 1000 °C (APR16-W13 run; Table 1). In detail, the NWA assemblage of Gl (~1 wt.% H_2O_f) + Cpx at 1225 °C is well simulated by Rhyolite-MELTS particularly when the calculations are performed using an initial water content similar to the APR16 L.O.I. value (0.61 wt.%; Figure 8). In turn, for hydrous experiments the paragenesis of Gl (~7 wt.% H_2O_f) + Cpx + Amph + Opx + Ox at *T* = 1000 °C is modelled by Rhyolite-MELTS at slightly lower temperature (~970 °C; Figure 8a). At lower temperatures, olivine is unstable and replaced by Opx (Figure 8). Notably, experiments and Rhyolite-MELTS calculations show that orthopyroxene crystallises in the APR16 magma at H_2O-rich conditions (≥5 wt.% in the melt). This unexpected result indicates that at high pressure, hydrous conditions the phases driving the liquid line of descent of the primitive magmas of the Phlegrean Fields could be different from those modelled at lower pressure (e.g. Fowler et al., 2007).

The subalkaline basaltic composition of CM42 shows a higher degree of mismatch between experimental and Rhyolite-MELTS results (Figure 8b). While the paragenesis of the damp run (~2 wt.% H_2O_i) at 1110 °C (CM42-2; Table 1) is Gl (~5 wt.% H_2O_f) + Cpx + Ol + Opx + Plg + Ox, that computed by Rhyolite-MELTS is Gl + Cpx + Opx + Ox. Analogously, the paragenesis of the wet run (~5 wt.% H_2O_i) at the 1050 °C run (CM42-1) is Gl (~7 wt.% H_2O_f) + Cpx + Ol + Amph + Ox, whereas that predicted by Rhyolite-MELTS modelling is Opx + Cpx + Ox + Amph at temperatures <960 °C and with H_2O contents in the residual melt between 11 and 14 wt.%. The coexistence of Ol and Opx is never predicted for CM42 basalt at any of the *T*-H_2O conditions investigated. Moreover, Rhyolite-MELTS yields Plg crystallisation exclusively when the H_2O_i in the system is lower than or equal to 3 wt.% and *T* = 1110 °C.

As regards the basanite composition of MF, phase relations modelled by Rhyolite-MELTS are fully consistent with experimental results of Conte et al. (2009; Figure 8c). In the anhydrous run at 1275 °C (PC185) and in the hydrous run (3 wt.% H_2O_i) at 1200 °C (PC106) the glasses (1.6 and 4 wt.% H_2O_f, respectively) are at equilibrium with Ox, Ol and Cpx. Rhyolite-MELTS is unable to predict the Ox crystallisation at experimental conditions of PC106 run (*T* = 1200 °C; 3 wt.% H_2O_i); this may be due to the fO_2 imposed for calculations. Further differences concern the temperatures of Phlog saturation, which occurs at equilibrium with Ol + Cpx + Ox + Gl (8 wt.% H_2O_f) in the charge at 1200 °C and at equilibrium with Cpx + Ox + Gl (5 wt.% H_2O_f) in the charge at 1150 °C. The temperatures provided by Rhyolite-MELTS for Phlog crystallisation are lower than ~100 °C (Figure 8c).

3.4.2. Effect of alkali on the amphibole stability

Experimental results show that amphibole crystallises from both APR16 and CM42 in the hydrous experiments (~5 wt.% H_2O_i) at 1000 °C (APR16-W13) and 1050 °C (CM42-1), respectively.

In these runs, Amph is in equilibrium with a melt containing ~7 wt.% H_2O_f. Conversely, in runs with lower water content in the melt, amphibole does not crystallise (e.g., APR16-7W; Figure 9a; Table 1). This agrees with many experimental studies on similar compositions showing that at the similar *P*-*T*-H_2O-fO_2 conditions, amphibole crystallises from liquids with H_2O contents higher than ~6 wt.% (Krawczynski et al., 2012; Melekhova et al., 2015 and references

therein). The most relevant differences between APR16 and CM42 amphiboles are K_2O contents (1.11 and 0.67 wt.% in APR16 and CM42, respectively) and Mg# compositions (0.75 and 0.70 in APR16 and CM42, respectively). While the compositional diversity of the respective starting material (i.e., 1.52 and 0.84 wt.% K_2O for APR16 and CM42 whole rocks, respectively) could explain the different K_2O contents in amphiboles, this cannot justify the aforementioned differences in Mg# (0.63 and 0.69, APR16 and CM42 whole rocks, respectively). Our experiments show that amphibole crystallises at about 150 °C below the liquidus temperature, after olivine, pyroxenes and oxides crystallisation significantly modifying the bulk chemistry of coexisting melt. In this context, identifying which chemical component exerts a primary control on amphibole stability on the base of starting material compositions is not straightforward (Figure 8a-c). However, some considerations can be attempted as follows. Interestingly, we find that amphibole crystallising at higher temperature (i.e., 1050 °C; Figure 9b) is in equilibrium with a melt (i.e., CM42-1 melt) characterised by a lower Mg# and sodium content ($Mg\#_{0.52}$ and $Na_2O \approx 2$ wt.%) with respect to that crystallising at lower temperature (i.e., 1000 °C; Figure 9a) from APR16-W13 melt ($Mg\#_{0.56}$ and ~4 wt.% Na_2O). Despite the activity of sodium is generally considered of paramount importance for amphibole stability in arc magmas (e.g. Cawthorn and O'Hara, 1976; Martin, 2007; Nandedkar et al., 2014 and references therein), our experiments, according to those realised on similar compositions (e.g., Pilet et al., 2010; Melekhova et al., 2015), underline that the increase of Na_2O/K_2O ratio (up to 2.04 in our experiments; see Table C8 for comparison with literature data) is actually more effective in stabilising amphibole than the absolute sodium content in the melt. The diagrams in Figure 9a-c show that the amphibole crystallisation at 1050 °C in the CM42 magma is associated with the increase of water and Na_2O/K_2O ratio, but not with the variation of sodium content in the melt. Pilet et al (2010) show that K_2O in amphiboles increases with increasing Mg# and/or temperature. High temperature would indeed promote the increase of K_2O accompanied by a decrease of Na_2O (and then a decrease of Na_2O/K_2O ratio), due to an isostructural exchange of K for Na in the A site of amphibole. On the other hand, the increasing Fe component in the amphibole would favour the Na substitution (increase Na_2O/K_2O ratio in Amph). Thus, we consider the effects of liquid composition (i.e., degree of differentiation) to prevail on those of

temperature for our amphiboles crystallised at constant pressure, as suggested by Pilet et al. (2010). The comparison of phase relations obtained at 800 MPa on the CM42 composition with those obtained with both Rhyolite-MELTS modelling and experiments on the MF leucite-basanite composition (Figure 8c), confirms that Na_2O/K_2O ratio in magmas plays a role on amphibole stability. According to Rhyolite-MELTS, amphibole never crystallises from the MF (Figure 8c), irrespective of the absolute amount of sodium in the melt. Experimental glasses reported by Conte et al. (2009) for the 1000 MPa hydrous experiments on the MF show Na_2O contents comparable to those obtained in the present study on CM42 (Na_2O ≈2 wt.%; Figure 9b), however, their Na_2O/K_2O ratios are lower than ours (<0.8 compared to ≥0.9, respectively; Figure 9c). Thus, the near-primary ultrapotassic character of the MF composition (high Mg# = 0.75) favours the early crystallisation (i.e. at 1200 °C) of phlogopite rather than amphibole in the experimental runs.

On the other hand, the occurrence of amphiboles in the lava flows of the Colli Albani Volcanic District (6-11 wt.% K_2O; Gaeta and Freda, 2001; Gozzi et al., 2014; Gaeta et al., 2016) indicates that the inhibition of amphibole crystallisation in ultrapotassic magmas is not caused by the high activity of potassium but, according to our experiments, it depends on the low Na_2O/K_2O ratios of magmas.

3.5. Conclusions

An alkaline (sample APR16) and a calc-alkaline (sample CM42) primitive basaltic liquids from the Phlegraean Volcanic District (South Italy) and the Capo Marargiu Volcanic District (Sardinia, Italy) are experimentally crystallised at deep crustal pressures under hydrous conditions. The experiments aim to investigate the effects of alkali on the stability of amphibole during the early stages of fractionation in alkaline/calc-alkaline magmas. Clinopyroxene is always present; orthopyroxene crystallises in the calc-alkaline composition for H_2O contents <5 wt.% and, unexpectedly, it also occurs in the alkaline composition. Amphibole stability is achieved in the calc-alkaline composition at 1050 °C and >5 wt.% H_2O in the melt, while its crystallisation is restricted at lower temperature (i.e. 1000 °C) in the alkaline composition. This is unexpected by virtue of the relatively high Na_2O content in the experimental alkaline glasses, which is thought to favour amphibole crystallisation under a wider range of physico-chemical conditions.

Therefore, we interpret amphibole crystallisation in our experiments as being mostly controlled by the Na_2O/K_2O ratio of the residual melt rather than by its absolute sodium content. The comparison of our results with those obtained from Rhyolite-MELTS simulations and experiments on ultrapotassic compositions from literature demonstrated that, at deep crustal level, the crystallisation of amphibole from primitive liquids depends not only on the water contents but also on the Na_2O/K_2O ratio, that should be ≥0.9.

Acknowledgements

This research has been conducted with the financial support of the HP-HT Laboratory of the Earth Science Department, Sapienza - University of Rome and contains part of the first author's master thesis. We are grateful to an anonymous referee for his very constructive reviews. We are also indebted to Editor S. Mollo for him thoughtful and useful comments. The authors thank M. Serracino (CNR-IGAG) for assistance during EPM analyses and M. Albano (CNR-IGAG) for his help in the SEM analyses.

References

Allen, J.C., Boettcher, A.L., 1983. The stability of amphibole in andesite and basalt at high-pressures. American Mineralogist 68, 307-314.

Alonso-Perez, R., Müntener, O., Ulmer, P., 2009. Igneous garnet and amphibole fractionation in the roots of island arcs: experimental constraints on andesitic liquids. Contributions to Mineralogy and Petrology 157, 541-558.

Anderson, A.T., 1980. Significance of hornblende in calc-alkaline andesites and basalts. American Mineralogist 65, 837-851.

Asimow, P.D., Ghiorso, M.S., 1998. Algorithmic modifications extending MELTS to calculate subsolidus phase relations. American Mineralogist 83, 1127-1132.

Barclay, J., Carmichael, I.S.E., 2004. A hornblende basalt from Western Mexico: water-saturated phase relations constrain a pressure-temperature window of eruptibility. Journal of Petrology 45, 486-506.

Blatter, D.L., Carmichael, I.S.E., 1998. Plagioclase-free andesites from Zita´cuaro (Michoaca´n), Mexico: petrology and experimental constraints. Contributions to Mineralogy and Petrology 132, 121-138.

Cawthorn, R.G., O'Hara, M.J., 1976. Amphibole fractionation in calcalkaline magma genesis. American Journal of Science 276, 309-329.

Conte, A.M., Dolfi, D., Gaeta, M., Misiti, V., Mollo, S., Perinelli, C., 2009. Experimental constraints on evolution of leucite-basanite magma at 1 and 10-4 GPa: implications for parental compositions of Roman high-potassium magmas. European Journal of Mineralogy 21, 763-782.

Davidson, J., Turner, S., Handley, H., Macpherson, C., Dosseto, A., 2007. Amphibole ''sponge'' in arc crust?. Geology 35, 787-790.

D'Antonio, M., Civetta, L., Di Girolamo, P., 1999. Mantle source heterogeneity in the Campanian Region (South Italy) as inferred from geochemical and isotopic features of mafic volcanic rocks with shoshonitic affinity. Mineralogy and Petrology 67, 163-192.

De Astis, G., Pappalardo, L., Piochi, M., 2004. Procida Volcanic History: new insights in the evolution of the Phlegraean Volcanic District (Campania Region, Italy). Bulletin of Volcanology 66, 622-641.

Devine, J.D., Gardner, J.E., Brack, H.P., Laynet, G.D., Rutherford, M.J., 1995. Comparison of microanalytical methods for estimating H_2O contents of silicic volcanic glasses. American Mineralogist 80, 319-328.

Fowler, S.J., Spera, F.J., Bohrson, W.A., Belkin, H.E., De Vivo, B., 2007. Phase equilibria constraints on the chemical and physical evolution of the Campanian Ignimbrite. Journal of Petrology 48, 459-493.

Gaeta, M., Freda, C., 2001. Strontian fluoro-magnesiohastingsite in Alban Hills lavas (Central Italy): constraints on crystallization conditions. Mineralogical Magazine 65, 787-795.

Gaeta, M., Freda, C., Marra, F., Arienzo, I., Gozzi, F., Jicha, B., Di Rocco, T., 2016. Paleozoic metasomatism at the origin of Mediterranean ultrapotassic magmas: Constraints from time-dependent geochemistry of Colli Albani volcanic products (Central Italy). Lithos 244, 151-154.

Ghiorso, M.S., Sack, R.O., 1995. Chemical mass transfer in magmatic processes IV. A revised and internally consistent thermodynamic model for the interpolation and extrapolation of liquid-solid equilibria in magmatic systems at elevated temperatures and pressures. Contributions to Mineralogy and Petrology 119, 197-212.

Gozzi, F., Gaeta, M., Freda, C., Mollo, S., Di Rocco, T., Marra, F., Dallai, L., Pack, A., 2014. Primary magmatic calcite reveals origin from crustal carbonate. Lithos 190-191, 191-203.

Graham, C.M., Powell, R., 1984. A garnet-hornblende geothermometer: calibration, testing, and application to the Pelona Schist, Southern California. Journal of Metamorphic Geology 2, 13-31.

Grove, T.L., Donnelly-Nolan, J.M., Housh, T., 1997. Magmatic processes that generated the rhyolite of Glass Mountain, Medicine Lake Volcano, N. California. Contributions to Mineralogy and Petrology 127, 205-223.

Grove, T.L., Elkins-Tanton, L.T., Parman, S.W., Chatterjee, N., Müntener, O., Gaetani, G.A., 2003. Fractional crystallization and mantle-melting controls on calc-alkaline differentiation trends. Contributions to Mineralogy and Petrology 145, 515-533.

Gualda, G.A., Ghiorso, M.S., Lemons, R.V., Carley, T.L., 2012. Rhyolite-MELTS: a modified calibration of MELTS optimized for silica-rich, fluid-bearing magmatic systems. Journal of Petrology 53, 875-890.

Hammarstrom, J.M., Zen, E., 1986. Aluminium in hornblende: an empirical igneous geobarometer. American Mineralogist 71, 1297-1313.

Hawthorne, F.C., Oberti, R., 2007. Classification of the Amphiboles. In: Amphiboles: crystal chemistry, occurrence and healts issues. (eds): F.C. Hawthorne, R. Oberti, G. Della Ventura, A. Mottana. Reviews in Mineralogy and Geochemistry 67, 55-88.

Helz, R.T., 1973. Phase relations of basalts in their melting range at P_{H2O} = 5 kbar as a function of oxygen fugacity. 1. Mafic phases. Journal of Petrology 14, 249-302.

Helz, R.T., 1976. Phase relations of basalts in their melting ranges at P_{H2O} = 5 kbar. 2. Melt compositions. Journal of Petrology 17, 139-193.

Helz, R.T., 1982. Phase relations and compositions of amphiboles produced in studies of the melting behavior of rocks. Reviews in Mineralogy 9B, 279-347.

Hilyard, M., Nielsen, R.L., Beard, J.S., Patinõ-Douce, A., Blencoe, J., 2000. Experimental determination of the partitioning behavior of rare earth and high field strength elements between pargasitic amphibole and natural silicate melts. Geochimica et Cosmochimica Acta 64, 1103-1120.

Holland, T.J.B., Richardson, S.W., 1979. Amphibole zonation in metabasites as a guide to the evolution of metamorphic conditions. Contributions to Mineralogy and Petrology 70, 143-148.

Hollister, L.S., Grissom, G.C., Peters, E.K., Stowell, H.H., Sisson, V.B., 1987. Confirmation of the empirical correlation of Al in hornblende with pressure of solidification of calc-alkaline plutons. American Mineralogist 72, 231-239.

Holloway, J.R., Burnham, C.W., 1972. Melting relations of basalt with equilibrium water pressure less than total pressure. Journal of Petrology 13, 1-29.

Holloway, J.R., 1973. The system Pargasite-H_2O-CO_2: A model for melting of a hydrous mineral with a mixed-volatile fluid-I. Experimental results to 8 kbar. Geochimica et Cosmochimica Acta 37, 651-666.

Krawczynski, M.J., Grove, T.L., Behrens, H., 2012. Amphibole stability in primitive arc magmas: effects of temperature, H_2O content, and oxygen fugacity. Contributions to Mineralogy and Petrology 164, 317-339.

Kress, V.G., Charmichael, I.S.E., 1991. The compressibility of silicate liquids containing Fe_2O_3 and the effect of composition, temperature, oxygen fugacity and pressure on their redox state. Contributions to Mineralogy and Petrology 108, 82-92.

Le Bas, M.J., Le Maitre, R.W., Streckeisen, A., Zanettin, R., 1986. A chemical classification of volcanic rocks based on the total alkali-silica diagram. Journal of Petrology 27, 745-750.

Le Maitre, R.W.B., Dudek, P., Keller, A., Lameyre, J., Le Bas, J., Sabine, M.J., Zanettin, A.R., 1989. A classification of igneous rocks and glossary of terms: Recommendations of the International Union of Geological Sciences, Subcommission on the Systematics of Igneous Rocks (No. 552.3 CLA). International Union of Geological Sciences.

Martin, R.F., 2007. Amphiboles in the igneous environment. Reviews in Mineralogy and Geochemistry 67, 323-358.

Masotta, M., Keppler, H., 2015. Anhydrite solubility in differentiated arc magmas. Geochimica et Cosmochimica Acta 158, 79-102.

Medard, E., Grove, T.L., 2008. The effect of H_2O on the olivine liquidus of basaltic melts: experiments and thermodynamic models. Contributions to Mineralogy and Petrology 155, 417-432.

Melekhova, E., Blundy, J., Robertson, R., Humphreys, M.C.S., 2015. Experimental evidence for polybaric differentiation of primitive arc basalt beneath St. Vincent, Lesser Antilles. Journal of Petrology 56, 161-192.

Moore, G., Carmichael, I.S.E., 1998. The hydrous phase equilibria (to 3 kbar) of an andesite and basaltic andesite from western Mexico: constraints on water content and conditions of phenocrysts growth. Contributions to Mineralogy and Petrology 130, 304-319.

Morimoto, N., Fabries, J., Ferguson, A.K., Ginzburg, I.V., Ross, M., Seifert, F.A., Zussman, J., Aoki, K., Gottardi, D., 1988. Nomenclature of pyroxenes. American Mineralogist 62, 53-62.

Middlemost, E.A., 1975. The basalt clan. Earth-Science Reviews 11, 337-364.

Müntener, O., Ulmer, P., 2006. Experimentally derived high-pressure cumulates from hydrous arc magmas and consequences for the seismic velocity structure of lower arc crust. Geophysical Research Letters 33, 21.

Nabelek, C.R., Lindsley, D.H., 1985. Tetrahedral Al in amphibole: a potential thermometer for some mafic rocks. Geological Society of America, Abstract Programs, (United States) 17, CONF-8510489.

Nandedkar, R.H., Ulmer, P., Müntener, O., 2014. Fractional crystallization of primitive, hydrous arc magmas: an experimental study at 0.7 GPa. Contributions to Mineralogy and Petrology 167, 1-27.

Philpotts, A., Ague, J., 2009. Principles of igneous and metamorphic petrology. Cambridge University Press.

Pichavant, M., Macdonald, R., 2007. Crystallization of primitive basaltic magmas at crustal pressures and genesis of the calcalkaline igneous suite: experimental

evidence from St Vincent, Lesser Antilles arc. Contributions to Mineralogy and Petrology 154, 535-558.

Pichavant, M., Scaillet, B., Pommier, A., Iacono-Marziano, G., Cioni, R., 2014. Nature and evolution of primitive Vesuvius magmas: an experimental study. Journal of Petrology 55, 2281-2310.

Pilet, S., Ulmer, P., Villiger, S., 2010. Liquid line of descent of a basanitic liquid at 1.5 GPa: constraints on the formation of metasomatic veins. Contributions to Mineralogy and Petrology 159, 621-643.

Prouteau, G., Scaillet, B., 2003. Experimental constraints on the origin of the 1991 Pinatubo dacite. Journal of Petrology 44, 2203-2241.

Ridolfi, F., Renzulli, A., Puerini, M., 2010. Stability and chemical equilibrium of amphibole in calc-alkaline magmas: an overview, new thermobarometric formulations and application to subduction-related volcanoes. Contributions to Mineralogy and Petrology 160, 45-66.

Ridolfi, F., Renzulli, A., 2012. Calcic amphiboles in calcalkaline and alkaline magmas: thermobarometric and chemometric empirical equations valid up to 1,130°C and 2.2 GPa. Contributions to Mineralogy and Petrology 163, 877-895.

Rutherford, M.J., Devine, J.D., 1988. The May 18, 1980, eruption of Mount St. Helens 3. Stability and chemistry of amphibole in the magma chamber. Journal of Geophysical Research 93, 949-11, 959.

Seck, H.A., 1971. Koexisterend alkali-feldspate und plagioclase in system $NaAlSi_3O_8$-$KAlSi_3O_8$-$CaAl_2Si_2O_8$ bei temperature von 650 °C bis 900 °C. Neues Jahrbuch für Mineralogie-Abhandlungen 155, 315-395.

Sisson, T.W., Grove, T.L., 1993. Experimental investigations of the role of H_2O in calc-alkaline differentiation and subduction zone magmatism. Contributions to Mineralogy and Petrology 113, 143-166.

Tecchiato, V., Gaeta, M., Mollo, S., Perinelli, C., Scarlato, P., 2015. High porphyritic calc-alkaline basalts from the Cenozoic Capo Marargiu Volcanic District (Sardinia, Italy). Goldschmidt Conference Abstracts 3098.

Toplis, M.J., 2005. The thermodynamics of iron and magnesium partitioning between olivine and liquid: criteria for assessing and predicting equilibrium in

natural and experimental systems. Contributions to Mineralogy and Petrology 149, 22-39.

Weaver, S.L., Wallace, P.J., Johnstonm, A.D., 2013. Experimental constraints on the origins of primitive potassic lavas from the Trans-Mexican Volcanic Belt. Contributions to Mineralogy and Petrology 166, 825-843.

Chapter 3: Figures

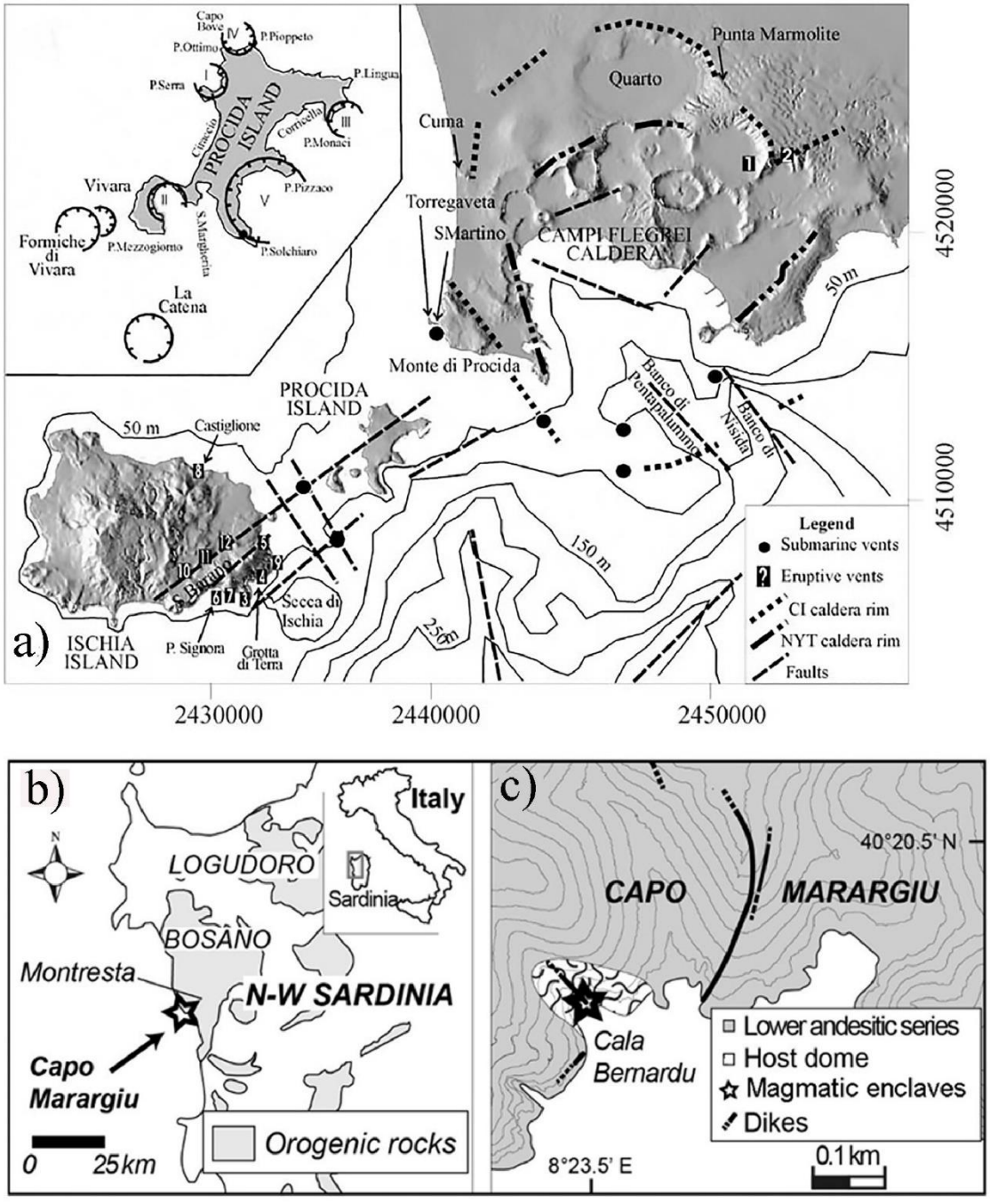

Figure 1. Sketch map of the Phlegraean Volcanic District (modified from De Astis et al., 2004), showing main tectonic structures, caldera rims and vent locations; the inset map shows an enlarged view of Procida Island and the outcrop (empty star) of the sample APR16 (a). Geological sketch map of the NW sector of Sardinia (b) and of Capo Marargiu Volcanic District (c); the black star in (c) shows the outcrop of the sample CM42.

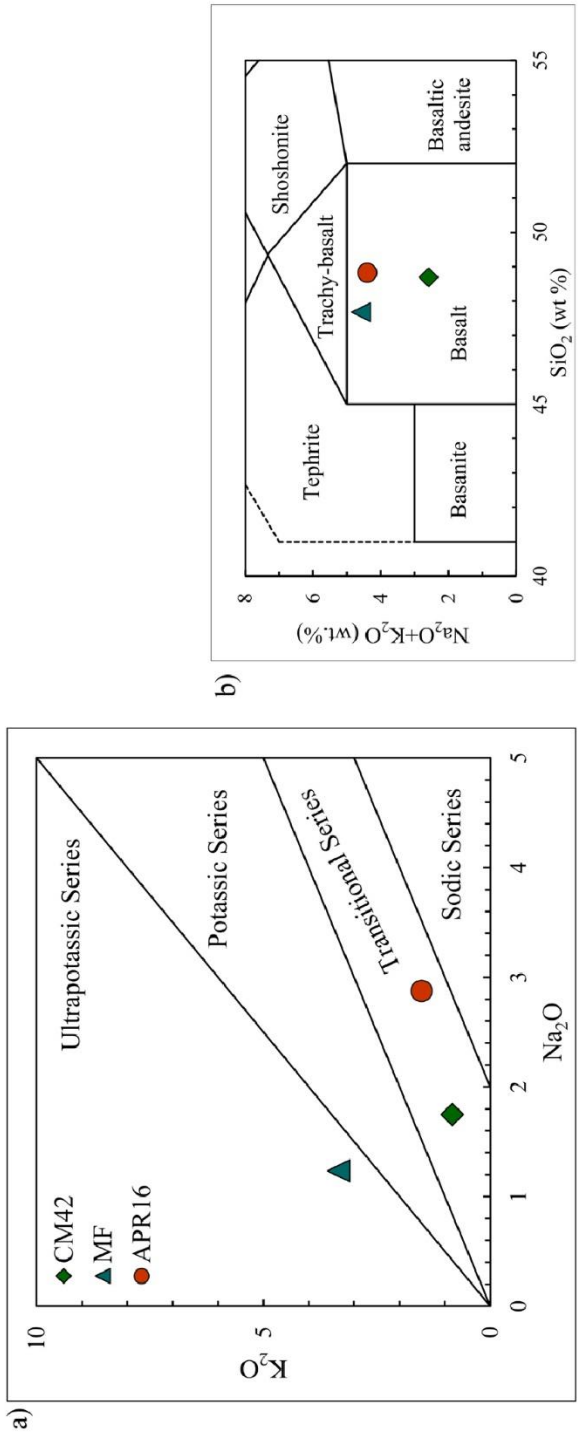

Figure 2. a) Total Alkali Silica (TAS, Le Bas et al., 1986) diagram showing the composition of primitive basalts (APR16 and CM42) used as starting materials for the experiments; b) APR16 and CM42 are plotted into the K_2O vs. Na_2O diagram which shows the fields for ultrapotassic, potassic, transitional and sodic alkaline series (Middlemost, 1975; Le Maitre, 1989). Also plotted in the diagrams is the leucite-basanite experimentally studied by Conte et al. (2009) whose results are used for comparison.

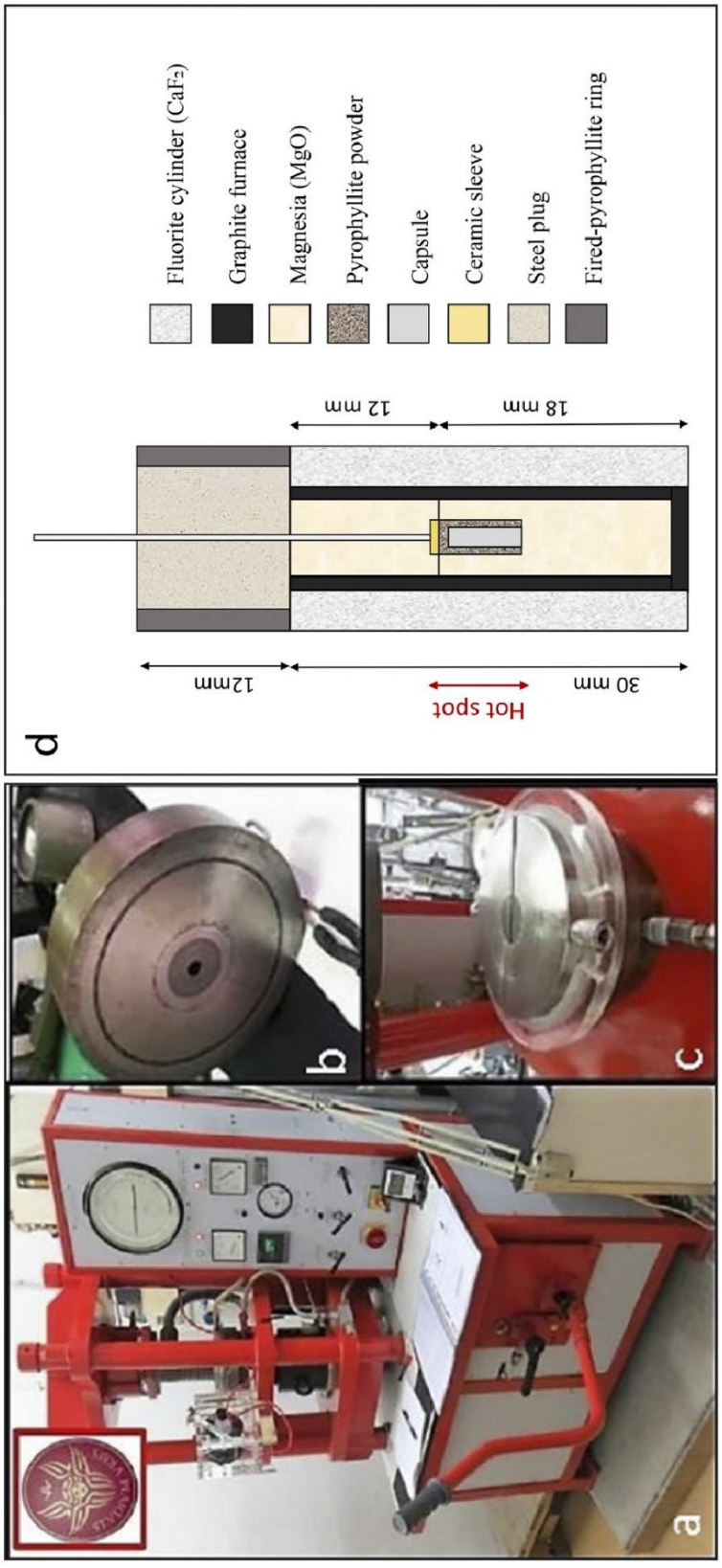

Figure 3. Piston cylinder apparatus at the HP-HT Laboratory of the Earth Science Department, “Sapienza” University of Rome (a); ½ inch pressure vessel (b); thermocouple plate (c), cross section of the experimental assembly (d).

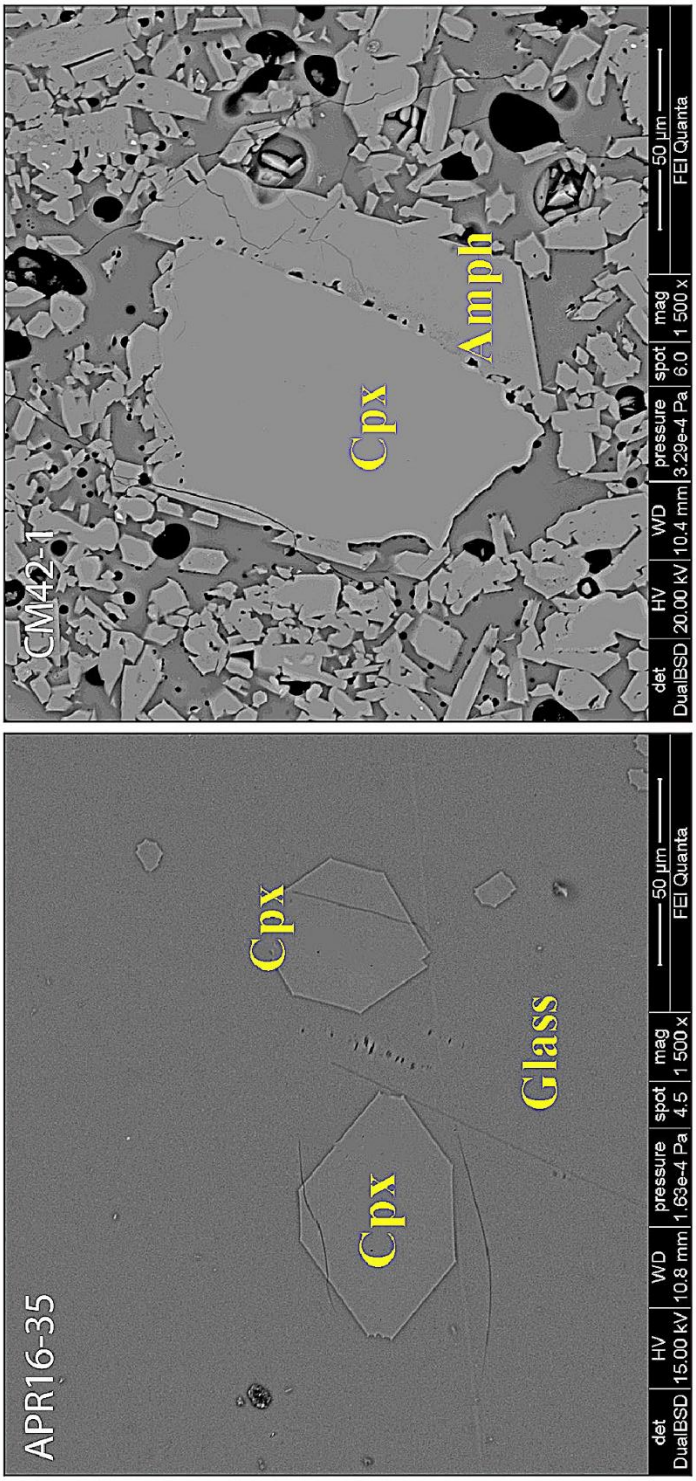

Figure 4. Backscattered SEM images of APR16-35 and CM42-1 runs; Cpx = clinopyroxene, Gl = glass.

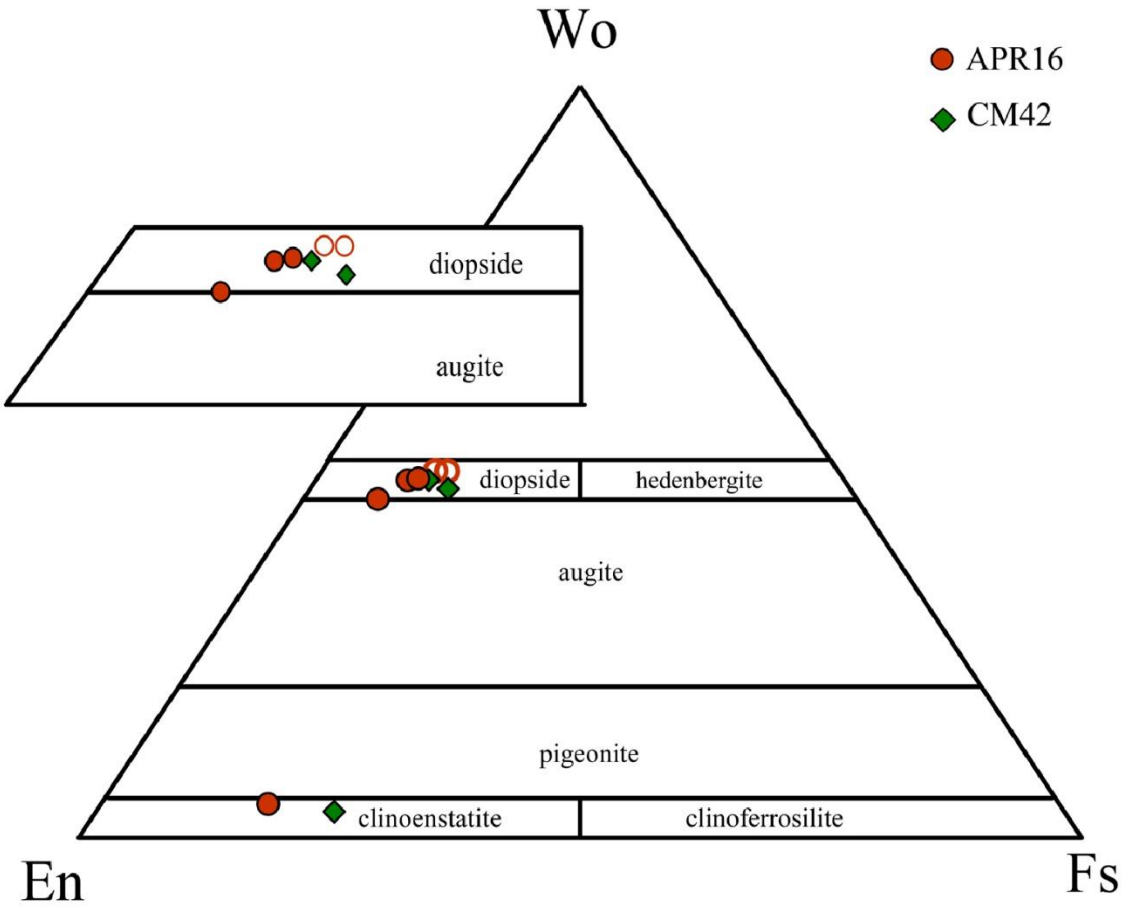

Figure 5. Pyroxene compositions plotted into the pyroxene classification diagram (Morimoto et al., 1988). Wo: wollastonite; En: enstatite; Fe: ferrosilite. Empty symbols refer to NWA experiments.

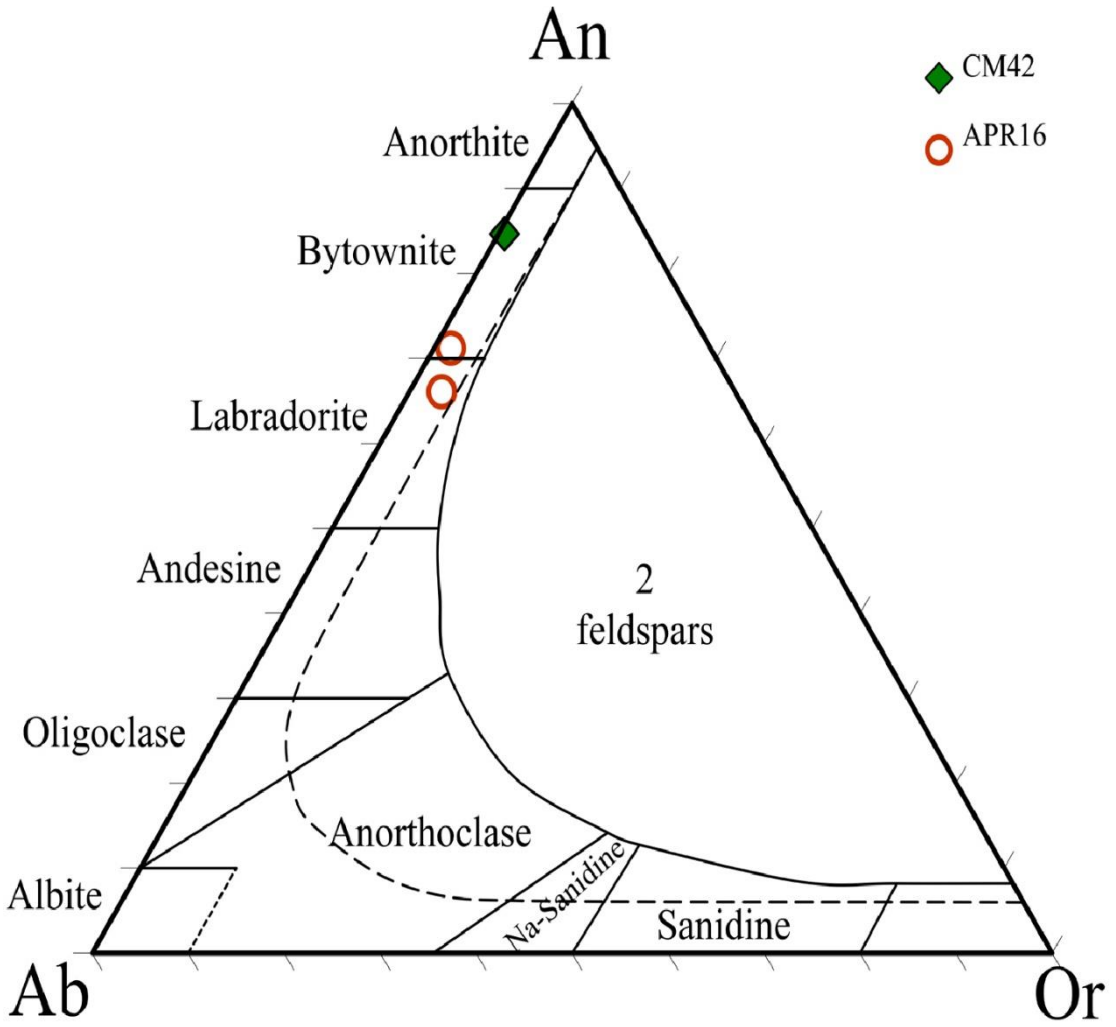

Figure 6. Feldspar compositions plotted in the Ab: albite; Or: orthoclase; An: anorthite classification diagram. Dashed line represents the solvus at 750 °C, P_{H2O} = 100 MPa (Seck, 1971).

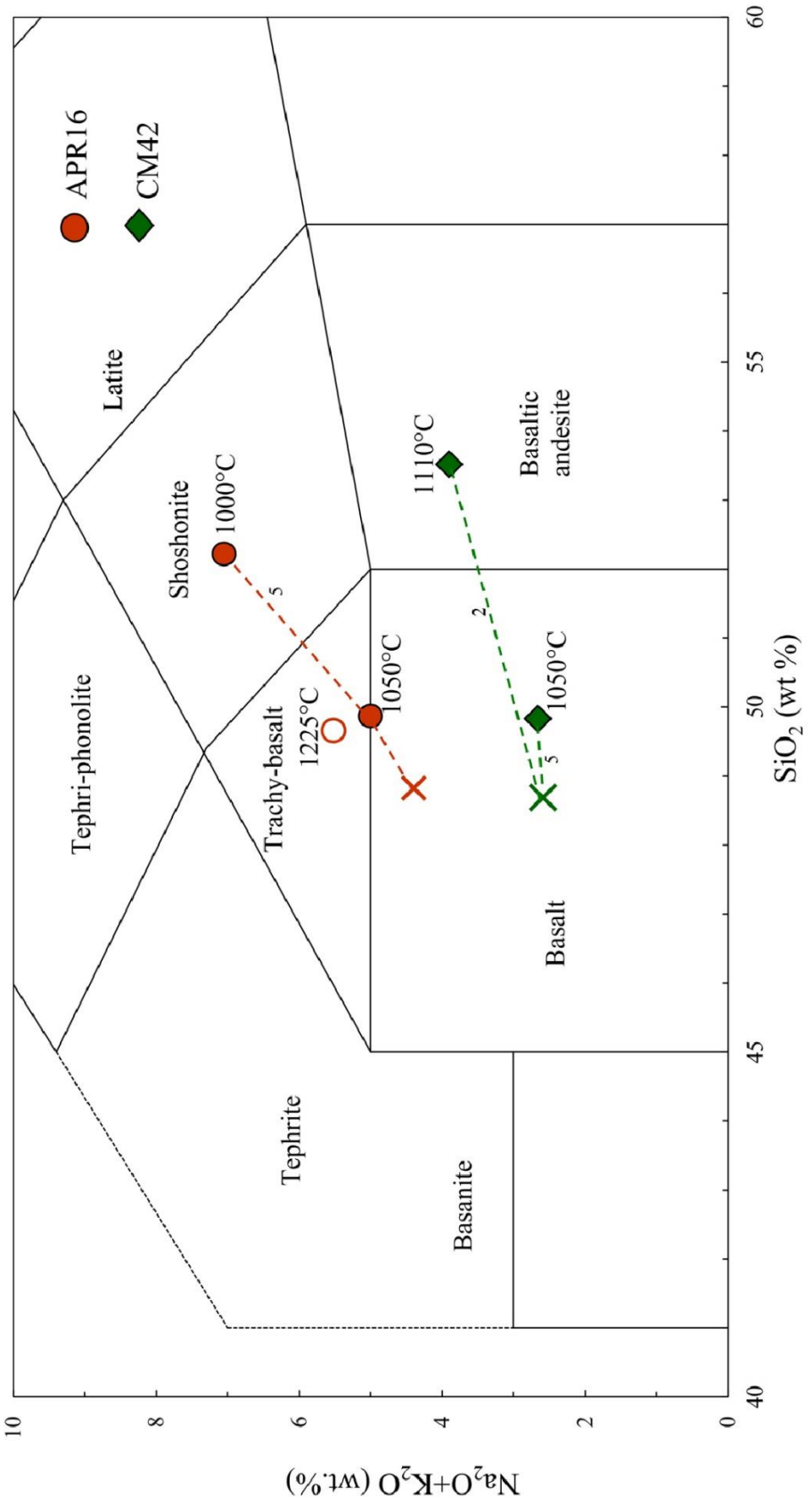

Figure 7. Composition of the APR16 and CM42 experimental glasses reported in the TAS diagram; crosses indicate starting material. Damp (2 wt.% H_2O_i) and wet (5 wt.% H_2O_i) runs are indicated by the numbers near to the dashed lines.

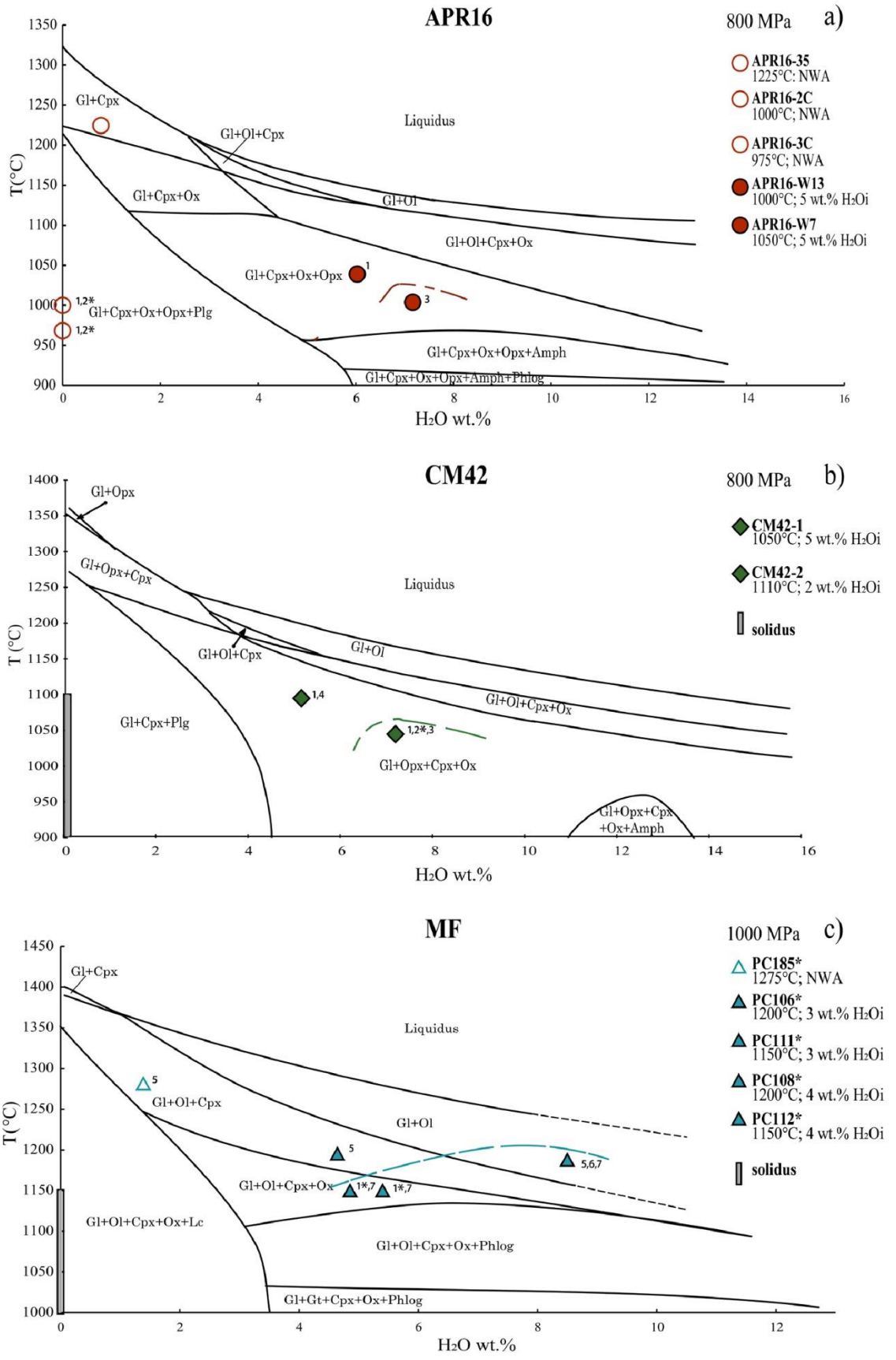

Figure 8. T (°C) vs. H_2O_f (i.e. H_2O in the melt phase) diagrams showing the phase relations at P = 800 MPa for APR16 (a) and CM42 (b) compositions and P = 1000

MPa for MF (c) composition obtained by means of the Rhyolite-MELTS calculations. The diagrams also display the data obtained from the piston cylinder experiments; dashed lines represent the amphibole/phlogopite saturation curves extrapolated from the experimental data. Numbers near symbols indicate phases crystallized in the experiments but not predicted by Rhyolite-MELTS modelling: 1 = Ol, 2 = Opx, 3= Amph, 4 = Plg, 5 = Ox, 6 = Cpx, 7 = Phlog. 1* = absence of Ol in experimental runs; 2* = absence of Opx in experimental runs. The asterisk (*) indicates data from Conte et al. (2009). Amph: amphibole, Cpx: clinopyroxene; Gl: glass; Lc: leucite; Ol: olivine; Opx: orthopyroxene, Ox: oxide, Phlog: phlogopite, Plg: plagioclase.

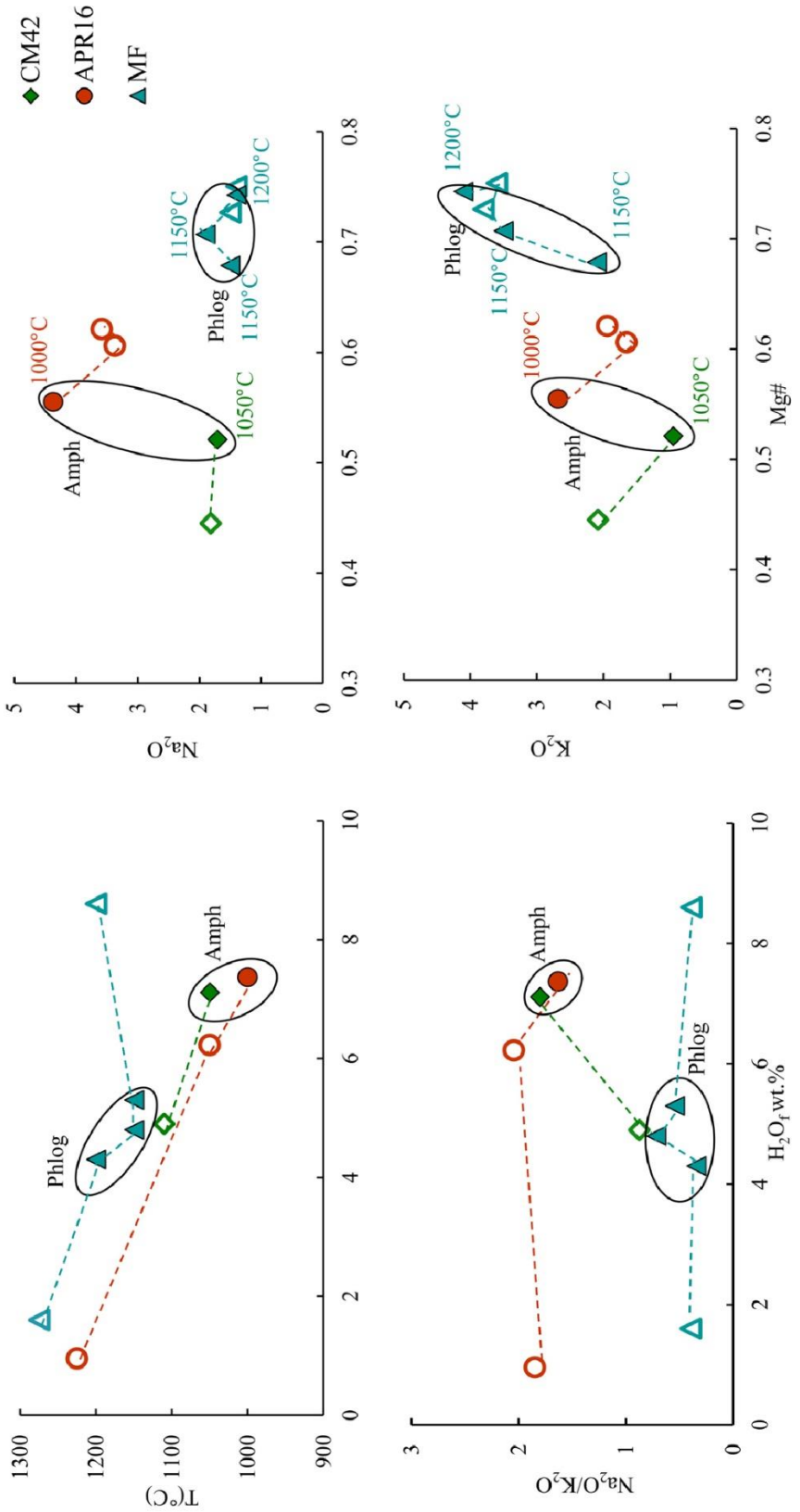

Figure 9. Experimental glasses of the samples APR16, CM42 and MF reported in the T °C vs H_2O_f (a), Na_2O vs Mg# (b), Na_2O/K_2O vs H_2O_f (c) and K_2O vs Mg# (d) diagrams.

Chapter 3: Tables

Table 1. Experimental run conditions, phase assemblages and proportions.

Run#	T (°C)	P (MPa)	Time (h)	H_2O_i	H_2O_f	Phase assemblage
APR16-35	1225	800	6	NWA	1.70	Gl (96) + Cpx (4)
APR16-2C	1000	800	3	NWA	-	Gl†(3) + Cpx (50) + Ol (10) + Plg (28) + Ox (9)
APR16-3C	975	800	3	NWA	-	Cpx (51) + Ol (10) + Plg (32) + Ox (7) ± KFld (trace) †
APR16-W7	1050	800	3	4.7	6.2	Gl (78) + Cpx (15) + Ol (5) + Opx (2) + Ox (trace) †
APR16-W13	1000	800	3	4.8	7.4	Gl (58) + Cpx (21) + Opx (1) + Amph (18) + Ox (2)
CM42-2	1110	800	3	2	4.9	Gl (42) + Cpx (23) + Ol (11) + Opx (0.2) + Plg (22.8) + Ox (1)
CM42-1	1050	800	3	5	7.1	Gl (67) + Cpx (8) + Ol (3) + Amph (21) + Ox (1)
PC185*	1275	1000	18	NWA	1.6	Gl (83.5) + Ox (0.9) + Ol (3.7) + Cpx (11.9)
PC106*	1200	970	27	3	4.3	Gl (78.6) + Ox (2) + Ol (5.2) + Cpx (14.2)
PC111*	1150	1000	70	3	5.3	Gl (54.8) + Ox (1.8) + Cpx (30.5) + Phlog (12.9)
PC108*	1200	1000	35	4	8.6	Gl (86.2) + Ox (1.2) + Ol (3.9) + Cpx (6.4) + Phlog (2.3)
PC112*	1150	1000	70	4	4.8	Gl (55.9) + Ox (0.6) + Cpx (23.8) + Phlog (19.7)

NWA = no water added; H_2O_i% of water added to the charge. H_2O_f as determined by the by-difference calculation method (respect to the total of EMP analyses).

Gl = glass; Cpx = clinopyroxene; Ol = Olivine; Plg = plagioclase; Phlog = phlogopite; Amph = amphibole; Ox = oxide; KFld = KFeldspar. † phases too small for analysis; *: data from Conte et al., 2009.

Concluding remarks

This PhD project investigated the early magmatic differentiation of basaltic to andesitic products at Capo Marargiu Volcanic District (CMVD). Petrographic and geochemical evidence from natural rocks (i.e., crystal-rich enclaves, host dome, crystal clots, dikes) and experimental data from piston cylinder runs all converge in the following conclusions:

1) The CMVD plumbing system is a complex polybaric structure developed from the base of Sardinian crust to hypabyssal depths. Thermometric, barometric, hygrometric and oxygen barometric estimates (see Chapter 1) indicate that hydrous (5-6 wt.% H_2O) high-Mg basalts produced by partial melting of spinel lherzolites variably metasomatised by slab-derived fluids undergo a first differentiation stage (Step 1; Chapter 1) at *P-T-f*O_2 conditions of 0.5-0.7 GPa, 1030-1180 °C, NNO – NNO+2. Textural relations (i.e., early crystallising Fo-rich olivine, diopsidic clinopyroxene, and high-Mg amphibole; Chapter 1), bulk-rock variation diagrams (especially Al_2O_3; Chapter 1), Type 1 + Type 2 clinopyroxene chemistry (Chapter 2), and experimental products (Chapter 3) fairly confirm the hydrous and deep evolution of high-Mg basalts towards basaltic andesitic compositions (i.e., PBA magmas; Chapter 2). Under such conditions, the crystallisation of plagioclase is hampered leading to Al_2O_3-rich residual liquids. Moreover, bulk rock incompatible trace elements and clinopyroxene isotopic composition testify to important assimilation of the Hercynian basement (r = 0.16).

   Crystal clots apparently represent the solid fraction segregated at shallower levels in the crust (0.2-0.4 GPa; Chapter 1) to produce andesitic melts from basaltic andesitic magmas (Step 2; Chapter 1). These andesites ultimately degas and crystallise anhydrous minerals (two pyroxenes and Na-rich plagioclase) during the emplacement in hypabyssal regions (Chapter 1).

2) Enclaves are hybrid products formed in an open system region of the CMVD plumbing system. Indeed, Type 1 + Type 2 clinopyroxenes (Chapter 2) and amphiboles (Chapter 1) represent the cumulitic material left behind during the

hydrous high-Mg basaltic to basaltic andesitic differentiation in the lower crust (HMB to PBA; Chapter 2). These early segregated crystals show strong disequilibrium textures caused by entrainment in a volatile-poor basaltic andesitic magma (i.e., EBA; Chapter 2), responsible for the final crystallisation of a distinctly more evolved population of clinopyroxenes (i.e., Type 3; Chapter 2). Bulk rock trace element composition (especially TiO_2, Sc and V abundances; Chapter 1) clearly account for the hybrid nature of these puzzling rocks.

Outlook

Understanding the petrology of crystal-rich enclaves and the differentiation processes of CMVD products was the main goal of this PhD project. Despite the results presented in the previous chapters provide qualitative and quantitative answers to these issues, the following aspects (and maybe more) still remain poorly explored in this research:

1) The scattering of Sr-isotopic data for Type 1 clinopyroxenes with Mg#>90 (Chapter 2) suggests the presence of a heterogeneous mantle source at CMVD, consistently with the geochemical variability observed for high-Mg basaltic rocks outcropping in different localities of the island. Considering that Sardinian orogenic products mainly denote two differentiation trends, i.e., tholeiitic and calc-alkaline, it would be interesting to investigate if and how, at regional scale, the primary variability of basalts influences the magmatic differentiation paths. Moreover, since Sardinian orogenic magmatism was strictly related to the extensional tectonic affecting the back-arc region of Apennine chain, it would be challenging to understand if there is an interplay between the structural evolution of Sardinian crust and the development of calc-alkaline vs. tholeiitic trends. Thus, from these two open questions, a third point concerns about the relationship between the regional geodynamic evolution and the nature of mantle metasomatic agents/processes.
2) Trace element data on anorthitic plagioclase from basaltic andesitic host dome (Tecchiato et al., in preparation) suggests the occurrence of two types of primitive plagioclases. Preliminary results from geochemical modelling of

melts at equilibrium with these plagioclases suggest a multiple magmatic contribution. Interestingly, this evidence remarks the occurrence of two different types of basaltic andesitic magmas at equilibrium with Type 2 and Type 3 clinopyroxenes from enclaves (Chapter 2), questioning the effect of magma mixing in the genesis of CMVD mafic to intermediate rocks.

3) Answering to the previous questions would provide an overall scenario about Sardinian magmatism and would help, at the scale of a single volcanic district like CMVD, to conceive a physical model describing both magma reservoir geometry and the dynamics of differentiation processes.

Acknowledgements

Looking back at all the exciting experiences I had, and at all the friends that I knew during these three years of hard work, I feel extremely lucky, grateful and indebted with many people.

Thanks to Prof. Mario Gaeta for his support and for feeding my passion for igneous petrology. Mario, thanks for your sincerity, friendship, and for the beautiful time spent together. I tried to do my best and I hope you are satisfied for our scientific achievements in that amazing island that is Sardinia.

I am really grateful to Prof. Silvio Mollo for his precious help in so many occasions. Silvio, I have no words to express my gratitude. Thanks for helping me to improve my scientific writing and for all the international experiences, from the Goldschmidt in Prague and Yokohama to the visit at ETH. Even if sometimes I was close to freak out for your comments, working with you helped me to grow scientifically and personally. Thank you.

A special thanks to Prof. Olivier Bachmann for his kind and warm hospitality. Thank you, Olivier, for giving me the privilege of working for several months in one of the best university of the world. It was a great honour to chat with you, and a big pleasure to have a couple of dinners at your place.

Thanks to Dr. Albrecht von Quadt for his kindness, his collaboration in the preparation of samples for isotopic measurements, and for the analytical work.

A massive acknowledgement to Dr. Cristina Perinelli, Dr. Piergiorgio Scarlato, and to Barbara Bonechi for their important contribution to this PhD project.

Thanks to Dr. Matteo Masotta and Dr. Marco Brenna for the review of this thesis. I apologise again for the raw version of the text submitted.

Huge thanks and warm hugs to my ETH friends for their help and for the funny moments spent together: il Parmi and family, Fraforni, Dawid, Ben (+ Dana and Seby), Fabio, Jakub, Alina, Italo, Ozge, Jörn (stronzio), Yannick, Cindy, Nico, Jule, Stephane, Juliane, il Galli, Max, Giuliano, Simon… sorry if I forgot someone.

To my Sapienza friends: thanks to Irene, Paolo, Livio, Carolina, Flavio, Gian Marco, Matteo, Danilo, il mitico Domenico Mannetta… and to all the PhD students from XXX ciclo.

Special thanks to my friends Carlo and Valentina (and Diego), Stefano R. and family, Andrea and Alexandra, Paolo and Sonia, Stefano G. and Erika, Zia Stefy and Gilberto, Cristian e Silvia, Giuliana, Angela, Andrea, Mirco, Domenico, il Piase, Dario… and many others.

A sweet thanks to Valentina for her love and patience. You have taught me something special every day since the beginning. I love you. Thanks Maria.

The biggest acknowledgement to my family: my parents Danilo and Concetta and my nonna Maria. Spero che i traguardi dei vostri figli ripaghino il vostro sudore. Thanks to my brothers Antonio and Sira and to their families. A thought goes to my grandparents nonno Bruno, nonna Dina, and nonno Toni, and to my aunt zia Assunta and my uncle zio Carlo.

Thank you for reading these pages and sorry if I forgot your name.